THESIS ON NATURAL AND EXACT SCIENCES B210

Study of Kesterite Solar Cell Absorbers by Capacitance Spectroscopy Methods

ERKKI KASK

TUT
PRESS

TALLINN UNIVERSITY OF TECHNOLOGY
Faculty of Science
Department of Physics

This dissertation was accepted for the defence of the degree of Doctor of Philosophy in Applied Physics on April 29, 2016.

Supervisor: Prof. Jüri Krustok
Department of Physics, Tallinn University of Technology, Estonia

Opponents: Dr. Paweł Zabierowski, Faculty of Physics, Warsaw University of Technology, Poland

Dr. Indrek Jõgi, Institute of Physics, Faculty of Science and Technology, University of Tartu, Estonia

Defence of the thesis: June 7, 2016

Declaration:
Hereby I declare that this doctoral thesis, my original investigation and achievement, submitted for the doctoral degree at Tallinn University of Technology, has not been submitted for doctoral or equivalent academic degree.

Erkki Kask

ISSN 1406-4723
ISBN 978-9949-23-949-8 (publication)
ISBN 978-9949-23-950-4 (PDF)

LOODUS- JA TÄPPISTEADUSED B210

Kesteriitsete päikesepatareide absorbermaterjalide uurimine mahtuvusspektroskoopiliste meetoditega

ERKKI KASK

TTÜ KIRJASTUS

TABLE OF CONTENTS

LIST OF PUBLICATIONS

The thesis is based on the following publications, which are referred to in the text by the Roman numerals I–III:

I. **E. Kask**, T. Raadik, M. Grossberg, R. Josepson, J. Krustok. Deep defects in Cu_2ZnSnS_4 monograin solar cells. Energy Procedia 10 (2011) 261-265.

II. **E. Kask**, M. Grossberg, R. Josepson, P. Salu, K. Timmo, J. Krustok. Defect studies in $Cu_2ZnSnSe_4$ and $Cu_2ZnSn(Se_{0.75}S_{0.25})_4$ by admittance and photoluminescence spectroscopy. Materials Science in Semiconductor Processing 16(3) (2013) 992 - 996.

III. **E. Kask**, J. Krustok, S. Giraldo, M. Neuschitzer, S. López-Marino, E. Saucedo. Temperature dependent electrical characterization of thin film $Cu_2ZnSnSe_4$ solar cells. Journal of Physics D: Applied Physics 49(8) (2016) 085101.

In Appendix A, copies of these papers are included.

AUTHOR'S CONTRIBUTION TO THE PUBLICATIONS

The contribution by the author to the papers included in this thesis is as follows:

I. Characterization of Cu_2ZnSnS_4 solar cells by admittance spectroscopy: measurements, analysis of results and major part of writing.

II. Characterization of $Cu_2ZnSnSe_4$ and $Cu_2ZnSn(Se_{0.75}S_{0.25})_4$ solar cells by admittance spectroscopy: measurements, analysis of results and major part of writing.

III. Characterization of $Cu_2ZnSnSe_4$ solar cells by impedance spectroscopy: measurements, analysis of results and major part of writing.

INTRODUCTION

Higher energy prices, increasing energy consumption and depleting fossil fuels remind of the need of alternative energy sources like solar energy, wind power, hydropower, and other resources. The global energy demand is expected to rise further. Importantly, as a result, the studies in the field of solar energy have increased too. Renewable energy sources provide sustainable, clean green and environmentally friendly energy. As the Sun is freely shining, we need only to collect, convert and save its radiation energy. Hence, it is worth of finding out the most efficient way to do that, which should involve production of low-cost high efficient solar panels with minimum possible harm to the environment.

To convert solar energy to electrical energy, semiconductor devices can be used. The creation of electric current is based on the photovoltaic effect in a semiconductor that is under light illumination. In a heterojunction solar cell, this effect occurs in the junction area formed by combining different semiconductor layers, i.e. absorber and buffer layers. However, producing such devices involves the possibility for creating material inhomogeneity as well as defects. This means that some energy levels in semiconductors band gap are created. These defects are caused during fabrication by different technology methods. These levels or states can capture charge carriers or as well give somehow a better solution for converting solar energy into electrical energy. For example, with specific defects, we are able to change the type of semiconductor conductivity and tune its magnitude. Thus, some defects can be bad, while other ones can be beneficial.

To produce more efficient solar cells, it is required to characterize the defect levels in the prepared solar cells. This can be done, for example, by capacitive measurements methods, like capacitance-frequency dependence, capacitance-voltage dependence and admittance spectroscopy (AS). For not to blame or criticize other methods, it is reasonable to mention that different methods give additional valuable knowledge, and vice versa, capacitive measurements methods include an essential extra picture for them.

According to Losee [1], the capacitance spectroscopy and admittance spectroscopy are particularly suitable methods for detecting defect levels. Also, deep level transient spectroscopy (DLTS) can be used to analyze semiconductor materials [2]. This technique investigates the properties of trap states by time resolved measurements of the depletion region admittance at a fixed frequency. Moreover, admittance spectroscopy is an effective and non-destructive method for studying deep defects in solar cells, giving values for defect level activation energies. It is suitable for understanding some of the basic physical properties of absorber materials and will help to make it possible to achieve a breakthrough and show higher efficiencies.

Currently, there are different solar cell technologies available, such as devices made with a silicon photoabsorber, and thin film or monograin layer solar cells with novel direct band gap absorbers. The production of large-scale Si

wafers for silicon solar cells is time consuming and expensive compared to thin film or monograin technologies. Moreover, silicon is an indirect band gap semiconductor, i.e. a thicker Si material layer is needed in the solar cell compared to the absorber material layer in solar cells with a direct band gap semiconductor, for example, $Cu(In,Ga)Se_2$ (CIGSe) or CdTe. Record efficiencies for CIGSe and CdTe thin film solar cells are 22.3% and 21.5% [3], respectively.

Unfortunately, CIGSe is not a good option as it includes rare and hence expensive element In [4, 5, 6]. Since Cd is toxic, the CdTe absorber is not a better solution either. Consequently, competitive absorber materials that consist of non-poisonous elements are in sufficient reserve in the Earth crust [7, 8, 9].

This thesis studies multinary compounds such as Cu_2ZnSnS_4 (CZTS) [I], $Cu_2ZnSnSe_4$ (CZTSe) [II, III] and their solid solutions $Cu_2ZnSn(S,Se)_4$ (CZTSSe) [II]. These materials have kesterite crystal structure and belong to the class of kesterites. They all have direct band gap and high absorption coefficient ($> 10^4$ cm^{-1}) [10] and are promising candidates for other solar cells with absorbers made from non-toxic and abundant elements [11, 12, 13, 14, 15]. For example, the quaternary compound $Cu_2ZnSnSe_4$ is an analogue of $CuInSe_2$, where rare and expensive In is replaced with Zn and Sn [10, 16, 17].

It is known that intrinsic point defects in absorbers are playing a major role in determining their properties. Record efficiencies for best solar cells with absorbers CZTS, CZTSe and CZTSSe are correspondingly 8.4% [18], 11.6% [19] and 12.6% [20]. The calculated maximum theoretical efficiency of these types of single junction solar cells is around 28% - 31% [21]. However, without understanding the basic physical properties of these absorbers it will be impossible to make a breakthrough similar to $CuInGaSe_2$ solar cells that show efficiencies over 21% [22]. The reason for further defect studies lies here.

In this work, solar cells made with CZTS [I], CZTSe [II] and CZTSSe [II] monograin absorber layer and CZTSe [III] thin film solar cells were studied by exploiting the usefulness of the capacitive spectroscopy methods. The aim was to characterize the defect structure in these materials and to study a role of grain boundaries in thin film polycrystalline CZTSe solar cells.

LIST OF ABBREVIATIONS

AC	Alternating current
AS	Admittance spectroscopy
a. u.	Arbitary units
C-f	Capacitance-frequency dependence
CIGSe	$Cu(In,Ga)Se_2$
CPE	Constant phase element
CZTS	Cu_2ZnSnS_4
CZTSe	$Cu_2ZnSnSe_4$
CZTSSe	$Cu_2ZnSn(S,Se)_4$
DC	Direct current
DLTS	Deep level transient spectroscopy
EQE	External quantum efficiency
E_A	Activation energy
IS	Impedance spectroscopy
I-V	Current-voltage characteristics
MGL	Monograin layer
PL	Photoluminescence
R_s	Series resistance
R_p	Parallel resistance
SCR	Space charge region
Y	Admittance
Z	Impedance
η	Power conversion efficiency

1. LITERATURE OVERVIEW

Quaternary compounds $Cu_2ZnSn(S_{1-x}Se_x)_4$ (CZTSSe) are promising non-toxic semiconductor materials for the absorber layer in solar cells [7]. Nevertheless, it is very difficult to grow pure absorbers, i.e CZTS or CZTSe, because different secondary phases like ZnS and Cu_2SnS_3 are very easily formed and large compositional nonuniformity is present. For CZTS and CZTSe absorber materials, bandgaps of ~1.6 eV [23, 24, 25] and ~1 eV [16, 26] have been attributed, respectively. Optimal bandgap for solar energy conversion is achievable by choosing suitable S to Se ratio for the CZTSSe solid solution [27, 28].

Photovoltaic performance is hindered by a large variety of intrinsic lattice defects, which influence optical and electrical properties of solar cells. Information about the defect structure of CZTS, CZTSe and CZTSSe in the literature is scarce. Defects have been studied mostly by photoluminescence spectroscopy (PL) [29, 16, 30, 31] and by capacitive spectroscopy methods. Capacitance and photoluminescence spectroscopy have proven to be very efficient methods in the defect studies of various semiconductors. To our knowledge, few papers cover capacitance spectroscopy of CZTS, CZTSSe and CZTSe. Hence, many physical properties of $Cu_2ZnSn(S_{1-x}Se_x)_4$ compounds are still unknown and CZTS/CdS, CZTSe/CdS and CZTSSe/CdS heterojunctions have not been analyzed in detail. Moreover, there is lack of information about the point defects in these absorber materials [I, II, III].

Only few papers have described PL properties of CZTS. For example, a broad and asymmetric PL band at 1.3 eV has been detected in many papers [32, 33, 34, 35]. Oishi et al. [34] have measured also a second PL peak at 1.45 eV in CZTS films grown on Si (100) surface by vacuum evaporation. This peak was attributed to the donor-acceptor pair transition. Recently, even more PL peaks were measured in the vapour phase grown CZTS crystals, including DA1 peak at 1.496 eV and DA2 peak at 1.475 eV [33]. A low temperature ($T = 10$ K) bandgap energy was calculated to be $E_g = 1.519$ eV and the estimated room temperature bandgap energy was 1.43 eV. This bandgap value is definitely lower than the usually measured bandgap energy in CZTS thin film samples.

Recently, Chen at al. [36] made first-principles calculations of defect structure of the quaternary absorber CZTS. They found that the p-type conductivity of CZTS is mainly determined by the Cu_{Zn}^{-} antisite defect that has quite deep level at $E_A = 0.12$ eV. At the same time, they showed that even deeper acceptors Zn_{Sn} and Cu_{Sn} can be found in CZTS with $E_A > 0.2$ eV.

Fernandes et al. [37] determined CZTS defect activation energies 44.7 meV and 112.7 meV by admittance spectroscopy. They analyzed AS of Cu_2ZnSnS_4 (CZTS) solar cells, applying various equivalent circuits to fit the measured data. They calculated deviation between measured and fitted data and found that their fitting of measured data is satisfied only by a quite complicated model. Usually,

the more elements are used in an equivalent circuit, the better the fit found is, but in that case, the interpretation is inappropriate or impossible.

Besides point defects, the presence of various defect clusters is possible. It has been found that the formation energies of defect clusters are lower than the formation energies of individual defects [36, 38, 39, 40], which means that they are easily formed. Also, structural disorder in the lattice causes defect clusters to form. For example, one reason may be the disorder among the Cu and Zn cations, which means that not all the Cu and Zn atoms are located on the correct crystallographic sites [41]. Ordering in structure is determined by the proportion of atoms located on the correct lattice sites in the relevant substructure. While the perfectly ordered structure is the ground state (0 K), the entropy associated with the introduction of disorder acts in opposition, leading to a state where the crystal is being in dynamic equilibrium, with thermal fluctuations inducing interchange of atoms between lattice sites with quite small energetic differences [41]. Moreover, the degree of disorder depends on the cooling rate after sample synthesis [39]. Slow cooling rate helps to create ordered structure in the absorber material lattice [42, 43]. One effect that results from ordered and disordered material structure is different bandgap energy.

These defect clusters may behave as recombination centres or trap charge carriers and hence affect solar cells performance, while being more prevailing in CZTS than in CZTSe [38].

In CZTSe, it was observed once that narrow PL peaks and a visible exciton emission indicated a good quality of crystals, where potential fluctuations were not seen. However, in addition to the edge emission, even these good crystals show a very wide PL band at 1.33 eV. It is obvious that this deep PL band must be related to deeper defects. For CZTSe, shallow defect levels with activation energies $E_A = 27$ meV and $E_A = 7$ meV have been found by photoluminescence, as presented in Ref. [44]. In addition, CZTSe monocrystalline powders have been studied by PL and a low-temperature PL band was found at 0.946 eV that results from band-to-impurity recombination. The ionization energy of the corresponding acceptor defect was found to be 69 meV [16].

Some studies are also for CZTSSe. Gunawan et al. [45] have studied $Cu_2ZnSn(S_{1-x}Se_x)_4$ absorber layer in solar cells by admittance spectroscopy and have found E_A values in the range 0.13-0.20 eV.

Frequently, it is quite difficult to interpret results of capacitance spectroscopy because choosing a correct equivalent circuit to describe complicated measurement data is not straightforward. According to Weiss et al.'s studies [46] of modelling equivalent circuit responses in kesterite solar cells, the evaluation of the admittance data cannot be performed simply with the as-measured capacitance data, as an increasing series resistance with decreasing temperature results in a capacitance step within *C-f* profile. For instance, they suppose that measurements data need to be discarded at higher frequencies and at lower temperatures. In addition, they used volt-ampere characteristics (*I-V*) to extract series and shunt resistances, but resistances found by direct current (DC)

measurements are not perfectly suitable for replacing resistance values of alternating current (AC) measurements. Moreover, they used as-measured capacitance (meaning no series resistance exists) and later applied series resistance to it.

Goodman [47] showed that accurate measurement of capacitance requires both $R_s << R_p$ and $R_s << (\omega C)^{-1}$, so that the capacitive impedance Z is the dominant circuit element. Ordinarily, the quantity C is assumed to be frequency independent, but in an experiment, this is not always true. The reason may be, for example, in charge relaxation times. In general, such effects tend to disappear with increasing frequency and may place a lower limit on the trustworthy frequency range. Moreover, measurement equipment limitation may place further restriction upon the measurement frequency. These restrictions require that the resistance and the geometry of a solar cell be suitably chosen.

According to Friesen et al.'s studies [48] of thin film CdTe solar cell, as commonly applied equivalent circuit models consist only of frequency-independent circuit elements, they cannot be used to describe the frequency dispersion of the thin film solar cell. They replaced the capacitor with a frequency-dependent non-ideal capacitor called constant phase element (CPE). It is generally assumed that the non-ideal capacitance behaviour originates from a distribution in the current density due to material inhomogeneity and/or the grain-boundaries [48, 49]. The use of CPE gives a better fit for the depressed semicircle in the Nyquist plot, i.e Z' versus $-Z''$ graph, where Z' and $-Z''$ are real and imaginary parts of impedance, correspondingly [III].

Usually, impedance spectroscopy (IS) and AS measurements are conducted at higher temperatures because models are then being easily applied and understood. Unfortunately, at very low temperatures, interpreting of IS spectra is quite difficult. In fact, low temperature measurements show that some interesting changes appear. For example, cooling down of recombination processes occur. This thesis analyzes these complicated IS measurement data at very low temperatures also. Moreover, frequency range limits of IS measurements are shown and results of *I-V* measurements and IS of the CZTSe thin film solar cell are presented and analyzed.

2. THEORY

Generally, in solar cells, the capacitance C represents the capacitance of the space charge region (SCR), which can be approximately described by a parallel plate capacitor with the equation:

$$C = \frac{\varepsilon\varepsilon_0 A}{w}, \quad (1)$$

where ε is the relative permittivity of the semiconductor material used in the solar cell and ε_0 is the permittivity of free space, A is the contact area and w is the width of the junction. w is determined by the concentration and occupation of electrically active shallow levels and centres. For example, if a p-n junction contains only shallow acceptors and donors, the capacitance C represents the width of the space charge region, provided the majority carriers can respond at the frequency f of the measurement. In this case, the response of the majority carriers is limited by the dielectric relaxation time. The majority carriers cease to respond when the angular modulation frequency $\omega = 2\pi f$ exceeds the inverse of the dielectric relaxation time. The critical frequency will show a thermally activated shift. In addition, the free carriers freeze out at very low temperatures [50].

Thus, at higher frequencies and/or at very low temperatures, the whole semiconductor behaves like a dielectric between two parallel plates and C reduces to the value determined by the sample geometry. The geometric capacitance is inversely proportional to the thickness of the device [50]. Due to the reason that as-measured capacitance data are not well suitable, it is advisable to measure impedance or admittance and then choose proper equivalent circuit and calculate capacitance. Both, impedance Z and its inverse admittance $Y = 1/Z$ are complex functions, composed of real and imaginary parts. For example, $Z = R + iX$, where R is resistance and X is reactance. Further, $Y = G + iB$, where G is conductance and B is susceptance. Also, $Y = G + i\omega C$. Impedance and admittance spectroscopy are methods where correspondingly, impedance and admittance dependence of frequency $f = \omega/2\pi$ with varied temperature is studied. In particular, they are very useful to describe electrical and physical properties of solar cells. The admittance of the heterostructure is a superposition of the free carrier capacitance across the width of the space charge region and the contribution from the charging and discharging of deeper defect levels within the SCR of the junction [I]. Hence, the total capacitance consists of the free carrier capacitance across the width of the SCR and the additional capacitance contribution from charging and discharging of defect states at a location where the energy of electron (hole) states equals the electron (hole) quasi-Fermi level. In addition, energetically continuous but locally discrete density of interface states at junction contributes to total capacitance. The time constant for charging and recharging of defect states at energy equal to the quasi-Fermi level determines the inflection frequency, i.e. step in the capacitance vs. frequency

spectrum (see Fig. 1). The additional capacitance occurs if the AC modulation allows the establishment of equilibrium between the occupation of the defect levels and the free carriers [51].

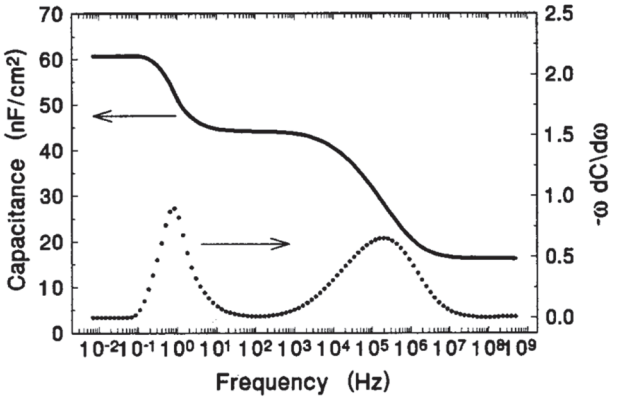

Fig. 1. The two inflection points in the *C-f* plot correspond to the maxima in the -ωdC/dω vs ω graph [52].

2.1. Impedance spectroscopy

Impedance spectroscopy is a powerful non-destructive tool for the characterization of semiconductors. The IS detects the AC response of a system to a small AC voltage signal with varied frequency. The impedance can be calculated by $Z=V/I$. The angle θ between R and X (real and imaginary part of impedance, respectively) can be calculated by $\theta = \arctan(-X/R)$. From the complex impedance, the capacitance can be calculated, but this requires a certain equivalent circuit to be known. Fitting of high temperature ($T \gtrsim 150$ K) IS curves of a solar cell is usually satisfactory with an equivalent circuit, where a series resistor is followed by a resistor and a capacitor connected in parallel, see Fig. 2.

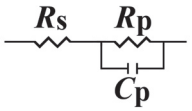

Fig. 2. Equivalent circuit commonly used for fitting high temperature ($T \gtrsim 150$ K) impedance measurement data of a typical solar cell.

At every measured temperature, values of the equivalent circuit elements can be found by exploiting the ZView (Scribner, USA) computer program for fitting. In

turn, R_s values can be used to calculate the capacitance. When assuming the series inductance to be insignificant or absent, this equivalent circuit can be described by the following equation [53]:

$$Z = R_S + \frac{R_P}{1+(\omega R_P C)^2} - i\frac{R_P^2 C\omega}{1+(\omega R_P C)^2}, \tag{2}$$

where ω, C, and R_P are angular frequency, capacitance, and parallel resistance, correspondingly. After rewriting (2), the capacitance can be found by:

$$C = \frac{-Z''}{\left[(Z'-R_S)^2+(-Z'')^2\right]\cdot\omega}, \tag{3}$$

where Z' and −Z'' are the real and imaginary part of the complex impedance, respectively. Equation (3) can be used for capacitance calculation if the mentioned equivalent circuit is applied for the fittings.

When measuring impedance Z and phase angle θ vs frequency f, then in (3) angular frequency $\omega=2\pi f$, and real and imaginary parts of impedance Z (see Fig. 3) can be calculated by the formulas:

$$Z' = Z\cdot cos\left(\theta\frac{\pi}{180°}\right) \tag{4}$$

$$Z'' = Z\cdot sin\left(\theta\frac{\pi}{180°}\right). \tag{5}$$

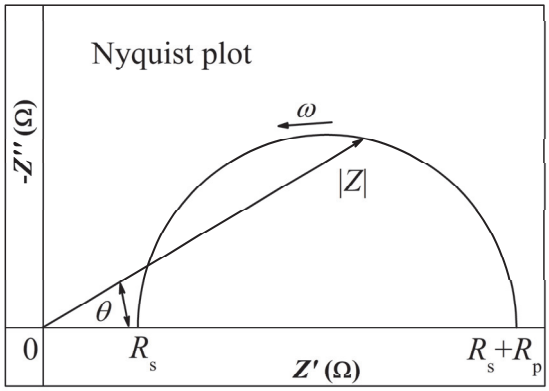

Fig. 3. Nyquist plot showing properties of an impedance semicircle.

Capacitance versus frequency plot (see Fig. 4) shows a rapid decrease of capacitance at higher frequencies. Corresponding frequency of the capacitance response inflection point is a defect characteristic frequency. The same capacitance step is also visible in the capacitance versus temperature graph, but this brings us to the admittance spectroscopy.

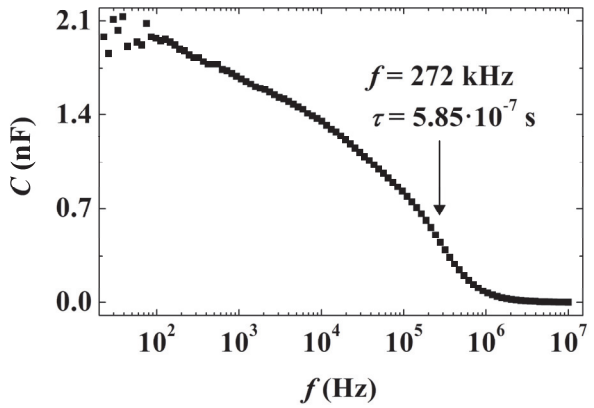

Fig. 4. Capacitance versus frequency plot of the CZTS solar cell at 280 K [I]. The inflection point frequency with the time constant are shown.

2.2. Admittance spectroscopy

Admittance spectroscopy involves measuring the junction capacitance as a function of frequency ω and temperature T. The admittance of the heterostructure is a superposition of the free carrier capacitance across the width of the SCR and the contribution from the charging and discharging of deeper defect levels within the SCR of the junction [54]. In the case of heavily doped n-type buffer layer (i.e Schottky barrier), the rectifying junction capacitance is given similar to that shown previously by the SCR capacitance [53]:

$$C_d = \frac{dQ}{dV} = \frac{d(qN_a wA)}{d(qN_a w^2/2\varepsilon\varepsilon_0)} = \frac{\varepsilon\varepsilon_0 A}{w} = \frac{\varepsilon\varepsilon_0 A}{\sqrt{2\varepsilon\varepsilon_0 V_{bi}/qN_a}} = A\left(\frac{\varepsilon\varepsilon_0 qN_a}{2V_{bi}}\right)^{\frac{1}{2}}, \quad (6)$$

where Q is space charge, V is voltage, q is elementary charge, N_a is the acceptor concentration in p-type absorber, w is the SCR width, A is the contact area, ε is the relative permittivity of the semiconductor material used in the solar cell, ε_0 is the permittivity of free space, and V_{bi} is the built-in voltage. In a semiconductor, V_{bi} equals the potential difference across the depletion region in thermal equilibrium. In thermal equilibrium, no external voltage is applied to the device. Moreover, the Fermi energy is constant throughout the heterostructure and the

built-in voltage equals the difference between the Fermi energies respectively in the buffer and the absorber, divided by the elementary charge.

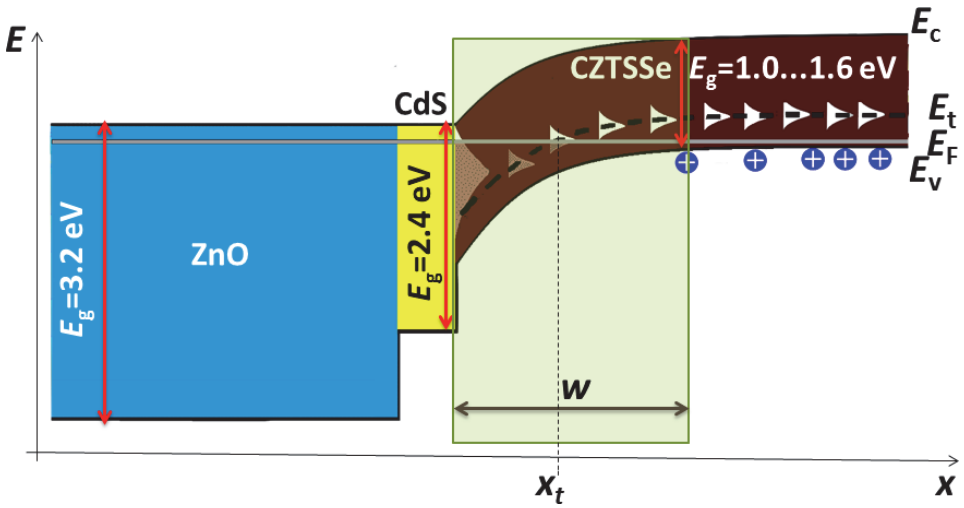

Fig. 5. Schematic of model semiconductor junction consisting of a CZTSSe absorber and having interface states and deep levels.

If deeper carrier traps are present, the band bending in the SCR causes the Fermi level E_F to cross the trap level E_t at some distance from the interface (see Fig. 5), at the crossing point x_t. A small AC oscillating voltage with the frequency $\omega=2\pi f$ causes the electric charge accumulated by traps to oscillate in the vicinity of this crossing point x_t. The trapped electric charge follows the applied voltage oscillations and contributes to the total capacitance only if their frequency does not exceed the trap characteristic frequency ω_t. Therefore, in the case of low frequency $\omega_{lf} << \omega_t$, the trap related capacitance is $C_t = C_{lf}$, where C_{lf} is the low frequency capacitance. The high frequency ($\omega_{hf} >> \omega_t$) measurements give the junction, i.e depletion area capacitance $C_d = C_{hf}$, where C_{hf} is the high frequency capacitance. Accordingly, in the case of a single majority carrier trap level, the total junction capacitance can be described by the equation [53, 55]:

$$C(\omega) = C_d + \frac{C_{lf} - C_d}{1 + \omega^2 \tau^2}, \tag{7}$$

where τ is the characteristic trapping time that depends on the trap density N_t, the acceptor concentration N_a, and the depletion layer width. In the case of a small trap concentration N_t, the characteristic frequency ω_t for the charging and discharging of defect levels is $\omega_t=1/\tau$ [56]. The inflection frequency ω_t can be obtained from the analysis of the first derivative of the capacitance, $dC/d\omega$, which should demonstrate a maximum at the frequency ω_t. The temperature

dependence of the inflection frequency ω_t is determined by the following equation [53]:

$$\omega_t(T) = 2e_t(T) = 2N_{c,v}\upsilon_{th}\sigma_{n,p}\exp\left(-\frac{E_A}{kT}\right) = 2\xi_0 T^2\exp\left(-\frac{E_A}{kT}\right), \quad (8)$$

where e_t is the emission rate, $N_{c,v}$ is the effective density of states in the conduction and valence band, v_{th} is the thermal velocity of the minority carriers at the interface, $\sigma_{n,p}$ is the capture cross-section for electrons and holes, $E_A = E_t - E_{be}$ is the activation energy of the defect level E_t with respect to the band edge E_{be}, k is the Boltzmann constant, and ξ_0 covers all the temperature independent parameters [53]. After rewriting equation (8), it is clear that the activation energy of a defect level E_A can be obtained from the temperature dependence of the capacitance spectra, i.e. from the Arrhenius plot of the quantity $\ln(\omega_t/T^2)$ versus $1000/T$, where the linear trend corresponds to the equation:

$$\ln\left(\frac{\omega_t}{T^2}\right) = -\frac{E_A}{k\cdot 1000}\cdot\frac{1000}{T} + ln(2\xi_0), \quad (9)$$

where $-\frac{E_A}{k\cdot 1000}$ is the slope of linear fit of the graph and knowing the value of the slope, the activation energy E_A of a defect level E_t can be calculated by $E_A = -\text{slope}\cdot k\cdot 1000$. Moreover, activation energy of interface states shows the location of the Fermi level E_F at the interface.

Since interface states and bulk defects show similar dependencies, measurements at different bias voltages can be done to distinguish between the two. For example, if capacitance-frequency dependence is measured at different bias voltages, which changes band bending near the interface, then it alters the crossing between interface states and the Fermi level. Consequently, time constant of charging and discharging of interface states varies with bias voltage [57] and hence, a maximum in capacitance derivative shifts on the frequency axis. If this happens, we have a contribution of interface states. Bulk defects do not reveal this behaviour. In the case of interface states, the activation energy found by admittance spectroscopy corresponds to the position of the electron quasi-Fermi level at the interface [50].

The theory described above is useful as it enables studies of solar cells and their properties, identification of defect levels or interface states, and finding out activation energy values. This theory was applied to the analysis of kesterite solar cells.

3. EXPERIMENTAL

3.1. Fabrication of monograin layer solar cells

Monograin layer solar cells were prepared at the Department of Materials Science in Tallinn University of Technology. Monograin is a crystalline powder particle consisting of one single crystal (~40 – 60 μm) or several single-crystalline blocks grown into a compact grain [58]. The CZTS, CZTSe and CZTSSe monograin powder materials used for the solar cells studied were synthesized from binary compounds in a molten KI flux in an isothermal recrystallization process. Further details of the monograin powder general production process can be found in papers [14, 59]. The single phase composition of the CZTS, CZTSe and CZTSSe monograin powder crystals was confirmed by Raman spectroscopy. The chemical composition was determined by energy dispersive X-ray analysis: Cu/(Zn+Sn)=0.9, Zn/Sn=1.1 for CZTS [I] and Cu/(Zn+Sn)=0.88, Zn/Sn=1.0 for CZTSe and Cu/(Zn+Sn)=0.93, Zn/Sn=0.99 for $Cu_2ZnSn(Se_{0.75}S_{0.25})_4$ [II].

Monograin crystals with diameters of 63–75 μm were selected by sieving and were used in the formation of a monolayer in the monograin layer (MGL) solar cell. The MGL solar cells have a layer of monograins in their structure. Powder grains are embedded into a polymer resin so that the upper part of the grains remains uncovered. CdS buffer layer was chemically deposited onto powder crystals, followed by RF-sputtering of i-ZnO and conductive ZnO:Al layers. Finally, highly conductive grid contacts are evaporated on top of the ZnO window layer, and the structure is glued onto a glass or on some flexible transparent substrate. For back contact, the bottom side of the MGL is polished to remove epoxy from powder crystals and to clear monograins before applying graphite contacts [58]. In summary, MGL solar cell structure is: graphite/$Cu_2ZnSn(S_{1-x}Se_x)_4$/CdS/ZnO/glass [59], see Fig. 6. Typically, the MGL solar cells prepared have an area of about ~4 mm^2. Firstly, 15 CZTS monograin layer solar cells were checked and measured at room temperature, while 2 best of them were chosen for temperature dependant measurements. Secondly 6 CZTSe and 16 CZTSSe monograin layer solar cells were chosen for temperature dependant measurements after room temperature measurements of about 18 CZTSe and 60 CZTSSe monograin layer solar cells. Results of one CZTS, one CZTSe, and one CZTSSe monograin solar cell are shown in this thesis.

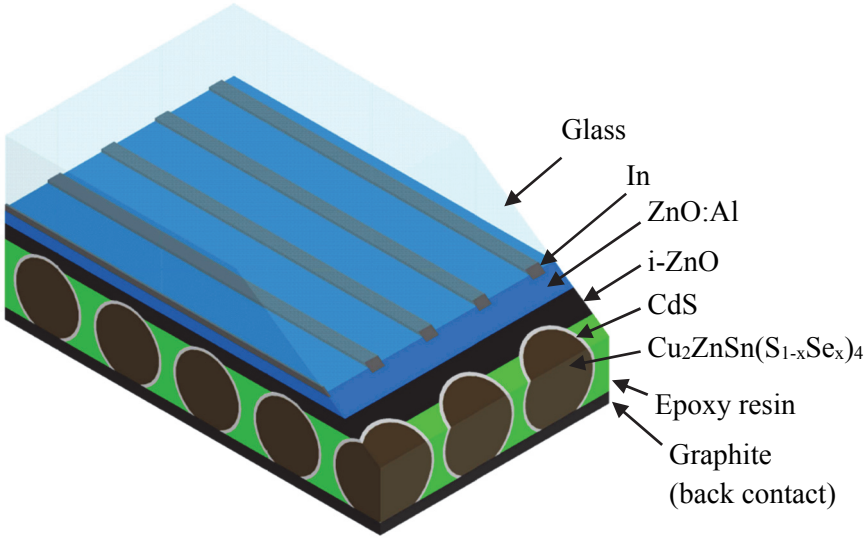

Fig. 6. The structure of a monograin layer solar cell.

3.2. Fabrication of thin film solar cells with CZTSe absorber

Thin film solar cells were fabricated at Catalonia Institute for Energy Research, IREC, in Barcelona, Spain. They prepared a CZTSe absorber used in this study by reactive thermal annealing of metallic Cu/Sn/Cu/Zn precursor stack deposited by DC magnetron sputtering onto Mo coated soda lime glass substrates, as described elsewhere in more detail [60]. The CZTSe absorber composition was measured by X-ray florescence spectroscopy, showing cation ratios of Cu/(Zn+Sn)=0.69, Zn/Sn= 1.45, Cu/Zn=1.16, and Cu/Sn=1.69 [III]. The highest device performance is reported in this Cu poor Zn rich compositional range. According to a recent study, this was attributed even to very Cu poor absorber layer devices with especially high V_{oc} values [61]. Solar cells were finished by depositing a CdS buffer layer by chemical bath deposition followed by DC-pulsed sputtered i-ZnO (50 nm) and In_2O_3:SnO_2 (90/10 wt.%; 350 nm, $R_{\square}$=50 Ωcm^{-1}) window layer [60, 62]. Prior to CdS deposition, the CZTSe absorber was etched using an oxidizing etching to remove possible ZnSe secondary phases from the surface, as reported in [60]. The compositional values presented here were measured prior to the specific surface etching because time between surface etching and buffer layer deposition is crucial to avoid surface contamination. Thus, a reduction in Zn composition is expected in the final CZTSe absorber layer [63]. Totally we got 144 thin film solar cells (each sized with dimensions of 3x3 mm). About half of them were not working. 10 better solar cells were chosen for temperature dependant measurements after room temperature *I-V* and IS measurements. The best individual solar cell used for our capacitance spectroscopy study and presented in this thesis showed a power

conversion efficiency of η = 6.6% with J_{sc} = 27.2 mA·cm^{-2}, V_{oc} = 383 mV, and FF = 64% [III].

3.3. Admittance spectroscopy and impedance spectroscopy

AS and impedance spectroscopy measurements were done with the same instruments and setup. The impedance Z and phase angle θ were both measured as functions of frequency f and temperature T. The temperature varied from 10 K to 325 K with a step ΔT = 5 K. For temperature dependent measurements, the selected monograin and thin film solar cells were mounted in the closed-cycle He cryostat (Janis). The frequency used in our experiments varied in the range of 20 Hz to 10 MHz. In order to maintain the linearity of the response signal, AC voltage was kept as low as 10 mV. AC measurements were conducted in the dark and different DC biases were used, i.e 0 V and −0.5 V. The admittance and impedance spectra curves were recorded by a Wayne Kerr 6500B impedance analyzer. After each measurement, the real and imaginary part of the impedance Z' and $-Z$'' were calculated respectively. Measured data were fitted by using the ZView (Scribner, USA) computer program, which gives values for the elements used in an equivalent circuit, for example, parallel (R_p) and serial resistances (R_s), as well as parallel capacitance C_p.

3.4. *I-V* and PL measurements. Temperature dependence of EQE

Volt-ampere curves of solar cells were recorded using Keithley SourceMeter 2401 under 100 mW/cm^2 illumination. A standard 250 W halogen lamp with calibrated intensity was used as a light source.

In addition, some monograin powders were studied by photoluminescence spectroscopy in the temperature range of 10 K to 140 K. For PL measurements, a He-Cd laser with the wavelength of 441 nm was used for PL excitation. The PL spectra were recorded by a computer controlled SPM-2 monochromator (f = 40 cm) together with an InGaAs detector and a DSP Lock-In amplifier SR 810 [II].

To analyze the temperature dependence of the external quantum efficiency (EQE) curves, a 250 W calibrated halogen lamp as a light source together with a computer controlled SPM-2 prism monochromator were used. Temperature range was as wide as from 10 K to 300 K to find changes in the spectral response. The generated short circuit current was detected with a DSP Lock-In (SR 810) [I].

All measurement instruments were controlled by a highly automated computer program written in LabVIEW graphical software programming environment.

4. RESULTS AND DISCUSSION

4.1. CZTS monograin layer solar cells (Paper I)

Fig. 7 gives the *I-V* curve of a CZTS solar cell. As can be seen, this cell shows quite poor parameters: V_{oc} = 582.4 mV, J_{sc} = 7.13 mA/cm^2 and the fill factor FF = 32%, resulting in a solar energy conversion efficiency of only η = 1.3%. It is known that a low efficiency of CZTS cells is mainly related to the high recombination losses [64], which can be caused by deep defect levels that act as carrier traps or by interface states. However, there are quite few experimental results about the deep defect levels in CZTS. Knowledge about the absorber surface properties and defect structure enables the electrical properties of the CZTS material to be improved by changing the surface composition, e.g. by the additional thermal and chemical treatments [14].

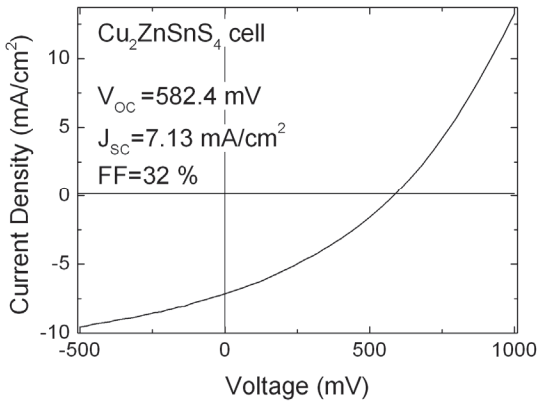

Fig. 7. Current-voltage characteristic of a CZTS solar cell with conversion efficiency η = 1.3%.

To study the defects in such CZTS monocrystalline powders, AS was applied to that CZTS MGL solar cell. Fig. 8 shows the frequency dependence of the capacitance of a CZTS solar cell in the temperature range from 95 K to 300 K. An equivalent circuit shown in Fig. 2 was used for the measured impedance data fittings and hence for applying equation (2). Formula (3) was used in the capacitance calculation. Spectra in Fig. 8 show two steps labelled N1 and N2 (similarly found for $CuInSe_2$ in [50]) that are attributed to the charging and discharging of two deep levels within the SCR of the heterojunction. The N2 capacitance step appears at lower frequencies and higher temperatures and corresponds therefore to a contribution of deeper defect level than N1. In accordance with the theory, the steps in the *C-f* spectrum shift towards higher frequencies with increasing temperature *T*. The height of the capacitance steps corresponds to the defect level contribution to the total capacitance.

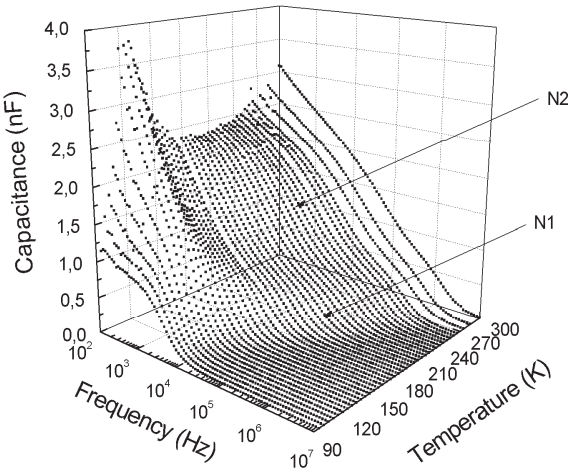

Fig. 8. The capacitance spectra of a CZTS solar cell as a function of frequency and temperature at 0 V bias. Two steps labelled N1 and N2 are indicated by arrows.

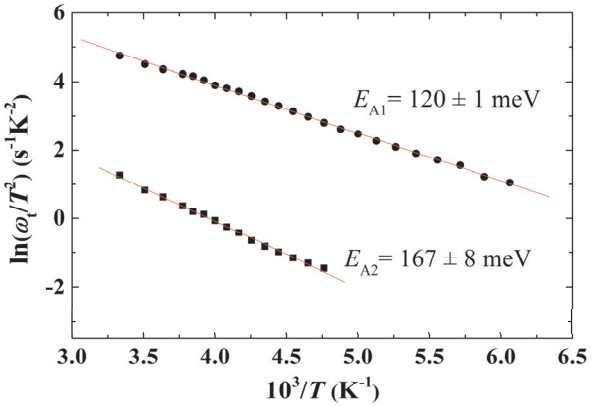

Fig. 9. The Arrhenius plot showing the calculated activation energies of the defect levels E_{A1} = 120 meV and E_{A2} = 167 meV corresponding to the two capacitance steps N1 and N2, respectively, measured at bias 0 V.

For the two capacitance steps, an Arrhenius plot of the quantity $\ln(\omega_t/T^2)$ versus $1000/T$ is shown in Fig. 9. The inflection frequencies ω_{t1} and ω_{t2} for every temperature corresponding to steps N1 and N2, respectively, were determined from the analysis of the first derivative $dC(\omega)/d\omega$. The obtained activation energies $E_{A1} = 120 \pm 1$ meV and $E_{A2} = 167 \pm 8$ meV are attributed to a defect

distribution peaking at the corresponding energetic distance from the delocalized band edges.

The deep defect state with an activation energy of 120 ± 1 meV was present in different CZTS solar cells while the second state with an activation energy of 167 ± 8 meV had somewhat different properties in different cells. The activation energy of the latter defect state varied in different cells and was dependent on the applied bias voltage (0 V, -1 V). This is not expected for bulk defect states, which do not depend on different bias voltage. On the other hand, in the case of reverse biasing, the SCR is widened and the position of the interface states with respect to the Fermi level and the band edges changes. Consequently, we attributed the N2 capacitance step to the contribution of interface states.

The temperature dependence of the external quantum efficiency curves of the corresponding monograin layer solar cells shows a shift of the long wavelength edge with increasing temperature by about 110 meV towards higher energy, see Fig. 10. At long wavelength side, no light is absorbed with lower than the bandgap energy. In reality, the EQE for solar cells is reduced due to recombination losses, low diffusion lengths and reflections. The inset in Fig. 10 plots EQE curves with energy response is reduced at low energy side. Fig. 10 shows also the maximum points of the first derivatives of the external quantum efficiency curves at different temperatures. This shift seems to be related to the first defect state found from AS experiments. At low temperatures, this (probably acceptor) state contributes to the absorption and causes a shift of the EQE curve. According to the first-principles calculations made by Chen *et al.* [36], the *p*-type conductivity of CZTS is mainly determined by a Cu_{Zn}^{-} acceptor defect having a quite deep level at $E_A = 0.12$ eV. Accordingly, the deep acceptor level observed in AS measurements with the matching activation energy could be assigned to Cu_{Zn}^{-} acceptor defect. Later, other research groups have come to the same conclusions [65, 66].

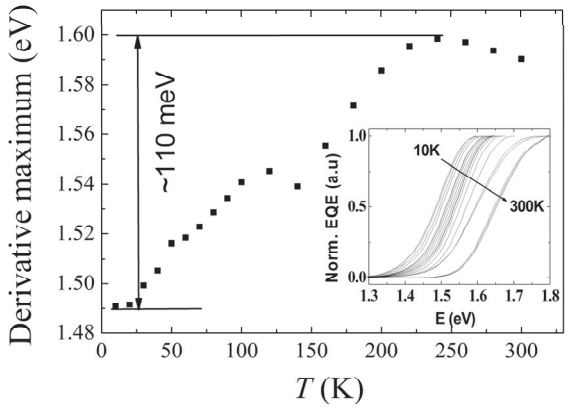

Fig. 10 Temperature dependence of the maximum points of the first derivative of the EQE curves.

4.2. CZTSe and CZTSSe monograin layer solar cells (Paper II)

Defect levels in CZTSe and CZTSSe monograin layer solar cells were investigated by admittance and photoluminescence spectroscopy. Two defect states were seen in both materials by AS. While the prepared CZTSe/CdS heterojunction was measured twice by AS, the first measurement after the preparation is referred to as the measurement of the fresh device. Then, two months later, the same CZTSe/CdS heterojunction (called aged device) was measured again. Between the measurements, no treatments on this heterojunction were performed. Different solar cell CZTSSe/CdS heterojunctions were studied and results of $Cu_2ZnSn(Se_{0.75}S_{0.25})_4$ absorber material are presented.

4.2.1. Results found by admittance spectroscopy measurements

Admittance spectroscopy studies of CZTSe/CdS heterojunctions showed that properties of a solar cell change during time. In this chapter, these results are presented.

The temperature dependence of Z' versus -Z'' graph of an aged CZTSe/CdS heterojunction is shown in Fig. 11. At any temperature, each curve consists of one arc, and the corresponding equivalent circuit (see Fig. 11 inset) was used for fitting the arcs. From the fittings, the series resistance R_s values at each temperature were found. The R_s values were used to calculate the capacitance. The capacitance C versus ω graphs are shown in Fig. 12.

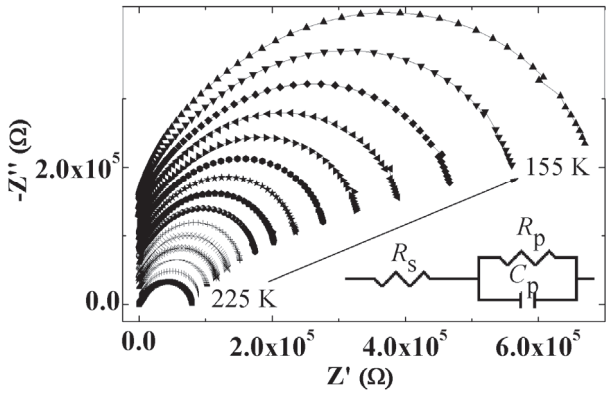

Fig. 11. *Z*' versus -*Z*'' graph of the aged CZTSe/CdS heterojunction. Equivalent circuit shown was used for fitting the arcs and finding R_s values at each temperature. Y-axis offset for arcs is set to 50%.

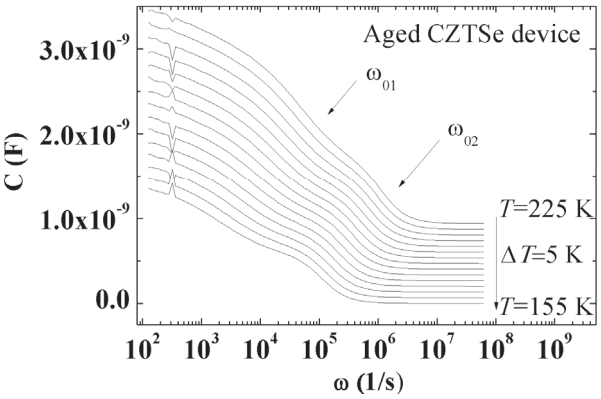

Fig. 12. The capacitance *C* versus *ω* graph of the aged CZTSe/CdS heterojunction. Steps corresponding to inflection frequencies are indicated by arrows. Y-axis offset for lines is set to 25%.

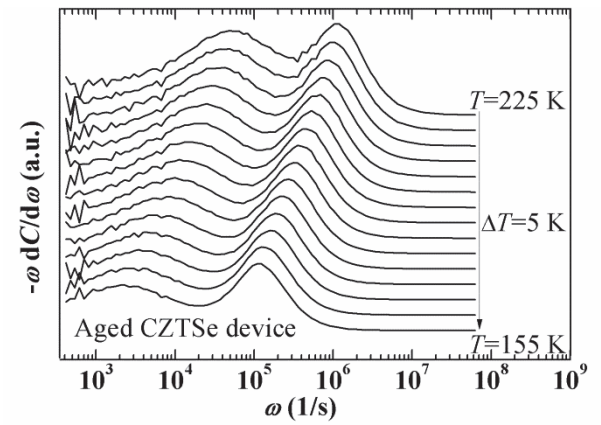

Fig. 13. The derivative -*ω*dC/d*ω* versus *ω* graph of the aged CZTSe/CdS heterojunction depicts maxima where corresponding inflection frequencies ω_0 are used for Arrhenius plot. Y-axis offset for lines is set to 50%.

Fig. 13 shows the –*ω*dC/d*ω* versus *ω* graph of an aged CZTSe/CdS heterojunction. This graph shows two maxima. Analogous dependences were found in the CZTSSe/CdS heterojunction. Fig. 14 shows Arrhenius plots for all CZTSe measurements. All activation energies found by AS are presented in Table. 1. The value of the activation energy at the higher frequency corresponding to E_{A2} state showed almost no changes during the ageing time.

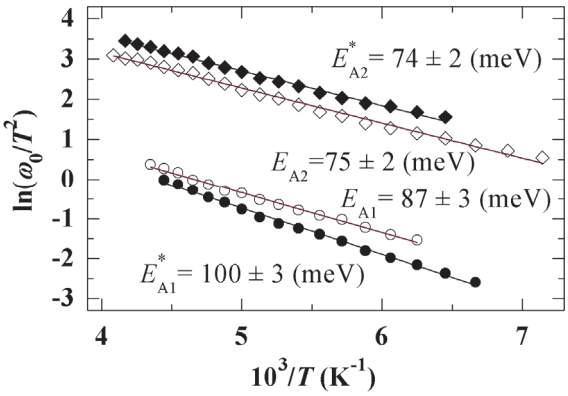

Fig. 14. The Arrhenius plot of the CZTSe/CdS heterojunction showing the activation energy values, where E_{A2} are for defect state and E_{A1} for interface states. White symbols and E_{A2} and E_{A1} correspond to the fresh device measurement, the black filled symbols and E_{A2}^* and E_{A1}^* show results for an aged device. All dependencies were fitted with a linear function.

At lower frequency (E_{A1} state), the fresh heterojunction shows quite different activation energy (87 ± 3 meV) compared to the same but aged heterojunction (100 ± 3 meV). These activation energies were found by measuring impedance Z and phase angle θ versus frequency f, and calculating capacitance C by employing an equivalent circuit, where a series resistor R_s is followed by a resistor R_p and a capacitor connected in parallel, (R_s and R_p cover series resistance of a structure, wires, contacts etc., and shunt resistance of the junction, accordingly). Inverse temperature versus the natural logarithm of angular frequencies ω that correspond to the capacitance step showed linear dependence and was used to calculate activation energy.

Table 1. Activation energies found by AS of the measured heterojunctions and by PL of the monograin powders. Results for an aged device are in brackets.

Material	AS results		PL results
	E_{A1}, meV	E_{A2}, meV	E_T, meV
$Cu_2ZnSn(Se_{0.75}S_{0.25})_4$	154 ± 7	25 ± 5	39 ± 5
$Cu_2ZnSnSe_4$	87 ± 3 (100 ± 3)	75 ± 2 (74 ± 2)	69 ± 4

The change (from 87 ± 3 to 100 ± 3 meV) in the second activation energy corresponding to E_{A1} state can probably be assigned to interface states. Possible change of interface properties with time could cause this change of activation energy. The stable activation energy at 74 ± 2 meV is obviously related to some deep acceptor defect state. In CZTS, the activation energy of 120 ± 1 meV belonged to Cu_{Zn}^{-} acceptor defect [I, II]. Considering that the activation energy of a defect varies with the bandgap of different materials, i.e for similar compounds $CuInSe_2$ and $CuInS_2$ [67, 68], 74 ± 2 meV of CZTSe could to be related to the same Cu_{Zn}^{-} acceptor defect. But this assumption needs some further studies. As in CZTSe, the *p-d* hybridization is smaller and the valence band is higher, it is expected that the activation energy of the Cu_{Zn}^{-} defect decreases with increasing Se concentration in $Cu_2ZnSn(Se_xS_{1-x})_4$ [69]. As materials inspected are deficient in copper, V_{Cu}^{-} acceptors should also be present. Moreover, donor-acceptor defect complexes are also expected in this material. In CZTS and CZTSe, the Cu_{Zn}^{-} antisite is a deeper acceptor than V_{Cu}^{-} [36] and therefore can be detected by AS.

In CZTSSe, activation energies of $E_{A1} = 154 \pm 7$ meV and $E_{A2} = 25 \pm 5$ meV were found (see Fig. 15). The E_{A1} with changing properties was attributed to the interface states and the second E_{A2} belongs to some acceptor defect.

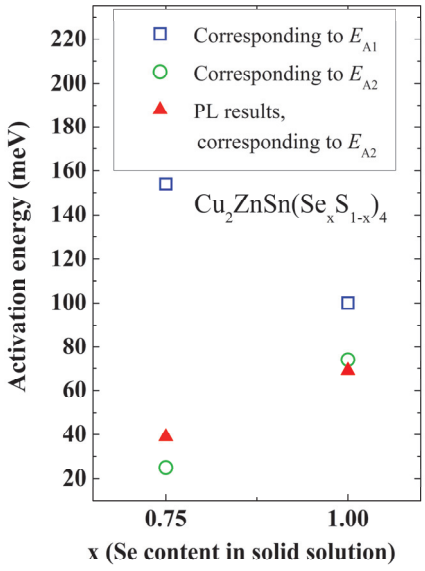

Fig. 15. Activation energies in CZTSSe solid solution found by AS and PL measurements.

4.2.2. Photoluminescence measurements

CZTSe and CZTSSe absorber materials were studied also by photoluminescence spectroscopy. Fig. 16 (b) shows normalized PL spectra of the CZTSe and $Cu_2ZnSn(Se_{0.75}S_{0.25})_4$ monograins measured at $T = 10$ K. Both PL spectra show an asymmetric PL band at 0.946 eV for CZTSe and at 1.028 eV for $Cu_2ZnSn(Se_{0.75}S_{0.25})_4$. The asymmetric shape of the PL bands is an indication of the presence of spatial potential fluctuations in the material [70] that is caused by high concentration of randomly distributed charged defects. The potential fluctuations are often found in multinary compounds where the native defect concentrations are usually very high [16, 26, 29]. These potential fluctuations lead to a local perturbation of the electronic band structure, thus broadening the defect level distribution and forming band tails [70]. Radiative recombination in the material containing spatial potential fluctuations can mainly arise from three different recombination channels. First, in a band-to-band recombination, a free electron recombines with a free hole. Second, in a band-to-tail recombination, a free electron recombines with a hole that is localized in the potential wells of the valence band tail. Third, in a recombination, a free electron recombines with a hole that is localized on a deep acceptor level, deep enough not to overlap with the valence band tail.

Temperature dependent and excitation power dependent measurements of the PL spectra indicate that the PL bands result from the band-to-impurity recombination. A strong blue-shift with a magnitude of 17 meV per decade for CZTSe and 11 meV per decade for $Cu_2ZnSn(Se_{0.75}S_{0.25})_4$ with increasing excitation power was detected. Arrhenius plots derived from the temperature dependencies of the PL spectra [29] together with the fitting curves are presented in Fig. 16 (a). For fitting the temperature dependence of the integral intensity, the following formula was used [71]:

$$I(T) = I_0 /(1 + c_1 T^{\frac{3}{2}} + c_2 T^{\frac{3}{2}} \exp(-E_T / kT)), \qquad (10)$$

where E_T is the activation energy. ln I versus $10^3/T$ is used for Arrhenius plot that shows linear behaviour at high temperatures, which is characteristic for BI-recombination. The obtained defect ionization energies E_T can be found in Table 1.

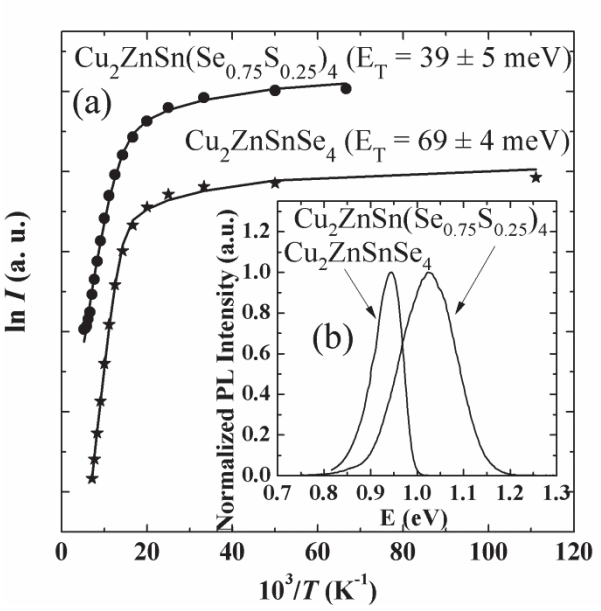

Fig. 16. The normalized PL spectra at 10 K (b) [29] and Arrhenius plot derived from the temperature dependencies of these PL spectra (a).

By summarizing these AS and PL results, defect ionization energies found by PL are attributed to the same acceptor defects that were found from AS measurements, correspondingly (see Fig. 15). In CZTSSe, the activation energy of the E_{A2} state seems to be unrelated to the same defect as in CZTSe or CZTS.

4.3. Thin film solar cells with a CZTSe absorber (Paper III)

Impedance spectroscopy and current–voltage characteristics measurements were applied to investigate properties of the thin film solar cell made with the $Cu_2ZnSnSe_4$ absorber material. The solar cell showed efficiency of 6.6%. Temperature dependence of the open circuit voltage (V_{oc}) derived from *I-V* measurements with varied temperature from T = 10 K to T = 325 K showed a linear part in the range of 250 K to 325 K (see Fig. 17). It is known that the temperature dependence of V_{oc} near the room temperature can be presented as in [72, 73, 74]:

$$V_{oc} = \frac{E_{A,Voc}}{q} - \frac{nkT}{q}\ln\left(\frac{I_{00}}{I_L}\right), \tag{11}$$

where I_L, $E_{A,Voc}$, n, k are the photocurrent, an activation energy, the diode ideality factor and the Boltzmann constant, respectively. The constant q is the electrical charge on the electron and I_{00} is obtained from the temperature

dependence of the dark saturation current I_0. In good solar cells $-I_L \approx I_{sc}$, where I_{sc} is a short circuit current, I_0 equals [72, 73]:

$$I_0 = I_{00} \exp\left(-\frac{E_{A,Voc}}{nkT}\right) \approx AT^3 \cdot \exp\left(-\frac{E_{A,Voc}}{nkT}\right), \tag{12}$$

In general, the activation energy $E_{A,Voc}$ and also I_{00} depend mostly on the dominating recombination mechanism in the solar cell. In the case of the bulk recombination $E_{A,Voc} \approx E_g$, where E_g is the bandgap energy of the absorber material.

Linear fitting of temperature dependence of V_{oc} showed that $E_{A,Voc}$= 962 ± 4 meV (see Fig. 17), which is in good agreement with the bandgap energy of CZTSe that is expected to be in the vicinity of 1 eV [75, 16]. Hence, the dominating recombination mechanism seems to be the bulk recombination.

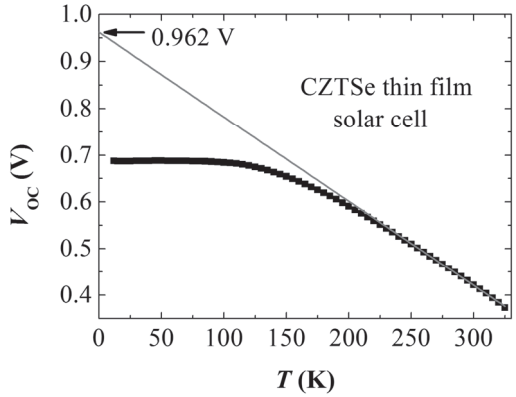

Fig. 17. Temperature dependence of V_{oc} of the best CZTSe thin film solar cell.

According to the temperature dependence of j_{sc}, three different temperature regions can be distinguished, see Fig. 18. Similar behaviour with different temperature ranges where electrical parameters change was also seen in CZTS [76]. At temperatures $T > 150$ K (region I), the series resistance R_s decreases with increasing temperature, indicating the thermal activation of carriers. In this region, R_s can be calculated by:

$$R_S = R_{S0} \exp(E_A / kT), \tag{13}$$

where R_{so} covers all parameters that are temperature independent and E_A is an activation energy. Using equation (13), the activation energy

$E_{AI} = 23.4 \pm 0.2$ meV was found in the temperature range from 175 K to 285 K (region I). Similar values in kesterites have been reported before, for example, 29 – 48 meV [77, 78]. In our sample, the activation energy of 23.4 meV is related to grain boundaries or some shallow acceptorlike defect.

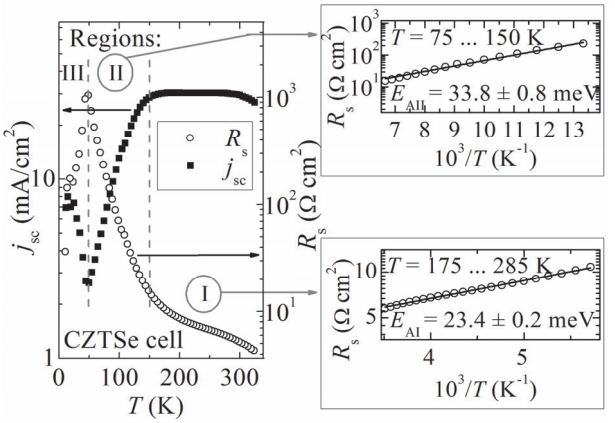

Fig. 18. Temperature dependence of j_{sc}. Insets show activation energies found in region I and II.

At intermediate temperatures (region II, $T = 50$ K to 150 K), another thermally activated process appears. Using equation (13), the activation energy $E_{AII} = 33.8 \pm 0.8$ meV was found in the temperature range from $T = 75$ K to 150 K. In our previous studies [29, 16, 26], this activation energy was related to the potential fluctuations of valence band edge, i.e. energy needed by holes to cross barriers created by these potential fluctuations. According to the literature, the root mean square depth of the potential well γ in CZTSe is usually in the range $\gamma = 20 – 30$ meV [29, 16, 26]. At the same time, it is shown that in region II, the dependence of the series resistance on the temperature changes and a typical Mott's variable-range hopping conduction starts to emerge [79]. This behaviour is expected in all heavily doped materials where spatial potential fluctuations create deep potential wells for holes. At the same time, we also expect the increasing role of bulk recombination in region II, as previously seen in CZTS [76]. At low temperatures ($T \lesssim 150$ K), the carriers, here holes, can occupy shallow acceptor states in the band gap. These states can arise from intrinsic defects or impurities or their interaction. At a sufficiently high concentration of these states, but below the critical Mott concentration, overlapping of carriers wave functions could form the so-called impurity band [80]. In such a case, charge carriers have the possibility of moving from one shallow impurity state to another one at their spatial neighbourhood and conduction in the impurity band is expected [79]. These different processes

could all be present and therefore we do not focus so much on activation energy here.

At low temperatures (region III, $T = 10$ K – 50 K), maximum of series resistance is present. By analyzing j_{sc} and *I-V* graphs (see Fig. 19), it can be seen that *I-V* curves have similar shapes symmetrically to both sides of 50 K. Also, impedance curves have quite the same patterns symmetrically to the temperature of $T = 50$ K in the Nyquist plot (compare the complex impedances at 10 K and 100 K in Fig. 20). The sudden drop of resistance below 50 K seems to be related to the blocking of the interface recombination. The rapid change in the series resistance can occur because of cooling down of recombination processes: generated holes are unable to tunnel through the potential barrier into the interface region between CZTSe and CdS. Therefore, the interface recombination rate must be very small at these very low temperatures ($T = 10$ K – 50 K). Similarly, in CZTS, at very low temperatures ($T < 40$ K), the effective bandgap energy E_g^* and series resistance R_s showed steep changes and this behaviour was interpreted as a hole blocking at a CZTSe/CdS heterojunction [76].

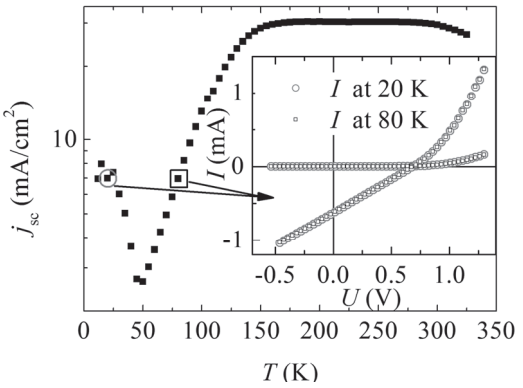

Fig. 19. Temperature dependence of j_{sc}. Inset shows *I-V* curve shape similiarity equally to both sides of 50 K at different temperatures.

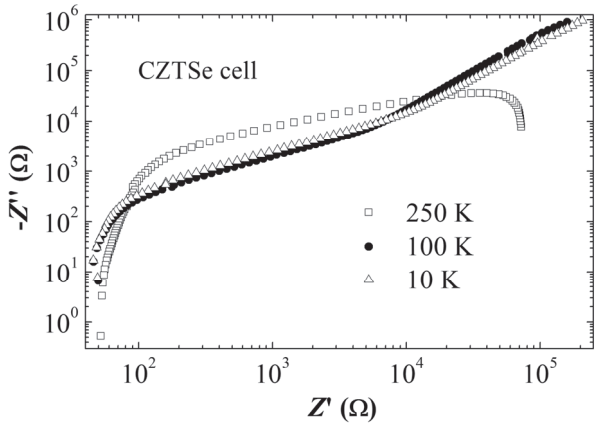

Fig. 20. Nyquist plots. Selection of impedance curves of the CZTSe thin film solar cell in the logarithmic scale at temperatures 250 K, 100 K and 10 K.

The temperature dependence of Z' and $-Z$'' of the CZTSe thin film solar cell is shown in Fig. 20.

Our measured impedance curves in the Nyquist plot in the whole temperature range can be fitted by applying an equivalent circuit, where a series resistor is followed by a resistor and a capacitor connected in parallel and followed by additional elements (R_{p2} and CPE) connected in parallel (circuit A in Fig. 21). The used complex impedance of a constant phase element Z_{CPE} is expressed by the equation:

$$Z_{CPE} = \frac{1}{C_{CPE} \cdot (i * \omega)^P}, \tag{14}$$

where C_{CPE} is equal to capacitance C if parameter $P = 1$. ω stands for an angular frequency. But fitting of high temperature IS curves is also satisfactory with an equivalent circuit, where a series resistor is followed by a resistor and a capacitor connected in parallel (circuit B in Fig. 21). Fig. 21 shows both theoretical fittings and experimental data curves. In Fig. 22, the deviation between theoretical and experimental impedance data is shown. It is clearly seen that at room temperature there is no difference between fittings with circuits A and B, but the deviation between fitted and measured $|Z|$ is increasing at higher frequencies. At low temperatures, i.e $T \lesssim 150$ K, the equivalent circuit B was not suitable at all, and the equivalent circuit A fitting deviation of measured $|Z|$ is enormously high (more than 50%) at quite high frequencies. Obviously, condition $R_s << (\omega C)^{-1}$ [47] is not satisfied at higher frequencies. It was checked by calculations and found that this condition is satisfied at frequencies $f < 3.7$ MHz at 100 K and at $f < 250$ kHz at room temperature.

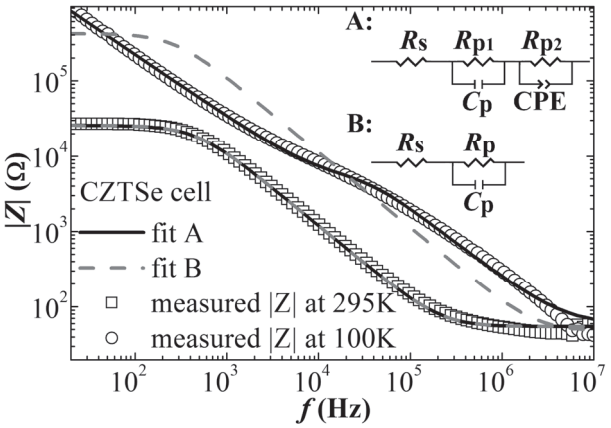

Fig. 21. Measured impedance of the CZTSe solar cell and fittings results with corresponding equivalent circuits. Better fit was obtained by A. Commonly used equivalent circuit B is unsuitable at lower temperatures $T \lesssim 150$ K. At room temperature, the difference was insignificant.

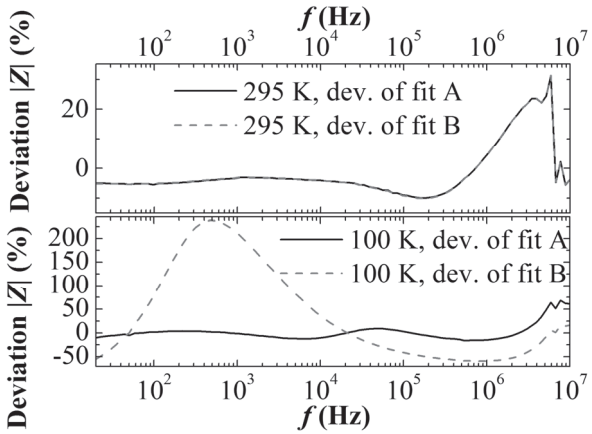

Fig. 22. Fitting deviations of $|Z|$ vs. frequency at temperatures 295 K and 100 K of the CZTSe solar cell.

Moreover, measurement instrumentation capabilities have limits and affect measurement data. At low frequency, fittings deviation of $|Z|$ was not significant. Hence, IS results at higher frequencies are not trustworthy, and the fittings

deviation of measured $|Z|$ coincides with neglecting of the condition $R_s << (\omega C)^{-1}$.

When assuming series inductance to be insignificant or absent, equivalent circuit B can be described by equation (2) and the capacitance can be calculated by (3) if the equivalent circuit B is applied to the fittings. In the equivalent circuit A, CPE is used and in this case, equations (2) and (3) would take much more complicated form and the calculation of capacitance is not straightforward. Thus, in the case of our studied CZTSe thin film solar cell capacitance should be derived by using equivalent circuit B and valid results are obtained only at higher temperatures ($T = 150$ K to 325 K). However, IS results are also beneficial in this low temperature range because they add complementary or confirmative details about the processes.

Temperature dependence of electrical parameters seen by IS in the CZTSe thin film solar cell at $T \lesssim 150$ K can be explained by grain boundaries, see Fig. 23. Some interface states at grain boundaries seem to be affected and change electrical properties of the studied cell at low temperatures. These states may not show a real capacitance, but can be explained by constant phase element in the equivalent circuit. This extra capacity is caused by holes being captured by interface states in grain boundaries, which are below the Fermi level and released by states, which are above the Fermi level. If the cell is contacted and is being electrically disturbed, then the band bending and hence crossing between the Fermi level and interface states change. As a result, the charging or discharging of these states appears and capacitance can be detected.

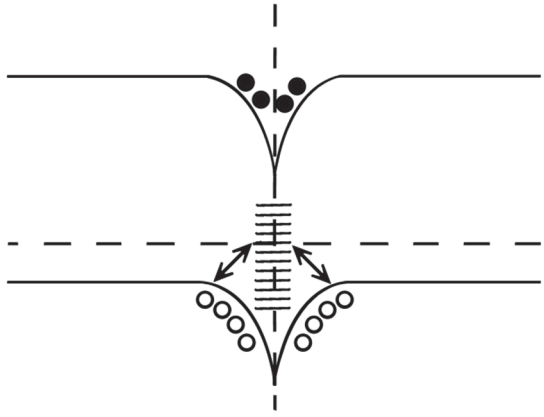

Fig. 23. Grain boundary between grains in a thin film solar cell. Some interface states are affected at quite low temperatures, which influences fittings of the measured data.

Resulting from such capacitance changes at low temperatures $T \lesssim 150$ K, where grain boundary states are affected, we need to add extra elements to our equivalent circuit. At high temperatures ($T = 150$ K – 325 K), where grain

boundary states do not contribute to capacitance, both equivalent circuits give an excellent result. This low temperature (T = 10 K – 150 K) behaviour, which requires the use of CPE and is present in the studied CZTSe thin film solar cells, was not seen in our previous research on monograin solar cells, where the role of grain boundaries was not so notable [I, II].

Studies of the CZTSe thin film solar cell by IS and current–voltage characteristics showed some differences between thin film and monograin solar cells. The results obtained contribute to knowledge about the processes in these solar cells.

5. CONCLUSIONS

1. Deep defects in CZTS monograin layer solar cells were studied by admittance spectroscopy and temperature dependence of the quantum efficiency curves.
    a. The AS studies revealed two deep defect states at $E_{A1} = 120 \pm 1$ meV and at $E_{A2} = 167 \pm 8$ meV that were assigned to a Cu_{Zn}^{-} deep acceptor defect and to interface states, respectively.
    b. A shift in the temperature dependence of the EQE curves by about 110 meV towards higher energy resulted from the contribution of this deep acceptor to the absorption at low temperatures.
2. Admittance spectroscopy and PL were used to investigate defect levels in CZTSe/CdS and $Cu_2ZnSn(Se_{0.75}S_{0.25})_4$/CdS monograin heterojunctions. Two defect states were observed in both materials.
    a. The unstable defect state showed activation energies from 87 ± 3 meV to 100 ± 3 meV in CZTSe. This was attributed to the interface states. The stable deep defect state in CZTSe was found to be at 74 ± 2 meV, which was attributed to Cu_{Zn}^{-} acceptor defect. A close activation energy was found also by PL.
    b. In CZTSSe, activation energies 154 ± 7 meV and 25 ± 5 meV were found by AS and were attributed to the interface states and to an acceptor defect, correspondingly. Similar activation energy was found by PL.
3. Impedance spectroscopy and volt-ampere measurements were used to characterize the CZTSe thin film solar cell. Three different temperature ranges where electrical properties change were obtained.
    a. IS showed that some interface states at grain boundaries are affected at low temperatures. These states were described by a constant phase element in an equivalent circuit.
    b. Dominating recombination mechanism was the bulk recombination.
    c. Temperature dependence of j_{sc} showed that in the range from 175 K to 285 K, some shallow acceptorlike defect or the grain boundaries dominate. At intermediate temperatures from 75 K to 150 K, different processes like carrier localization in potential wells, radiative recombination and Mott's variable-range hopping conduction start to affect. At low temperatures below 50 K, the blocking of the interface recombination is present.

REFERENCES

[1] D. L. Losee. Admittance spectroscopy of impurity levels in Schottky barriers. *Journal of Applied Physics* 46 (1975) 2204-2214.

[2] M. Igalson, H. W. Schock. The metastable changes of the trap spectra of $CuInSe_2$-based photovoltaic devices. *Journal of Applied Physics* 80 (1996) 5765.

[3] NREL, "Best Research-Cell Efficiencies," 2015 [Online]. Available: http://www.nrel.gov/ncpv/images/efficiency_chart.jpg. [Accessed 05 01 2016].

[4] A. Dhar, T. L. Alford. High quality transparent TiO_2/Ag/TiO_2 composite electrode films deposited on flexible substrate at room temperature by sputtering. *APL Materials* 1 (2013) 012102.

[5] C. Candelise, J. F. Speirs, R. J. K. Gross. Materials availability for thin film (TF) PV technologies development: A real concern? *Renewable and Sustainable Energy Reviews* 15 (2011) 4972-4981.

[6] P. A. Fernandes, P. M. P. Salomé, A. F. da Cunha. Precursors' order effect on the properties of sulfurized Cu_2ZnSnS_4 thin films. *Semiconductor Science and Technology* 24 (2009) 105013.

[7] D. B. Mitzi, O. Gunawan, T. K. Todorov, K. Wang, S. Guha. The path towards a high-performance solution-processed kesterite solar cell. *Solar Energy Materials and Solar Cells* 95 (2011) 1421-1436.

[8] H. Katagiri, N. Ishigaki, T. Ishida, K. Saito. Characterization of Cu_2ZnSnS_4 Thin Films Prepared by Vapor Phase Sulfurization. *Japanese Journal of Applied Physics* 40 (2001) 500-504.

[9] T. K. Todorov, J. Tang, S. Bag, O. Gunawan, T. Gokmen, Y. Zhu, D. B. Mitzi. Beyond 11% Efficiency: Characteristics of State-of-the-Art $Cu_2ZnSn(S,Se)_4$ Solar Cells. *Advanced Energy Materials* 3 (2013) 34-38.

[10] K. Ito, T. Nakazawa. Electrical and optical properties of stannite-type quaternary semiconductor thin films. *Japanese Journal of Applied Physics*

27 (1988) 2094-2097.

[11] H. Katagiri. Cu_2ZnSnS_4 thin film solar cells. *Thin Solid Films* 480-481 (2005) 426–432.

[12] K. Jimbo, R. Kimura, T. Kamimura, S. Yamada, W. S. Maw, H. Araki, K. Oishi, H. Katagiri. Cu_2ZnSnS_4-type thin film solar cells using abundant materials. *Thin Solid Films* 515 (2007) 5997-5999.

[13] H. Katagiri, K. Jimbo, W. S. Maw, K. Oishi, M. Yamazaki, H. Araki, A. Takeuchi. Development of CZTS-based thin film solar cells. *Thin Solid Films* 517 (2009) 2455-2460.

[14] E. Mellikov, M. Altosaar, J. Raudoja, K. Timmo, O. Volobujeva, M. Kauk, J. Krustok, T. Varema, M. Grossberg, M. Danilson, K. Muska, K. Ernits, F. Lehner, D. Meissner. $Cu_2(Zn_xSn_{2-x})(S_yS_{1-y})_4$ monograin materials for photovoltaics. *Materials Challenges in Alternative and Renewable Energy. Ceramic Transactions* 224 (2011) 137-141.

[15] T. K. Todorov, K. B. Reuter, D. B. Mitzi. High-efficiency solar cell with earth-abundant liquid-processed absorber. *Advanced Materials* 22 (2010) E156-E159.

[16] M. Grossberg, J. Krustok, K. Timmo, M. Altosaar. Radiative recombination in $Cu_2ZnSnSe_4$ monograins studied by photoluminescence spectroscopy. *Thin Solid Films* 517 (2009) 2489-2492.

[17] U. Rau, A. Jasenek, H. W. Schock, F. Engelhardt, T. Mayer. Electronic loss mechanisms in chalcopyrite based heterojunction solar cells. *Thin Solid Films* 361-362 (2000) 298-302.

[18] B. Shin, O. Gunawan, Y. Zhu, N. A. Bojarcczuk, S. J. Chey, S. Guha. Thin film solar cell with 8.4% power conversion efficiency using an earth-abundant Cu_2ZnSnS_4 absorber. *Progress in Photovoltaics: Research and Applications* 21 (2013) 72-76.

[19] Y. S. Lee, T. Gershon, O. Gunawan, T. K. Todorov, T. Gokmen, Y. Virgus, S. Guha. $Cu_2ZnSnSe_4$ Thin-Film Solar Cells by Thermal Co-evaporation with 11.6% Efficiency and Improved Minority Carrier Diffusion Length.

Advanced Energy Materials 5 (2015) 1401372-1401375.

[20] W. Wang, M. T. Winkler, O. Gunawan, T. Gokmen, T. K. Todorov, Y. Zhu, D. B. Mitzi. Device Characteristics of CZTSSe Thin-Film Solar Cells with 12.6% Efficiency. *Advanced Energy Materials* 4 (2014) 1301465.

[21] W. Shockley, H. J. Queisser. Detailed Balance Limit of Efficiency of pn Junction Solar Cells. *Journal of Applied Physics* 32 (1961) 510.

[22] P. Jackson, D. Hariskos, R. Wuerz, O. Kiowski, A. Bauer, T. M. Friedlmeier, M. Powalla. Properties of $Cu(In,Ga)Se_2$ solar cells with new record efficiencies up to 21.7%. *Physica Status Solidi - Rapid Research Letters* 9 (2015) 28-31.

[23] M. Grossberg, J. Krustok, J. Raudoja, T. Raadik. The role of structural properties on deep defect states in Cu_2ZnSnS_4 studied by photoluminescence spectroscopy. *Applied Physics Letters* 101 (2012) 102102.

[24] P. K. Sarswat, M. L. Free. A study of energy band gap versus temperature for Cu_2ZnSnS_4 thin films. *Physica B: Condensed Matter* 407 (2012) 108-111.

[25] H. Katagiri, K. Saitoh, T. Washio, H. Shinohara, T. Kurumadani, S. Miyajima. Development of thin film solar cell based on Cu_2ZnSnS_4 thin films. *Solar Energy Materials and Solar Cells* 65 (2001) 141-148.

[26] J. Krustok, R. Josepson, T. Raadik, M. Danilson. Potential fluctuations in $Cu_2ZnSnSe_4$ solar cells studied by temperature dependence of quantum efficiency curves. *Physica B* 405 (2010) 3186-3189.

[27] K. Timmo, M. Altosaar, J. Raudoja, K. Muska, M. Pilvet, M. Kauk, T. Varema, M. Danilson, O. Volobujeva, E. Mellikov. Sulfur-containing $Cu_2ZnSnSe_4$ monograin powders for solar cells. *Solar Energy Materials and Solar Cells* 94 (2010) 1889-1892.

[28] S. Bag, O. Gunawan, T. Gokmen, Y. Zhu, T. K. Todorov, D. B. Mitzi. Low band gap liquid-processed CZTSe solar cell with 10.1% efficiency. *Energy & Environmental Science* 5 (2012) 7060-7065.

[29] M. Grossberg, J. Krustok, J. Raudoja, K. Timmo, M. Altosaar, T. Raadik. Photoluminescence and Raman study of $Cu_2ZnSn(Se_xS_{1-x})_4$ monograins for photovoltaic applications. *Thin Solid Films* 519 (2011) 7403-7406.

[30] S. Oueslati, G. Brammertz, M. Buffiére, C. Köble, T. Oualid, M. Meuris, J. Poortmans. Photoluminescence study and observation of unusual optical transitions in $Cu_2ZnSnSe_4$/CdS/ZnO solar cells. *Solar Energy Materials and Solar Cells* 134 (2015) 340-345.

[31] M. V. Yakushev, I. Forbes, A. V. Mudryi, M. Grossberg, J. Krustok, N. S. Beattie, M. Moynihan, A. Rockett, R. W. Martin. Optical spectroscopy studies of $Cu_2ZnSnSe_4$ thin films. *Thin Solid Films* 582 (2015) 154-157.

[32] K. Tanaka, Y. Miyamoto, H. Uchiki, K. Nakazawa, H. Araki. Donor-acceptor pair recombination luminescence from Cu_2ZnSnS_4 bulk single crystals. *Physica Status Solidi (A)* 203 (2006) 2891-2896.

[33] K. Hönes, E. Zscherpel, J. Scragg, S. Siebentritt. Shallow defects in Cu_2ZnSnS_4. *Physica B: Condensed Matter* 404 (2009) 4949-4952.

[34] K. Oishi, G. Saito, K. Ebina, M. Nagahashi, K. Jimbo, W. S. Maw, H. Katagiri, M. Yamazaki, H. Araki, A. Takeuchi. Growth of Cu_2ZnSnS_4 thin films on Si (100) substrates by multisource evaporation. *Thin Solid Films* 517 (2008) 1449-1452.

[35] E. Mellikov, M. Altosaar, M. Krunks, j. Krustok, T. Varema, O. Volobujeva, M. Grossberg, L. Kaupmees, T. Dedova, K. Timmo, K. Ernits, J. Kois, I. Oja Acik, M. Danilson, S. Bereznev. Research in solar cell technologies at Tallinn University of Technology. *Thin Solid Films* 526 (2008) 7125-7134.

[36] S. Chen, J.-H. Yang, X. G. Gong, A. Walsh, S.-H. Wei. Intrinsic point defects and complexes in the quaternary kesterite semiconductor Cu_2ZnSnS_4. *Physical Review B* 81 (2010) 245204.

[37] P. A. Fernandes, A. F. Sartori, P. M. P. Salomé, J. Malaquias, A. F. da Cunha, M. P. F. Graça, J. C. González. Admittance spectroscopy of Cu_2ZnSnS_4 based thin film solar cells.

Applied Physics Letters 100 (2012) 233504.

[38] S. Chen, L.-W. Wang, A. Walsh, X. G. Gong, S.-H. Wei. Abundance of CuZn + SnZn and 2CuZn + SnZn defects clusters in kesterite solar cells. *Applied Physics Letters* 101 (2012) 223901.

[39] M. Grossberg, T. Raadik, J. Raudoja, J. Krustok. Photoluminescence study of defect clusters in Cu_2ZnSnS_4 polycrystals. *Current Applied Physics* 14 (2014) 447-450.

[40] D. Huang, C. Persson. Band gap change induced by defect complexes in Cu_2ZnSnS_4. *Thin Solid Films* 535 (2013) 265-269.

[41] J. J. S. Scragg, L. Choubrac, A. Lafond, T. Ericson, C. Platzer-Björkman. A low-temperature order-disorder transition in Cu_2ZnSnS_4 thin films. *Applied Physics Letters* 104 (2014) 041911.

[42] S. Schorr, H.-J. Hoebler, M. Tovar. A neutron diffraction study of the stannite-kesterite solid solution series. *European Journal of Mineralogy* 19 (2007) 65-73.

[43] S. Schorr. The crystal structure of kesterite type compounds: A neutron and X-ray diffraction study. *Solar Energy Materials and Solar Cells* 95 (2011) 1482-1488.

[44] F. Luckert, M. V. Hamilton, N. S. Beattie, G. Zoppi, M. Moynihan, I. Forbes, A. V. Karotki, A. V. Mudryi, M. Grossberg, J. Krustok, R. W. Martin. Optical properties of high quality $Cu_2ZnSnSe_4$ thin films. *Applied Physics Letters* 99 (2011) 062104.

[45] O. Gunawan, T. Gokmen, C. W. Warren, J. D. Cohen, T. K. Todorov, A. R. Barkhouse, B. Santanu, J. Tang, B. Shin, D. B. Mitzi. Electronic properties of the $Cu_2ZnSn(Se,S)_4$ absorber layer in solar cells as revealed by admittance spectroscopy and related methods. *Applied Physics Letters* 100 (2012) 253905.

[46] T. P. Weiss, A. Redinger, J. Luckas, M. Mousel, S. Siebentritt. Admittance spectroscopy in kesterite solar cells: Defect signal or circuit response. *Applied Physics Letters* 104 (2013) 202105-1 - 202105-4.

[47] A. M. Goodman. Metal—Semiconductor Barrier Height Measurement by the Differential. *Journal of Applied Physics* 34 (1963) 329-338.

[48] G. Friesen, M. E. Özsar, E. D. Dunlop. Impedance model for CdTe solar cells exhibiting constant phase element behaviour. *Thin Solid Films* 361-362 (2000) 303-308.

[49] G. Hanna, T. Glatzel, S. Sadewasser, N. Ott, H. P. Strunk, U. Rau, J. H. Werner. Texture and electronic activity of grain boundaries in $Cu(In,Ga)Se_2$ thin films. *Applied Physics A* 82 (2006) 1-7.

[50] R. Herberholz, M. Igalson, H. W. Schock. Distinction between bulk and interface states in $CuInSe_2$/CdS/ZnO by space charge spectroscopy. *Journal of Applied Physics* 83 (1998) 318-325.

[51] A. Kubiaczyk, M. Nawrocka, M. Igalson. Admittance measurements on CIGS solar cells. *Opto-Electronics Review* 8 (2000) 378-381.

[52] J. T. Heath, J. D. Cohen, W. N. Shafarman. Bulk and metastable defects in $CuIn_{1-x}Ga_xSe_2$ thin films using drive level capacitance profiling. *Journal of Applied Physics* 95 (2004) 1000-1010.

[53] H. Bayhan, A. S. Kavasoğlu. Admittance and Impedance Spectroscopy on $Cu(In,Ga)Se_2$ Solar Cells. *Turkish Journal of Physics* 27 (2003) 529-535.

[54] U. Rau, M. Schmitt, D. Hilburger, F. Engelhardt, O. Seifert, J. Parisi, W. Riedl, J. Rimmasch, F. Karg. Influence of Na and S incorporation on the electronic transport properties of $Cu(In,Ga)Se_2$ solar cells. *25th IEEE PVSC* (1996) 1005-1008.

[55] A. Jasenek, U. Rau, V. Nadenau, H. W. Schock. Electronic properties of $CuGaSe_2$-based heterojunction solar cells. Part II. Defect spectroscopy. *Journal of Applied Physics* 87 (2000) 594-602.

[56] A. S. Gilmore, V. Kaydanov, T. R. Ohno. The Study of Deep Levels in CdS/CdTe Solar Sells Using Admittance Spectroscopy and its Modifications. *MRS Proceedings, Symposium B* 763 (2003)

[57] T. Walter, R. Herberholz, C. Muller, W. Schock. Determination of defect

distributions from admittance measurements and application to $Cu(In,Ga)Se_2$ based heterojunctions. *Journal of Applied Physics* 80 (1996) 4411-4420.

[58] E. Mellikov, M. Altosaar, M. Kauk-Kuusik, K. Timmo, D. Meissner, M. Grossberg, J. Krustok, O. Volobujeva. Growth of CZTS-Based Monograins and Their Application to Membrane Solar Cells. In *Copper Zinc Tin Sulfide-Based Thin Film Solar Cells*, K. Ito (Ed.), 289-310, Wiley-V C H Verlag Gmbh, 2015.

[59] M. Altosaar, J. Raudoja, K. Timmo, M. Danilson, M. Grossberg, J. Krustok, E. Mellikov. $Cu_2Zn_{1-x}Cd_xSn(Se_{1-y}S_y)_4$ solid solutions as absorber materials for solar cells. *Physica Status Solidi (A)* 205 (2008) 167-170.

[60] S. López-Marino, Y. Sánchez, M. Placidi, A. Fairbrother, M. Espindola-Rodríguez, X. Fontané, V. Izquierdo-Roca, J. López-García, L. Calvo-Barrio, A. Pérez-Rodríguez, E. Saucedo. ZnSe etching of Zn-Rich $Cu_2ZnSnSe_4$: An oxidation route for improved solar-cell efficiency. *Chem. Eur. J.* 19 (2013) 14814-14822.

[61] A. Fairbrother, M. Dimitrievska, Y. Sanchez, V. Izquierdo-Roca, A. Perez-Rodrguez, E. Saucedo. Compositional paradigms in multinary compound systems for photovoltaic applications: a case study of kesterites. *Journal of Materials Chemistry A* 3 (2015) 9451-9455.

[62] M. Neuschitzer, Y. Sanchez, S. López-Marino, H. Xie, A. Fairbrother, M. Placidi, S. Haass, V. Izquierdo-Roca, A. Perez-Rodriguez, E. Saucedo. Optimization of CdS buffer layer for high-performance $Cu_2ZnSnSe_4$ solar cells and the effects of light soaking:elimination of crossover and red kink. *Progress in Photovoltaics: Research and Applications* 23 (2015) 1660-1667.

[63] J. Krustok, T. Raadik, M. Grossberg, S. Giraldo, M. Neuschitzer, S. López-Marino, E. Saucedo. Temperature dependent electroreflectance study of $Cu_2ZnSnSe_4$ solar cells. *Materials Science in Semiconductor Processing* 39 (2015) 251-254.

[64] K. Wang, O. Gunawan, T. Todorov, B. Shin, S. J. Chey, N. A. Bojarczuk, D. Mitzi, S. Guha. Thermally evaporated Cu_2ZnSnS_4 solar cells. *Applied*

Physics Letters 97 (2010) 143508.

[65] H.-S. Duan, W. Yang, B. Bob, C.-J. Hsu, B. Lei, Y. Yang. The Role of Sulfur in Solution-Processed $Cu_2ZnSn(S,Se)_4$ and its Effect on Defect Properties. *Advanced Functional Materials* 23 (2013) 1466-1471.

[66] S. Das, S. K. Chaudhuri, R. N. Bhattacharya, K. C. Mandal. Defect levels in $Cu_2ZnSn(S_xSe_{1-x})_4$ solar cells probed by current-mode deep level transient spectroscopy. *Applied Physics Letters* 104 (2014) 192106.

[67] J. H. Schön, E. Bucher. Characterization of intrinsic defect levels in $CuInS_2$. *Physica Status Solidi (A)* 171 (1999) 511-519.

[68] S. Zott, K. Leo, M. Ruckh, H.-W. Schock. Photoluminescence of polycrystalline $CuInSe_2$ thin films. *Applied Physics Letters* 68 (1996) 1144-1146.

[69] S. Chen, A. Walsh, J.-H. Yang, X. G. Gong, L. Sun, P.-X. Yang, J.-H. Chu, S.-H. Wei. Compositional dependence of structural and electronic properties of $Cu_2ZnSn(S,Se)_4$ alloys for thin film solar cells. *Physical Review B* 83 (2011) 125201.

[70] A. P. Levanyuk, V. V. Osipov. Edge luminescence of direct-gap semiconductors. *Physics-Uspekhi* 24 (1981) 187-215.

[71] J. Krustok, H. Collan, K. Hjelt. Does the low-temperature Arrhenius plot of the photoluminescence intensity in CdTe point towards an erroneous activation energy? *Journal of Applied Physics* 81 (1997) 1442-1445.

[72] J. Krustok, R. Josepson, M. Danilson, D. Meissner. Temperature dependence of $Cu_2ZnSn(Se_xS_{1-x})_4$ monograin solar cells. *Solar Energy* 84 (2010) 379-383.

[73] U. Rau, H. W. Schock. Electronic properties of $Cu(In,Ga)Se_2$ heterojunction solar cells–recent achievements, current understanding, and future challenges. *Applied Physics A* 69 (1999) 131-147.

[74] A. Jasenek, U. Rau, T. Hahn, G. Hanna, M. Schmidt, M. Hartman, H. W. Schock, J. H. Werner, B. Schattat, S. Kraft, K.-H. Schmid, W. Bolse.

Defect generation in polycrystalline Cu(In,Ga)Se_2 by high-energy electron irradiation. *Applied Physics A* 70 (2000) 667-680.

[75] J. M. Raulot, C. Domain, J. F. Guillemoles. Ab initio investigation of potential indium and gallium free chalcopyrite compounds for photovoltaic application. *Journal of Physics and Chemistry of Solids* 66 (2005) 2019-2023.

[76] M. Danilson, E. Kask, N. Pokharel, M. Kauk-Kuusik, T. Varema, J. Krustok. Temperature dependent current transport properties in Cu_2ZnSnS_4 solar cells. *Thin Solid Films* 582 (2015) 162-165.

[77] J. P. Leitão, N. M. Santos, P. A. Fernandes, P. M. P. Salomé, A. F. da Cunha, J. C. González, G. M. Ribeiro, F. M. Matinaga. Photoluminescence and electrical study of fluctuating potentials in Cu_2ZnSnS_4-based thin films. *Physical Review B* 84 (2011) 024120.

[78] V. Kosyak, M. A. Karmarkar, M. A. Scarpulla. Temperature dependent conductivity of polycrystalline Cu_2ZnSnS_4 thin films. *Applied Physics Letters* 100 (2012) 263903.

[79] N. F. Mott. Impurity band conduction. Experiment and theory. *Journal de Physique Colloques* 37 (1976) C4-301 - C4-306.

[80] X. Song, P. H. M. Böttger, O. B. Karlsen, T. G. Finstad, J. Taftø. Impurity band conduction in the thermoelectric material ZnSb. *Physica Scripta* T148 (2012) 014001.

ACKNOWLEDGEMENTS

I am deeply grateful to my supervisor Prof. Jüri Krustok for his support, guidance, encouragement and helpful discussions over the years of my studies.

My special thanks are due to Dr. Maarja Grossberg, Dr. Marit Kauk-Kuusik, Dr. Raavo Josepson, Dr. Taavi Raadik, Dr. Mare Altosaar, and PhD student Mati Danilson. I am very thankful to all colleagues in the lab for their support and guidance, especially PhD student Maris Pilvet, scientists Dr. Kristi Timmo, Dr. Tiit Varema, and Dr. Jaan Raudoja for useful discussions and help.

I am very thankful to Prof. Malgorzata Igalson from the Faculty of Physics, Warsaw University of Technology, for the opportunity provided for some measurements and acquisition of new knowledge in their lab, for Dr. Frederique Ducroquet from INP-Grenoble (IMEP-LAHC) for support with measurements, and for Dr. Edgardo Saucedo from Catalonia Institute for Energy Research for providing me with thin film solar cell samples for studies.

This work was supported by the Estonian Science Foundation grant G-8282 and ETF 9369, by the target financing by HTM (Estonia) No. SF0140099s08, Estonian Centre of Excellence in Research, Project TK117T, and by the materials technology program, by European Social Fund's Doctoral Studies and Internationalisation Programme DoRa. The support of the World Federation of Scientists National Scholarship Programme is gratefully acknowledged. This research was also supported by the institutional research funding IUT 19-28 of the Estonian Ministry of Education and Research, by the European Union through the European Regional Development Fund, Project TK141, and by FP7 project CHEETAH, EC grant agreement no. 609788, by project KESTCELLS (FP7-PEOPLE-2012-ITN-316488) and by European Regional Development Funds (ERDF, FEDER Programa Competitivitat de Catalunya 2007–2013). Authors from IREC and the University of Barcelona belong to the M-2E (Electronic Materials for Energy) Consolidated Research Group and the XaRMAE Network of Excellence on Materials for Energy of the "Generalitat de Catalunya". E.S. thanks the Government of Spain for the "Ramon y Cajal" fellowship (RYC-2011-09212).

My warmest gratitude belongs to my family for their unconditional support and encouragements during my studies and thesis writing.

ABSTRACT

The aim of the present thesis was to characterize monograin solar cells consisting of absorbers Cu_2ZnSnS_4, $Cu_2ZnSnSe_4$ and their solid solution $Cu_2ZnSn(S_xSe_{1-x})_4$, and thin film solar cells with a $Cu_2ZnSnSe_4$ absorber layer. The thesis is based on three publications. To study defects in these materials, we used mostly admittance and impedance spectroscopy methods. Volt-ampere characteristics, photoluminescence, and temperature dependence of the quantum efficiency were supplemental methods. Monograin solar cells were prepared by other researchers at the Department of Materials Science in Tallinn University of Technology (TUT). Thin film solar cells were sent to us from Catalonia Institute for Energy Research, IREC, in Barcelona, Spain. The author did his earlier measurements in the Department of Materials Science of TUT. Later, new equipment was set up by the author in the Department of Physics of TUT, where further measurements were conducted.

In CZTS, two deep defect states (E_{A1} = 120 meV and at E_{A2} = 167 meV) were found by admittance spectroscopy and assigned to a Cu_{Zn}^{-} deep acceptor defect and to interface states, respectively. A shift in the temperature dependence of the quantum efficiency curves by about 110 meV towards higher energy was suggested to result from the contribution of this deep acceptor to the absorption at low temperatures.

Admittance spectroscopy was also used to investigate defect levels in CZTSe/CdS and $Cu_2ZnSn(Se_{0.75}S_{0.25})_4$/CdS heterojunctions. Two defect states were observed in both materials by AS. The unstable defect state showed activation energies from 87 meV to 100 meV in CZTSe. This defect state was attributed to the interface states because a possible change of interface properties with time could cause a change of activation energy. The stable deep defect state in CZTSe was found to be at 74 meV and this could belong to Cu_{Zn}^{-} acceptor defect. However, this assumption needs further studies. In CZTSSe, activation energies 154 meV and 25 meV were found. In addition, these materials were studied by photoluminescence spectroscopy. Activation energies for CZTSe and for $Cu_2ZnSn(Se_{0.75}S_{0.25})_4$ found by AS were attributed to the same acceptor defects that was seen by PL.

Impedance spectroscopy and volt-ampere characterization were used to characterize the CZTSe thin film solar cell. Different temperature ranges where electrical properties change were observed. Fittings of impedance data showed that some interface states at grain boundaries are affected at low temperatures. These states can be described by constant phase element in an equivalent circuit. Linear fitting of temperature dependence of V_{oc} showed activation energy E_A = 962 meV, which is in good agreement with the bandgap of CZTSe. Hence, the dominating recombination mechanism seemed to be the bulk recombination in the studied thin film solar cell. From the temperature dependence of j_{sc}, the activation energies were found. In the temperature range from 175 K to 285 K,

the activation energy of E_{AI} = 23.4 meV is related to the energy needed to cross the grain boundaries or some shallow acceptorlike defect. At intermediate temperatures from 75 K to 150 K, different processes like carrier localization in potential wells, radiative recombination and Mott's variable-range hopping conduction start to affect, showing an activation energy of E_{AII} = 33.8 meV.

KOKKUVÕTE

Kaasaja päikeseenergeetika põhiprobleem on liiga kõrge energiahind. Odavamate päikesepatareide valmistamiseks saab kasutada näiteks uut tüüpi absorbermaterjale – kesteriite. Kuid nende materjalide kasutegurid on liiga madalad. Et teada saada, mis seda põhjustab, on vaja välja selgitada antud materjalide fundamentaalsed põhiomadused. Paraku on neid materjale eriti vähe uuritud just kõrgsageduslike mahtuvuslike meetoditega. Eesmärk oli täita see tühimik, kogudes teavet eksperimentaalsete mõõtmistega nende materjalide defektstruktuuri kohta.

Käesolevas kolmel publikatsioonil põhinevas doktoritöös on kasutatud põhiliselt näivjuhtivuse- ja impedantsspektroskoopia meetodeid, et uurida kesteriitide Cu_2ZnSnS_4, $Cu_2ZnSnSe_4$ ja nende tahke lahuse $Cu_2ZnSn(S_xSe_{1-x})_4$ baasil valmistatud päikesepatareisid. Lisaks kasutati volt-amper karakteristikuid, fotoluminestsentsspektroskoopiat ja kvantefektiivsuse spektrite temperatuursõltuvusi. Monoterakihilised päikesepatareid valmistati Tallinna Tehnikaülikooli materjaliteaduse instituudis. Õhukesekihilised päikesepatareid valmistati Barcelonas IREC-i keskuses.

Absorbermaterjalis Cu_2ZnSnS_4 leiti näivjuhtivuse spektroskoopiaga kaks defektitaset (E_{A1} = 120 meV ja E_{A2} = 167 meV), mis omistati vastavalt sügavale aktseptoritasemele Cu_{Zn}^{-} ja piirpinna olekutele. Lisaks ilmnes kvantefektiivsuse spektrite temperatuursõltuvusest, et see leitud sügav aktseptordefekt mõjutas neeldumist ning põhjustas efektiivse keelutsooni energia nihke suurusega 110 meV kõrgema energia suunas.

Näivjuhtivuse spektroskoopiat kasutati ka $Cu_2ZnSnSe_4$/CdS ja $Cu_2ZnSn(Se_{0.75}S_{0.25})_4$/CdS heterosiirete defektitasemete uurimiseks. Mõlemas materjalis leiti kaks defektitaset. Absorbermaterjali $Cu_2ZnSnSe_4$ ebastabiilse defektitaseme aktivatsioonienergiad muutusid aja jooksul vahemikus 87 meV kuni 100 meV. See tase omistati piirpinna olekutele, kuna ajas toimuvad piirpinna olekute muutused võivad põhjustada aktivatsioonienergia muutusi. $Cu_2ZnSnSe_4$ stabiilne defektitase oli aktivatsioonienergiaga 74 meV ja omistati Cu_{Zn}^{-} aktseptordefektile. Absorbermaterjalis $Cu_2ZnSn(Se_{0.75}S_{0.25})_4$ leiti elektriliselt aktiivsete defektide aktivatsioonienergiad 154 meV ja 25 meV. Lisaks uuriti neid materjale fotoluminestsentsspektroskoopiaga. Näivjuhtivuse spektroskoopiaga leitud defektide aktivatsioonienergiad langesid kokku fotoluminestsentsist leitud aktivatsioonienergiatega.

Õhukesekileliste $Cu_2ZnSnSe_4$ päikesepatareide uurimisel kasutati impedantsspektroskoopia ja volt-amper karakteristikute temperatuursõltuvusi. Tehti kindlaks erinevad temperatuuripiirkonnad, kus elektrilised omadused oluliselt ja erinevalt muutuvad. Impedantsspektroskoopia mõõtmised näitasid, et terade piirpinna olekud avaldavad erilist mõju madalatel temperatuuridel. Vastavaid olekuid saab elektriskeemis kirjeldada konstantse faasielemendiga.

Volt-amper karakteristikutest leitud avatud ahela pinge V_{oc} temperatuursõltuvusest saadi aktivatsioonienergia $E_A = 962$ meV, mis on energeetiliselt küllaltki sarnane $Cu_2ZnSnSe_4$ keelutsooni laiusega. Seega on uuritud päikesepatareide domineerivaks rekombinatsioonimehhanismiks rekombinatsioon absorberi neutraalses ruumiosas. Lühisvoolu j_{sc} temperatuursõltuvusest leiti samuti aktivatsioonienergiad. Näiteks, temperatuurivahemikus $T = 175$ - 285 K leiti aktivatsioonienergia $E_{AI} = 23.4$ meV, mis suure tõenäosusega on seotud teradevaheliste barjääridega. Keskmiste temperatuuride ($T = 75$ - 150 K) juures kerkivad esile laengulõksudena käituvad potentsiaaliaugud, kiirguslik rekombinatsioon ja Motti muutuva kaugusega hüpakjuhtivus, mis näitab aktivatsioonienergiat $E_{AII} = 33.8$ meV.

Töö tulemusena võib öelda, et mahtuvusspektroskoopiliste meetoditega on võimalik saada väga olulist teavet uuritud kesteriitsete materjalide defektstruktuuri kohta. Saadud tulemused näitavad, et neid meetodeid võib rakendada edaspidigi selliste materjalide uurimiseks. Nende uurimuste tulemusena on võimalik tõsta nendest materjalidest valmistatud päikesepatareide kasutegureid.

APPENDIX A1

Article I

E. Kask, T. Raadik, M. Grossberg, R. Josepson, J. Krustok. Deep defects in Cu_2ZnSnS_4 monograin solar cells. Energy Procedia 10 (2011) 261-265.

Available online at www.sciencedirect.com

SciVerse ScienceDirect

Energy Procedia 10 (2011) 261 – 265

Energy Procedia

European Materials Research Society Conference
Symp. Advanced Inorganic Materials and Concepts for Photovoltaics

Deep defects in Cu_2ZnSnS_4 monograin solar cells

E. Kask*, T. Raadik, M. Grossberg, R. Josepson, J. Krustok

Tallinn University of Technology, Ehitajate tee 5, Tallinn 19086, Estonia

Abstract

In this report Cu_2ZnSnS_4 (CZTS) monograin layer (MGL) solar cells were studied using admittance spectroscopy (AS) (frequency range 20Hz-10MHz) and temperature dependence of quantum efficiency (QE) curves (T=10K-300K). These studies revealed two deep defect states at E_{A1}= 120 meV and at E_{A2}= 167 meV. The first state was present in different CZTS cells while the second state had somewhat different properties in different cells. The temperature dependence of QE curves showed a shift of the long wavelength edge with increasing temperature by about 110 meV towards higher energy. The possible origin of the observed deep defect states is discussed.

Keywords: Cu_2ZnSnS_4; admittance spectroscopy; quantum efficiency; defects

1. Introduction

Cu_2ZnSnS_4 (CZTS) is a promising candidate for thin film solar cells with absorbers made from non-toxic and abundant elements [1-4]. At the same time it is very difficult to grow pure CZTS, because different secondary phases like ZnS, Cu_2SnS_3, and others are very easily formed and large compositional nonuniformity is present. This is a reason why even for such a fundamental parameter as the band gap energy agreement has not been reached: values between 1.4 eV and 1.6 eV have been reported [4-7]. Despite this fact the best solar cells based on CZTS have already shown efficiencies of almost 10 % [8]. However, without understanding the basic physical properties of CZTS it will be impossible to make a breakthrough similar to $CuInGaSe_2$ solar cells that show efficiencies of over 20 % [9].

It is known that intrinsic point defects in CZTS are playing a major role and determine the properties of CZTS. This is why more defect studies are needed. According to Losee [10], capacitance and admittance spectroscopy (AS) in particular are suitable methods for detecting defect levels. In defect studies also photoluminescence spectroscopy (PL) has proven to be a very efficient method. As far as we know there are no papers yet on capacitance spectroscopy studies of CZTS. So far only few papers about PL properties of CZTS have been published. A broad and asymmetric PL band at 1.3 eV has been detected in many papers [11-16]. Recently, even more PL peaks were detected in vapour phase grown CZTS crystals including a DA1 peak at 1.496 eV and a DA2 peak at 1.475 eV [12]. Both PL peaks are related to shallow defects with E < 30 meV. The first excitonic emission was also recorded in these crystals with a peak position at E=1.509 eV. From these measurements a low temperature (T=10K) band gap energy was calculated to

* Corresponding author. Tel.: +372-620-3210; fax: +372-620-3367.
E-mail address: erkki.kask@ttu.ee.

doi:10.1016/j.egypro.2011.10.188

be E_g=1.519 eV and the estimated room temperature band gap energy was 1.43 eV. In this paper we apply admittance spectroscopy and temperature dependent quantum efficiency (QE) measurements to study deep defects in CZTS solar cells.

2. Experimental

The CZTS monograin powder materials used for the solar cells studied were synthesized from binary compounds in a molten KI flux in an isothermal recrystallization process. The details of the monograin powder production process can be found in previous papers [4, 16]. The single phase composition of the monograin powder crystals was confirmed by Raman spectroscopy. The chemical composition was determined by energy dispersive X-ray analysis: Cu/(Zn+Sn)=0.9, Zn/Sn=1.1. Crystals with diameters of 63–75 μm were used in the formation of a monolayer in the monograin layer (MGL) solar cell structure: graphite/CZTS/CdS/ZnO [16]. The solar cells prepared have typically an area of about 4 mm^2.

We studied the solar cells by admittance spectroscopy. The solar cells were mounted on a cold finger of a closed-cycle helium cryostat (Janis) and a Wayne Kerr 6500B impedance analyzer was used for the electrical measurements. Impedance Z and phase angle θ were both measured as a functions of frequency f and temperature T. The used frequency range was from 20Hz to 10MHz and the temperature was varied from 95K to 300K with a step width ΔT of 5K. In order to maintain the linearity of the response signal, the alternating current (AC) voltage amplitude was kept as low as 10mV. The measurements were carried out in the dark and at 0V or -1V DC bias voltage.

For the temperature dependence of the QE curves a 250W calibrated halogen lamp was used as a light source together with a computer controlled SPM-2 prism monochromator. The temperature range was as wide as from 10K to 300K to find changes in the spectral response. The generated short circuit current was detected with a DSP Lock-In amplifier (SR 810).

I/V-measurements of CZTS cells were performed with a computer-controlled KEITHLEY 2400 SourceMeter at room temperature and under 100 mW/cm^2 illumination. As light source a standard halogen lamp with calibrated intensity was used.

3. Theory

Admittance spectroscopy involves measuring the junction capacitance as a function of frequency ω and temperature T. The admittance of the heterostructure is a superposition of the free carrier capacitance across the width of the space charge region (SCR) and the contribution from the charging and discharging of deeper defect levels within the SCR of the junction. The rectifying junction capacitance is given by the SCR capacitance [17]:

$$C_d = \frac{\varepsilon}{w} = \left(\frac{\varepsilon q N_a}{2V_{bi}} \right)^{1/2}, \tag{1}$$

where ε is the semiconductor's dielectric permittivity, w is the SCR width, N_a is the acceptor concentration in p-type absorber, and V_{bi} is the built-in voltage.

If deeper carrier traps are present, the band bending in the SCR causes the Fermi level E_F to cross the trap level E_t at some distance from the interface, at the crossing point x_t. The oscillating voltage with the frequency ω causes the electric charge accumulated by traps to oscillate in the vicinity of x_t. The trapped electric charge follows the applied voltage oscillations and contributes to the total capacitance only if their frequency does not exceed the characteristic trap frequency ω_t. Therefore, in the case of low frequencies $\omega_{lf} << \omega_t$, the trap related capacitance C_t is equal to C_{lf}, where C_{lf} is the low frequency capacitance. In high frequency ($\omega_{hf} >> \omega_t$) measurements the junction capacitance C_d is determined by C_{hf}, where C_{hf} is the high frequency capacitance. Accordingly, in the case of a single majority carrier trap level the total junction capacitance can be described by the equation [17]:

$$C(\omega) = C_d + \frac{C_{lf} - C_d}{1 + \omega^2 \tau^2}, \tag{2}$$

where τ is the characteristic trapping time that depends on the trap density N_t, the acceptor concentration N_a and on the SCR-width w. In the case of a small trap concentration N_t, the characteristic frequency ω_t for the hole trapping defects

is $\omega_t=1/\tau$ [18]. The inflection frequency ω_t can be obtained from the analysis of the first derivative of the capacitance, $dC/d\omega$, that should demonstrate a peak at the frequency ω_t.

The temperature dependence of the inflection frequency ω_t is described by the equation [17]:

$$\omega_t(T) = 2e_t(T) = 2N_{c,v}\nu_{Th}\sigma_{n,p}\exp(-E_A/kT) = 2\xi_0 T^2\exp(-E_A/kT), \quad (3)$$

where e_t is the emission rate, $N_{c,v}$ is the effective density of states in the conduction and valence band, υ_{Th} is the thermal velocity of the minority carriers at the interface, $\sigma_{n,p}$ is the capture cross-section for electrons and holes, $E_A=E_t-E_v$ is the activation energy of the defect level E_t with respect to the valence band edge E_v in p-type absorber and ξ_0 covers all the temperature independent parameters. The activation energy of a defect level E_A can be obtained from the temperature dependence of the capacitance spectra i.e. from the Arrhenius plot of the quantity $\ln(\omega_t/T^2)$ versus $1000/T$.

4. Results and discussion

The I-V curve of our here most studied CZTS solar cell is given in Fig.1. As can be seen, this cell shows quite poor parameters: V_{oc}=582.4 mV, J_{sc}=7.13 mA/cm^2 and fill factor FF=32%, resulting in a solar energy conversion efficiency of only 1.3%. It is known that a low efficiency of CZTS cells is mainly caused by the high rate of interface recombination [19]. Additional recombination losses can be caused by deep acceptor levels that act as carrier traps. However, there are no experimental results about the deep defect levels in CZTS. Knowledge about the absorber surface properties and defect structure enables to improve the electrical properties of the CZTS material by changing the surface composition e.g. by the additional thermal and chemical treatments [4].

In order to study the defects in such CZTS powders, admittance spectroscopy was applied to CZTS MGL solar cells. Fig. 2 shows the frequency dependence of the capacitance of a CZTS solar cell in the temperature range from 95K to 300K. These spectra show two steps labelled N1 and N2 (similarly found for $CuInSe_2$ in [20]) that are attributed to the charging and discharging of two deep levels within the space charge region (SCR) of the heterojunction. The N2 capacitance step appears at lower frequencies and higher temperatures and corresponds therefore to a contribution of deeper defect level than N1. In accordance with the theory, the steps in the capacitance spectrum shift towards higher frequencies with increasing temperature T. The height of the capacitance steps corresponds to the defect level contribution to the total capacitance.

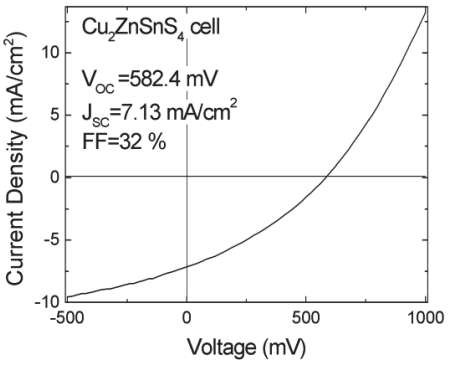

Fig. 1. Current-voltage characteristic of CZTS solar cell.

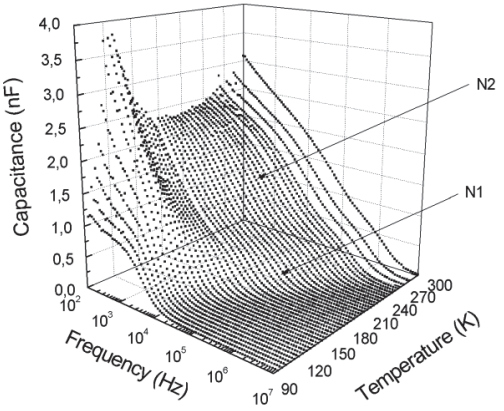

Fig. 2. The capacitance spectra of CZTS solar cell as a function of frequency and temperature at 0 V bias. Two steps, labelled N1 and N2 are indicated by arrows.

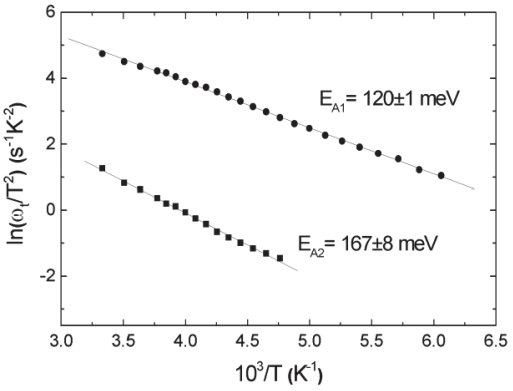

Fig. 3. The Arrhenius plot showing the calculated activation energies of the defect levels E_{A1}= 120 meV and E_{A2}= 167 meV corresponding to the two capacitance steps N1 and N2, respectively. Measured at bias 0 V.

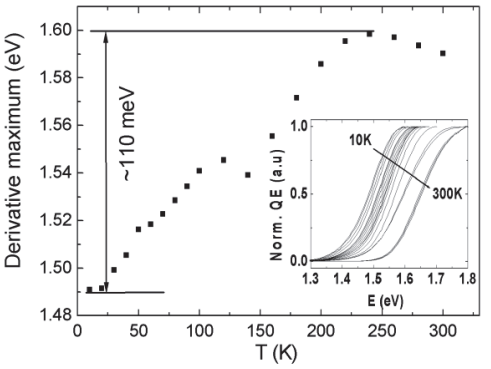

Fig. 4. Temperature dependence of the maximum points of the first derivative of the QE curves.

For the two capacitance steps, an Arrhenius plot of the quantity $\ln(\omega_t/T^2)$ versus $1000/T$ is shown in Fig. 3. The inflection frequencies ω_{t1} and ω_{t2} for every temperature corresponding to steps N1 and N2, respectively, were determined from the analysis of the first derivative $dC(\omega)/d\omega$. The obtained activation energies E_{A1}=120 ± 1 meV and E_{A2}=167 ± 8 meV are attributed to a defect distribution peaking at the corresponding energetic distance from the delocalized band edges.

The deep defect state with an activation energy of 120 meV was present in different CZTS solar cells while the second state with an activation energy of 167 meV had somewhat different properties in different cells. The activation energy of the latter defect state varied in different cells and was dependent on the applied bias voltage (0V, -1V). This is not expected for bulk defect states. On the other hand, in the case of reverse biasing the SCR is widened and the position of the interface states with respect to the Fermi level and the band edges changes. Consequently, we attributed the N2 capacitance step to the contribution of interface states.

The temperature dependence of the QE curves of the corresponding solar cells shows a shift of the long wavelength edge with increasing temperature by about 110 meV towards higher energy. Fig. 4 shows the maximum points of the first derivatives of the quantum efficiency (QE) curves at different temperatures. This shift seems to be related to the first defect state found from AS experiments. At low temperatures, this (probably acceptor) state contributes to the absorption and causes a shift of the QE curve. According to first-principles calculations made by Chen *et al.* [21] the *p*-type conductivity of CZTS is mainly determined by a Cu_{Zn} acceptor defect having a quite deep level at E_A= 0.12 eV. Accordingly, the deep acceptor level observed in AS measurements with the matching activation energy could be assigned to Cu_{Zn} acceptor defect.

5. Conclusions

Deep defects in CZTS monograin layer solar cells were studied by using admittance spectroscopy and temperature dependence of the quantum efficiency curves. The AS studies revealed two deep defect states at E_{A1}= 120 meV and at E_{A2}= 167 meV that were assigned to a Cu_{Zn} deep acceptor defect and to interface states, respectively. A shift in the temperature dependence of the quantum efficiency curves by about 110 meV towards higher energy was proposed to result from the contribution of this deep acceptor to the absorption at low temperatures.

Acknowledgements

This work was supported by the Estonian Science Foundation grant G-8282, by the target financing by HTM (Estonia) No. SF0140099s08, by European Social Fund's Doctoral Studies and Internationalisation Programme DoRa.

The support of the World Federation of Scientists National Scholarship Programme is gratefully acknowledged. The authors thank also the CZTSSe-team at the TUT.

References

[1] Katagiri H. Cu_2ZnSnS_4 thin film solar cells. Thin Solid Films 2005;**480-481**:426.
[2] Jimbo K, Kimura R, Kamimura T, Yamada S, Maw W S, Araki H, Oishi K, Katagiri H. Cu_2ZnSnS_4-type thin film solar cells using abundant materials. Thin Solid Films 2007;**515**:5997-5999.
[3] Katagiri H, Jimbo K, Maw W S, Oishi K, Yamazaki M, Araki H, Takeuchi A. Development of CZTS-based thin film solar cells. Thin Solid Films 2009;**517**:2455-2460.
[4] Mellikov E, Altosaar M, Raudoja J, Timmo K, Volobujeva O, Kauk M, Krustok J, Varema T, Grossberg M, Danilson M, Muska K, Ernits K, Lehner F, Meissner D. $Cu_2(Zn_xSn_{2-x})(S_yS_{1-y})_4$ monograin materials for photovoltaics. Materials Challenges in Alternative and Renewable Energy. Ceramic Transactions 2010;**224**:137-141.
[5] Katagiri H, Ishigaki N, Ishida T, Saito K. Characterization of Cu_2ZnSnS_4 Thin Films Prepared by Vapor Phase Sulfurization. Jpn. J. Appl. Phys. Part 1-Regular Pap. Short Notes Rev. Pap. 2001;**40**:500-504.
[6] Katagiri H, Saitoh K, Washio T, Shinohara H, Kurumadani T, Miyajima S. Development of thin film solar cell based on Cu_2ZnSnS_4 thin films. Sol. Energy Mater. Sol. Cells 2001;**65**:141-148.
[7] Fernandes P A, Salome P M P, da Cunha A F. Precursors' order effect on the properties of sulfurized Cu_2ZnSnS_4 thin films. Semicond. Sci. Technol. 2009;**24**:105013.
[8] Todorov T K, Reuter K B, Mitzi D B. High-efficiency solar cell with earth-abundant liquid-processed absorber. Adv. Mater. 2010;**22**:E156-E159.
[9] Jackson P, Hariskos D, Lotter E, Paetel S, Wuerz R, Menner R, Wischmann W, Powalla M. New world record efficiency for $Cu(In,Ga)Se_2$ thin-film solar cells beyond 20%. Prog. Photovolt: Res. Appl. 2011.
[10] Losee D L. Admittance spectroscopy of impurity levels in Schottky barriers. J. Appl. Phys. 1975;**46**:2204-2214.
[11] Tanaka K, Miyamoto Y, Uchiki H, Nakazawa K, Araki H. Donor-acceptor pair recombination luminescence from Cu_2ZnSnS_4 bulk single crystals. phys. stat. sol. 2006;**203**:2891-2896.
[12] Hönes K, Zscherpel E, Scragg J, Siebentritt S. Shallow defects in Cu_2ZnSnS_4. Physica B: Condensed Matter 2009;**404**:4949-4952.
[13] Oishi K, Saito G, Ebina K, Nagahashi M, Jimbo K, Maw W S, Katagiri H, Yamazaki M, Araki H, Takeuchi A. Growth of Cu_2ZnSnS_4 thin films on Si (100) substrates by multisource evaporation. Thin Solid Films 2008;**517**:1449-1452.
[14] Grossberg M, Krustok J, Raudoja J, Timmo K, Altosaar M, Raadik T. Photoluminescence and Raman study of $Cu_2ZnSn(Se_xS_{1-x})_4$ monograins for photovoltaic applications. Thin Solid Films (in press).
[15] Mellikov E, Altosaar M, Krunks M, Krustok J, Varema T, Volobujeva O, Grossberg M, Kaupmees L, Dedova T, Timmo K, Ernits K, Kois J, Oja Acik I, Danilson M, Bereznev S. Research in solar cell technologies at Tallinn University of Technology. Thin Solid Films 2008;**516**:7125-7134.
[16] Altosaar M, Raudoja J, Timmo K, Danilson M, Grossberg M, Krustok J, Mellikov E. $Cu_2Zn_{1-x}Cd_xSn(Se_{1-y}S_y)_4$ solid solutions as absorber materials for solar cells. phys. stat. sol. 2008;**205**:167-170.
[17] Bayhan H, Kavasoğlu A S. Admittance and Impedance Spectroscopy on $Cu(In,Ga)Se_2$ Solar Cells. Turk J Phys 2003;**27**:529-535.
[18] Gilmore A S, Kaydanov V, Ohno T R. The Study of Deep Levels in CdS/CdTe Solar Cells Using Admittance Spectroscopy and its Modifications. MRS Proceedings, Symposium B 2003.
[19] Wang K, Gunawan O, Todorov T, Shin B, Chey S J, Bojarczuk N A, Mitzi D, Guha S. Thermally evaporated Cu_2ZnSnS_4 solar cells. Applied Physics Letters 2010;**97**:143508.
[20] Herberholz R, Igalson M, Schock H W. Distinction between bulk and interface states in CuInSe2/CdS/ZnO by space charge spectroscopy. J. Appl. Phys. 1998;**83**:318-325.
[21] Chen S, Yang J-H, Gong X G, Walsh A, Wei S-H. Intrinsic point defects and complexes in the quaternary kesterite semiconductor Cu_2ZnSnS_4. Phys. Rev. B 2010;**81**:245204.

APPENDIX A2

Article II

E. Kask, M. Grossberg, R. Josepson, P. Salu, K. Timmo, J. Krustok. Defect studies in $Cu_2ZnSnSe_4$ and $Cu_2ZnSn(Se_{0.75}S_{0.25})_4$ by admittance and photoluminescence spectroscopy. Materials Science in Semiconductor Processing 16(3) (2013) 992 - 996.

Materials Science in Semiconductor Processing 16 (2013) 992–996

Contents lists available at SciVerse ScienceDirect

Materials Science in Semiconductor Processing

journal homepage: www.elsevier.com/locate/mssp

Defect studies in $Cu_2ZnSnSe_4$ and $Cu_2ZnSn(Se_{0.75}S_{0.25})_4$ by admittance and photoluminescence spectroscopy

E. Kask*, M. Grossberg, R. Josepson, P. Salu, K. Timmo, J. Krustok

Tallinn University of Technology, Department of Material Science, Ehitajate tee 5, 19086 Tallinn, Estonia

ARTICLE INFO

Available online 15 March 2013

Keywords:
$Cu_2ZnSnSe_4$
$Cu_2ZnSn(Se_{0.75}S_{0.25})_4$
Admittance spectroscopy
Photoluminescence spectroscopy
Defects

ABSTRACT

To achieve higher record efficiencies for solar cells containing $Cu_2ZnSnSe_4$ (CZTSe), Cu_2ZnSnS_4 (CZTS) or their solid solution $Cu_2ZnSn(Se_xS_{1-x})_4$ (CZTSSe) as an absorber, it is necessary to obtain more knowledge about defect structure of these materials. In this work, admittance spectroscopy (AS) and low temperature photoluminescence spectroscopy (PL) were used for defect studies. Admittance spectroscopy in the frequency range from 20 Hz to 10 MHz was used for studies of CZTSe/CdS and CZTSSe/CdS monograin layer heterojunctions. The measurement temperature varied from 140 K to 245 K. Two defect states (labelled E_{A1} and E_{A2}) were found in $Cu_2ZnSnSe_4$ and $Cu_2ZnSn(Se_{0.75}S_{0.25})_4$. In different CZTSe/CdS heterojunctions the E_{A2} state was present at 74 meV, but the second E_{A1} defect state changed from 87 meV to 100 meV during time and had varying properties. In $Cu_2ZnSn(Se_{0.75}S_{0.25})_4$ the E_{A2} state was found at 25 meV. The E_{A1} state at 154 meV showed the same properties as the two defect levels in CZTSe. In both cases the E_{A2} defect state was attributed to an acceptor defect and the E_{A1} state with changing properties to interface states. The detected PL bands were at 0.946 eV in CZTSe and at 1.028 eV in $Cu_2ZnSn(Se_{0.75}S_{0.25})_4$. Obtained by PL measurements, defect states at 69 meV in CZTSe and at 39 meV in $Cu_2ZnSn(Se_{0.75}S_{0.25})_4$ were attributed to the same acceptor defect that was found from the AS measurements.

1. Introduction

Quaternary compound $Cu_2ZnSnSe_4$ (CZTSe) is a promising non-toxic semiconductor material for absorber layer in solar cells [1]. CZTSe is an analogue of $CuInSe_2$ (CISe), where rare In is replaced with Zn and Sn. This CZTSe material has a direct band gap of about 1 eV [2,3] and high absorption coefficient ($>10^4\,cm^{-1}$) [4]. Bag et al. have studied CZTSe solar cells and conversion efficiency 10.1% was achieved [5]. $Cu_2ZnSn(S,Se)_4$ (CZTSSe) and Cu_2ZnSnS_4 (CZTS) devices with efficiencies of as high as 11.1% [6] and 8.4% [7], correspondingly, have been shown. Optimal band gap for solar energy conversion is achievable by choosing suitable S to Se ratio for CZTSSe solid solution. However, many physical properties of this compound are still unknown and CZTSe/CdS and CZTSSe/CdS heterojunctions have not been studied in detail. Furthermore, there is lack of information about the point defects in these absorber materials.

In fact, shallow defect levels with activation energies $E_A=27$ meV and $E_A=7$ meV have been found in CZTSe by photoluminescence (PL) as presented in Ref. [8]. We have previously studied CZTSe monograin powder by PL and found a low-temperature PL band at 0.946 eV that results from band-to-impurity (BI) recombination. The ionisation energy of the corresponding acceptor defect was found to be 69 meV [2].

The first-principles calculations have been made similar to CZTSe quaternary absorber CZTS by Chen et al. [9]. They found that the main acceptor defect in CZTS is Cu_{Zn}^- antisite defect that has quite deep level at $E_A=0.12$ eV. In our previous study the admittance spectroscopy (AS) on CZTS also showed deep acceptor level at $E_{A1}=0.12$ eV [10], that could be assigned to Cu_{Zn}^- acceptor defect.

* Corresponding author. Tel.: +372 620 3210.
E-mail address: erkki.kask@ttu.ee (E. Kask).

1369-8001/$ - see front matter © 2013 Elsevier Ltd. All rights reserved.
http://dx.doi.org/10.1016/j.mssp.2013.02.009

In addition, the second activation energy $E_{A2}=167$ meV was observed and attributed to the contribution of interface states. Similar results were attained by Fernandes et al. [11] who determined defect activation energies 44.7 meV and 112.7 meV. Gunawan et al. have studied CZTSSe absorber layer in solar cells by admittance spectroscopy and found E_A values in range 0.13–0.20 eV [12]. However, AS studies on CZTSe have not been reported so far. In the present paper AS and PL results of $Cu_2ZnSn(Se_{0.75}S_{0.25})_4$/CdS and $Cu_2ZnSnSe_4$/CdS monograin layer heterojunctions are presented.

2. Experimental

The CZTSe and CZTSSe monograin powders were synthesised from binary compounds. The chemical composition of monograin powder crystals was determined by energy dispersive X-ray analysis: Cu/(Zn+Sn)=0.88, Zn/Sn=1.0 for CZTSe and Cu/(Zn+Sn)=0.93, Zn/Sn=0.99 for $Cu_2ZnSn(Se_{0.75}S_{0.25})_4$. The single phase composition of CZTSe and CZTSSe was confirmed by Raman spectroscopy. Grains with diameters of 63–75 μm were selected by sieving and used for monolayer in the monograin layer CZTSe/CdS and CZTSSe/CdS heterojunctions. CdS buffer layer was chemically deposited onto powder crystals. Further details can be found in Ref. [13].

For temperature dependent AS measurements the CZTSe/CdS heterojunctions were mounted in the closed-cycle He cryostat (Janis) and the admittance spectra for CZTSe/CdS heterojunction were recorded by using a Wayne Kerr 6500B impedance analyser. Impedance Z and phase angle θ were both measured as functions of frequency and temperature. The used frequency range was from 20 Hz to 10 MHz and the temperature was varied from 140 K to 245 K with a step $\Delta T=5$ K. In order to maintain the linearity of the response signal, the AC voltage amplitude was kept as low as 10 mV. The measurements were carried out in the dark and with DC bias of 0 V.

In addition, the same monograin powders were studied by using photoluminescence (PL) spectroscopy in the temperature range of 10–140 K. For PL measurements, a He–Cd laser with the wavelength of 441 nm was used for PL excitation. The PL spectra were recorded by using a computer controlled SPM-2 monochromator ($f=40$ cm) together with an InGaAs detector and a DSP Lock-In amplifier SR 810.

The prepared CZTSe/CdS heterojunction was measured twice by AS. The first measurement after the preparation is referred to as the measurement of the fresh device in this paper. Then 2 months later the same CZTSe/CdS heterojunction (called aged device) was measured again. Between measurements no treatments on this heterojunction were performed.

3. Results and discussion

3.1. AS results

Admittance spectroscopy is a powerful tool for electrical characterisation of semiconductors. For defect studies, after each measurement the real and imaginary part of the impedance, Z' and $-Z''$ respectively, were calculated. The temperature dependence of Z' versus $-Z''$ graph of an aged CZTSe/CdS heterojunction is shown in Fig. 1. At every temperature curve consists of one arc and the corresponding equivalent circuit (see Fig. 1) was used for fitting the arcs. From the fittings the series resistance R_s values at each temperature were found. The R_s values were used to calculate the capacitance. Equivalent circuit, where serial resistor is followed by a resistor and a capacitor connected in parallel can be described by the following equation [14]:

$$Z = R_S + \frac{R_P}{1+(\omega R_P C)^2} - i\frac{R_P^2 C\omega}{1+(\omega R_P C)^2} \quad (1)$$

where ω, C, and R_P are angular frequency, capacitance, and parallel resistance, respectively. After rewriting (1), capacitance can be found by

$$C = \frac{-Z''}{\left[(Z'-R_S)^2+(-Z'')^2\right]\omega} \quad (2)$$

The capacitance C versus ω graphs are shown in Fig. 2.

The total capacitance consists of the free carrier capacitance across the width of the space charge region (SCR) and the additional capacitance contribution from charging and discharging of defect states at a location where the energy of electron (hole) states equals the electron (hole) quasi-Fermi level. Also, energetically continuous but locally discrete interface states contribute to total capacitance. The time constant for charging and recharging of defect states at energy equal to the quasi-Fermi level determines the inflection frequency i.e. step in the capacitance versus frequency spectrum. The additional capacitance occurs if the AC modulation allows the establishment of equilibrium between the occupation of the defect levels and the free carriers.

In case of an ideally discrete defect level, the dependence of the additional defect related capacitance C_d on the angular frequency ω is given by [15]:

$$C_d \propto \omega_0^2/(\omega_0^2-\omega^2) \quad (3)$$

where the inflection point at frequency ω_0 is related to the emission rate of the defect e_T. Therefore the temperature dependence of the inflection frequency ω_0 is presented by

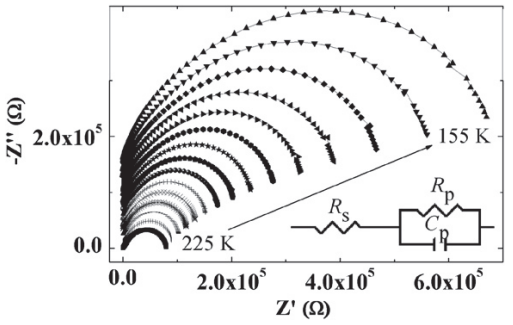

Fig. 1. Z' versus $-Z''$ graph of the aged CZTSe/CdS heterojunction. Equivalent circuit shown was used for fitting the arcs and finding R_s values at each temperature. The y-axis offset for arcs is set to 50%.

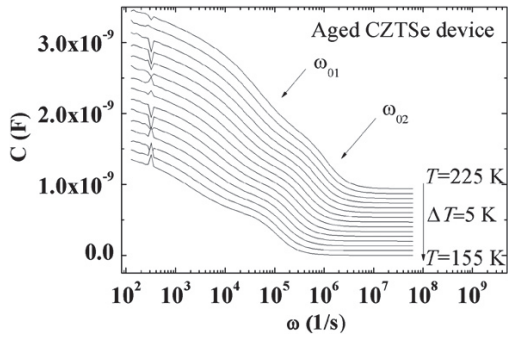

Fig. 2. The capacitance C versus ω graph of the aged CZTSe/CdS heterojunction. Steps, corresponding to inflection frequencies, are indicated by arrows. The y-axis offset for lines is set to 25%.

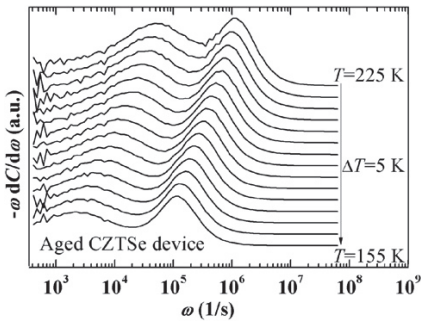

Fig. 3. The derivative $-\omega\,\mathrm{d}C/\mathrm{d}\omega$ versus ω graph of the aged CZTSe/CdS heterojunction depicts maxima which corresponding inflection frequencies ω_0 are used for the Arrhenius plot. The y-axis offset for lines is set to 50%.

[14–16]

$$\omega_0(T) = 2e_T(T) = 2N_{C,v}\upsilon_{th}\sigma_{n,p}\exp(-E_A/kT) = \\ = \xi_0 T^2\exp(-E_A/kT) \quad (4)$$

where $N_{c,v}$ is the effective density of states in the conduction and valence band, v_{th} is the thermal velocity of charge carriers, $\sigma_{n,p}$ represents the capture cross-section for electrons and holes by the defect level. The emission prefactor ξ_0 covers all the temperature independent parameters. E_A is the activation energy of the defect level with respect to the corresponding band edge. The inflection frequency ω_0 corresponds to a maximum of $-\omega\,\mathrm{d}C/\mathrm{d}\omega$ versus ω graph.

After finding the natural logarithm of the Eq. (4) one can draw the Arrhenius plot of the inflection frequencies, $\ln(\omega_0/T^2)$ versus $10^3/T$. The linear fit is used for calculating activation energy of the defect level.

The $-\omega\,\mathrm{d}C/\mathrm{d}\omega$ versus ω graph of an aged CZTSe/CdS heterojunction is given in Fig. 3. This graph shows two maxima. Analogical dependences were found in CZTSSe/CdS heterojunction. The Arrhenius plots for all CZTSe measurements are shown in Fig. 4. All activation energies found by AS are in Table 1. The value of the activation energy at the higher frequency corresponding to E_{A2} state showed almost no changes during ageing time. At lower frequency (E_{A1} state) the fresh heterojunction shows quite different activation energy compared to the same but aged heterojunction: 87 meV and 100 meV, respectively.

The change (from 87 to 100 meV) in the second activation energy corresponding to E_{A1} state can probably be assigned to interface states. Possible change of interface properties with time could cause this change of activation energy. The stable activation energy at 74 meV is obviously related to some deep acceptor defect state. In CZTS the activation energy of 120 meV belonged to Cu_{Zn}^{-} acceptor defect [9,10]. Considering that the activation energy of a defect varies with the band-gap of different materials, i.e. for similar compounds $CuInSe_2$ and $CuInS_2$ [17,18], 74 meV of CZTSe could to be related to the same Cu_{Zn}^{-} acceptor defect, but this assumption needs some further studies. As in CZTSe the p–d hybridisation is smaller and the valence band is higher, then it is expected that the activation energy of the Cu_{Zn}^{-} defect decreases

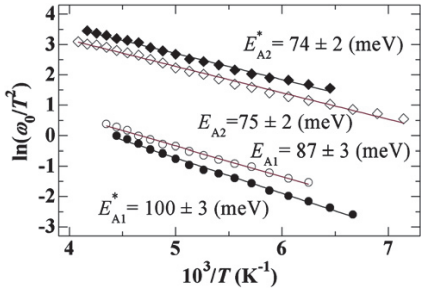

Fig. 4. The Arrhenius plot of the CZTSe/CdS heterojunction showing the activation energy values, where E_{A2} are for defect state and E_{A1} for interface states. White symbols and E_{A2} and E_{A1} correspond to the fresh device measurement, the black filled symbols and E^*_{A2} and E^*_{A1} show results for aged device. All dependencies were fitted with a linear function.

Table 1
Activation energies found by AS and PL of the measured heterojunctions. In brackets are results for aged device.

Material	AS results		PL results
	E_{A1} (meV)	E_{A2} (meV)	E_T (meV)
$Cu_2ZnSn(Se_{0.75}S_{0.25})_4$	154 ± 7	25 ± 5	39 ± 5
$Cu_2ZnSnSe_4$	87 ± 3 (100 ± 3)	75 ± 2 (74 ± 2)	69 ± 4

with increasing Se concentration in $Cu_2ZnSn(Se_xS_{1-x})_4$ [19]. As materials inspected are deficient in copper, V_{Cu}^{-} acceptors should also be present. Moreover, donor–acceptor defect complexes are also expected in this material. In CZTS and CZTSe the Cu_{Zn}^{-} antisite is deeper acceptor than V_{Cu}^{-} [9] and therefore can be detected by AS.

3.2. PL results

In Fig. 5(b) normalised PL spectra of the CZTSe and $Cu_2ZnSn(Se_{0.75}S_{0.25})_4$ monograins measured at $T = 10$ K are given. Both PL spectra show an asymmetric PL band at 0.946 eV for CZTSe and at 1.028 eV for $Cu_2ZnSn(Se_{0.75}S_{0.25})_4$. The asymmetric shape of the PL bands is an indication of the

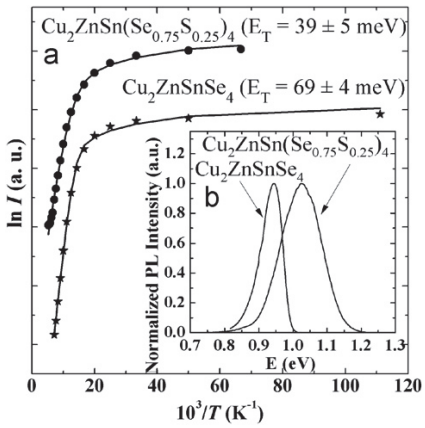

Fig. 5. The normalised PL spectra at 10 K (b) [21] and the Arrhenius plot derived from the temperature dependencies of these PL spectra (a).

presence of spatial potential fluctuations in the material [20] that are caused by high concentration of randomly distributed charged defects. The potential fluctuations are often found in multinary compounds where the native defect concentrations are usually very high [2,3,21]. These potential fluctuations lead to a local perturbation of the electronic band structure, thus broadening the defect level distribution and forming band tails [20]. Radiative recombination in the material containing spatial potential fluctuations can mainly arise from three different recombination channels. First, in band-to-band (BB) recombination a free electron recombines with a free hole. Second, in band-to-tail (BT) recombination a free electron recombines with a hole that is localised in the potential wells of the valence band tail. Third, in band-to-impurity (BI) recombination a free electron recombines with a hole that is localised on a deep acceptor level that is deep enough not to overlap with the valence band tail.

Temperature dependent and excitation power dependent measurements of the PL spectra indicate that the PL bands result from the BI—recombination. A strong blue-shift with a magnitude of 17 meV per decade for CZTSe and 11 meV per decade for $Cu_2ZnSn(Se_{0.75}S_{0.25})_4$ with increasing excitation power was detected. The Arrhenius plots derived from the temperature dependencies of the PL spectra [21] together with the fitting curves are presented in Fig. 5(a). For the fitting the temperature dependence of the integral intensity formula was used [22]

$$I(T) = I_0 / \left(1 + c_1 T^{3/2} + c_2 T^{3/2} \exp(-E_T/kT)\right) \quad (5)$$

where E_T is the activation energy. ln$I$ versus $10^3/T$ is used for the Arrhenius plot that shows linear behaviour at high temperatures which is characteristic for BI-recombination. The obtained defect ionisation energies, E_T can be found in Table 1.

By summarizing AS and PL results, defect ionisation energies found by PL are attributed to the same acceptor defects that were found from AS measurements, respectively. In CZTSSe the activation energy of the E_{A2} state seems not to be related to the same defect as in CZTSe or CZTS, but this behaviour needs further studies.

4. Conclusions

Admittance and photoluminescence spectroscopy were used for investigating defect levels in CZTSe/CdS and $Cu_2ZnSn(Se_{0.75}S_{0.25})_4$/CdS heterojunctions. Two defect states were observed in both materials by AS. The unstable defect state showed activation energies from 87 meV to 100 meV in CZTSe. This defect state was attributed to the interface states because possible change of interface properties with time could cause change of activation energy. The stable deep defect state in CZTSe was found to be at 74 meV and this could belong to Cu_{Zn}^{-} acceptor defect, but this assumption needs further studies. In CZTSSe activation energies 154 meV and 25 meV were found. In addition, these materials were studied by photoluminescence spectroscopy. An asymmetric PL band at 0.946 eV in CZTSe and at 1.028 eV in $Cu_2ZnSn(Se_{0.75}S_{0.25})_4$ were detected at 10 K. The obtained E_{A2} defect states at 69 meV for CZTSe and at 39 meV for $Cu_2ZnSn(Se_{0.75}S_{0.25})_4$ were attributed to the same acceptor defects that were found from AS measurements.

Acknowledgements

This work was supported by the Estonian Science Foundation Grants G-8282 and ETF 9369, by the Target Financing by HTM (Estonia) (No. SF0140099s08), Estonian Centre of Excellence in Research, Project TK117T, and by Materials Technology program. The support of the World Federation of Scientists National Scholarship Programme is gratefully acknowledged. The authors thank also the CZTSSe-team at the TUT.

References

[1] D.B. Mitzi, O. Gunawan, T.K. Todorov, K. Wang, S. Guha, Solar Energy Materials and Solar Cells 95 (2011) 1421.
[2] M. Grossberg, J. Krustok, K. Timmo, M. Altosaar, Thin Solid Films 517 (2009) 2489.
[3] J. Krustok, R. Josepson, T. Raadik, M. Danilson, Physica B 405 (2010) 3186.
[4] K. Ito, T. Nakazawa, Japanese Journal of Applied Physics 27 (1988) 2094.
[5] S. Bag, O. Gunawan, T. Gokmen, Y. Zhu, T.K. Todorov, D.B. Mitzi, Energy and Environmental Science 5 (2012) 7060.
[6] T.K. Todorov, J. Tang, S. Bag, O. Gunawan, T. Gokmen, Y. Zhu, D.B. Mitzi, Advanced Energy Materials 3 (2013) 34.
[7] B. Shin, O. Gunawan, Y. Zhu, N.A. Bojarczuk, S.J. Chey, S. Guha, Progress in Photovoltaics: Research and Applications 21 (2013) 72.
[8] F. Luckert, D.I. Hamilton, M.V. Yakushev, N.S. Beattie, G. Zoppi, M. Moynihan, I. Forbes, A.V. Karotki, A.V. Mudryi, M. Grossberg, J. Krustok, R.W. Martin, Applied Physics Letters 99 (2011) 062104.
[9] S. Chen, J.-H. Yang, X.G. Gong, A. Walsh, S.-H. Wei, Physical Review B 81 (2010) 245204.
[10] E. Kask, T. Raadik, M. Grossberg, R. Josepson, J. Krustok, Energy Procedia 10 (2011) 261.
[11] P.A. Fernandes, A.F. Sartori, P.M.P. Salomé, J. Malaquias, A.F. da Cunha, et al., Applied Physics Letters 100 (2012) 233504.
[12] O. Gunawan, T. Gokmen, C.W. Warren, J.D. Cohen, T.K. Todorov, et al., Applied Physics Letters 100 (2012) 253905.
[13] M. Altosaar, J. Raudoja, K. Timmo, M. Danilson, M. Grossberg, J. Krustok, E. Mellikov, Physica Status Solidi A 205 (2008) 167.
[14] H. Bayhan, A.S. Kavasoğlu, Turkish Journal of Physics 27 (2003) 529.
[15] R. Herberholz, M. Igalson, H.W. Schock, Journal of Applied Physics 83 (1998) 318.

[16] A. Jasenek, U. Rau, V. Nadenau, H.W. Schock, Journal of Applied Physics 87 (1) (2000) 594.
[17] S. Zott, K. Leo, M. Ruckh, H.W. Schock, Applied Physics Letters 68 (1996) 1144.
[18] J.H. Schön, E. Bucher, Physica Status Solidi A 171 (1999) 511.
[19] S. Chen, A. Walsh, J.-H. Yang, X.G. Gong, L. Sun, P.-X. Yang, J.-H. Chu, S.-H. Wei, Physical Review B 83 (2011) 125201.
[20] A.P. Levanyuk, V.V. Osipov, Soviet Physics Uspekhi 24 (1981) 187.
[21] M. Grossberg, J. Krustok, J. Raudoja, K. Timmo, M. Altosaar, T. Raadik, Thin Solid Films 519 (2011) 7403.
[22] J. Krustok, H. Collan, K. Hjelt, Journal of Applied Physics 81 (3) (1997) 1442.

APPENDIX A3

Article III

E. Kask, J. Krustok, S. Giraldo, M. Neuschitzer, S. López-Marino, E. Saucedo. Temperature dependent electrical characterization of thin film $Cu_2ZnSnSe_4$ solar cells. Journal of Physics D: Applied Physics 49(8) (2016) 085101.

IOP Publishing Journal of Physics D: Applied Physics
J. Phys. D: Appl. Phys. **49** (2016) 085101 (6pp) doi:10.1088/0022-3727/49/8/085101

Temperature dependent electrical characterization of thin film $Cu_2ZnSnSe_4$ solar cells

E Kask[1], J Krustok[1], S Giraldo[2], M Neuschitzer[2], S López-Marino[2] and E Saucedo[2]

[1] Tallinn University of Technology, Ehitajate tee 5, 19086 Tallinn, Estonia
[2] Catalonia Institute for Energy Research, IREC, Jardins de les Dones de Negre 1, 08930 Sant Adrià del Besòs, Barcelona, Spain

E-mail: erkki.kask@ttu.ee

Received 16 August 2015, revised 15 November 2015
Accepted for publication 18 November 2015
Published 25 January 2016

Abstract

Impedance spectroscopy (IS) and current–voltage characteristics measurements were applied to study properties of a $Cu_2ZnSnSe_4$ (CZTSe) thin film solar cell. IS measurements were done in the frequency range 20 Hz to 10 MHz. The measurement temperature was varied from 10 K to 325 K with a step $\Delta T = 5$ K. Temperature dependence of V_{oc} revealed an activation energy of 962 meV, which is in the vicinity of the band gap energy of CZTSe and hence the dominating recombination mechanism in this solar cell is bulk recombination. Different temperature ranges, where electrical properties change, were found. Interface states at grain boundaries with different properties were revealed to play an important role in impedance measurements. These states can be described by introducing a constant phase element in the equivalent circuit.

Keywords: $Cu_2ZnSnSe_4$, impedance spectroscopy, current–voltage characteristics, grain boundaries

(Some figures may appear in colour only in the online journal)

1. Introduction

Quaternary compound $Cu_2ZnSnSe_4$ (CZTSe) with a direct band gap and high absorption coefficient ($>10^4$) [1] is a promising absorber material for photovoltaics. Moreover, CZTSe is a low-cost non-toxic semiconductor material, whose elemental constituents are abundant in the Earth's crust. The current power conversion efficiency record of a CZTSe device is 11.6% [2]. Photovoltaic performance is hindered by a large variety of intrinsic lattice defects, which have influence on optical and electrical properties of solar cells. Little information about the defect structure of CZTSe can be found in the literature.

Defects have been studied by photoluminescence spectroscopy [3–6] and also by capacitive spectroscopy methods. In our previous works [7, 8] we studied so-called monograin solar cells consisting of a microcrystal absorber material, and different defect levels were detected. In CZTSe two defect states were observed by admittance spectroscopy (AS). The unstable defect state showed activation energies from 87 meV to 100 meV and was attributed to the interface states because the possible change of interface properties with time could alter activation energy. The second state at 74 meV was assumed to belong to Cu_{Zn}. These activation energies were found by measuring impedance Z and phase angle θ versus frequency f, and calculating capacitance C by employing an equivalent circuit, where a series resistor R_s is followed by a resistor R_p and a capacitor connected in parallel, (R_s and R_p cover series resistance of a structure, wires, contacts, etc, and shunt resistance of the junction, accordingly). Inverse temperature versus the natural logarithm of angular frequencies ω that correspond to a capacitance step showed linear dependence and this was used for activation energy calculation.

Weiss *et al* [9] have studied modelling equivalent circuit responses in kesterite solar cells and found that the evaluation of the admittance data cannot be performed simply with the as-measured capacitance data, as an increasing series resistance with decreasing temperature results in a capacitance step within the *C–f* profile. For instance, they suppose that measurements data need to be discarded at higher frequencies and at lower temperatures. In addition, they used current–voltage characteristics (*I–V*) to extract series and shunt resistances, but resistances found by direct current measurements are not perfectly suitable for replacing resistance values of alternating current measurements. Moreover, they used as-measured capacitance (meaning no series resistance exists) and later applied series resistance to it.

Goodman [10] showed that accurate measurement of capacitance requires both $R_s \ll R_p$ and $R_s \ll (\omega C)^{-1}$ so that the capacitive impedance is the dominant circuit element. Ordinarily, the quantity C is assumed to be frequency independent, but in experiments this is not always true; reasons may be, for example, charge relaxation times. In general, such effects tend to disappear with increasing frequency and may place a lower limit on the trustworthy frequency range. Moreover, limitations with respect to measurement equipment may place further restrictions upon the measurement frequency. These restrictions require that the resistance and geometry of the solar cell are suitably chosen.

Fernandes *et al* [11] have studied AS of Cu_2ZnSnS_4 (CZTS) solar cells and also applied various equivalent circuits to fit measured data. They calculated the deviation between measured and fitted data and found that their fitting of measured data is satisfsctory only via a quite complicated model. Usually, the more elements used in an equivalent circuit the better fit found, but in this case the interpretation is impossible or inappropriate. Moreover, Friesen *et al* [12] studied a thin film CdTe solar cell and state that as commonly applied equivalent circuit models consist only of frequency-independent circuit elements they cannot be used to describe the frequency dispersion of a thin film solar cell. They replaced the capacitor with a frequency-dependent non-ideal capacitor, called the constant phase element (CPE). It is generally assumed that non-ideal capacitance behaviour originates from a distribution in the current density due to material inhomogeneity and/or the grain boundaries [12]. The use of a CPE provides a better fitting for a depressed semicircle in the Nyquist plot.

According to our previous temperature-dependent measurements [13], three different temperature ranges, where electrical parameters change, were seen in monograin CZTS solar cells. At very low temperatures ($T < 40$ K) the effective band gap energy E_g^* and series resistance R_s showed steep changes and this behaviour was interpreted as hole blocking at a CZTSe/CdS heterojunction. Therefore the interface recombination rate turns out to be very low at $T < 40$ K.

Usually, impedance spectroscopy (IS) and AS measurements are conducted at higher temperatures because models are then more easily applied and understood. Unfortunately, at very low temperatures interpreting IS spectra is quite difficult. In this work, we analyze this complicated IS measurements data at very low temperatures and correlate with grain boundaries properties. Also, IS measurements frequency range limits are shown and results of *I–V* measurements and IS for a CZTSe thin film solar cell are presented and analyzed.

2. Experiment

A CZTSe absorber for this study was prepared by reactive thermal annealing of a metallic Cu/Sn/Cu/Zn precursor stack deposited by dc magnetron sputtering onto Mo-coated soda lime glass substrates, as described elsewhere in more detail [14]. The CZTSe absorber composition was measured by x-ray florescence spectroscopy showing cation ratios of Cu/(Zn + Sn) = 0.69, Zn/Sn = 1.45, Cu/Zn = 1.16 and Cu/Sn = 1.69. The details of the preparation of the thin film solar cell device are given in [15]. The individual solar cell (with dimensions $3 \times 3\,mm^2$) used for this study shows power conversion efficiency of $\eta = 6.6\%$ with $J_{sc} = 27.2$ mA cm^{-2}, $V_{oc} = 383$ mV and $FF = 64\%$.

For temperature-dependent measurements the selected thin film solar cells were mounted in a closed-cycle He cryostat (Janis). *I–V* curves were recorded using a Keithley SourceMeter 2401 with 100 mW cm^{-2} illumination. For a light source a standard 250 W halogen lamp with calibrated intensity was used. The impedance spectra curves were recorded using a Wayne Kerr 6500B impedance analyzer. For IS the impedance Z and phase angle θ were both measured as functions of frequency f and temperature T. The temperature was varied from 10 K to 300 K with a step $\Delta T = 5$ K. The used frequency was in the range 20 Hz to 10 MHz. In order to maintain the linearity of the response signal, the ac voltage was kept as low as 10 mV. The ac measurements were carried out in the dark and dc biases of 0 V and −0.5 V were used. After each measurement, the real and imaginary parts of the impedance, Z' and $-Z''$ respectively, were calculated. Measured data were fitted using the ZView (Scribner, USA) computer program, which gives values for elements used in an equivalent circuit; for example, series resistance, R_s.

3. Results and discussion

The studied solar cell exhibited an efficiency of 6.6%. Temperature dependence of the open circuit voltage (V_{oc}) derived from *I–V* measurements with varied temperature from $T = 10$ K to $T = 325$ K was linear in the range 250 K to 325 K (see figure 1). It is known that the temperature dependence of V_{oc} near room temperature can be presented as [16, 17]

$$V_{oc} = \frac{E_{A,V_{oc}}}{q} - \frac{nkT}{q} \ln\left(\frac{I_{00}}{I_L}\right), \tag{1}$$

where I_L, $E_{A,V_{oc}}$, n, k are the photocurrent, an activation energy, the diode ideality factor and the Boltzmann constant, respectively. The constant q is the electrical charge of the electron and I_{00} is obtained from the temperature dependence of the dark saturation current I_0. In good solar cells $-I_L \approx I_{sc}$, where I_{sc} is a short circuit current. I_0 equals [16, 17]

$$I_0 = I_{00} \exp\left(-\frac{E_{A,V_{oc}}}{nkT}\right) \approx AT^3 \cdot \exp\left(-\frac{E_{A,V_{oc}}}{nkT}\right). \tag{2}$$

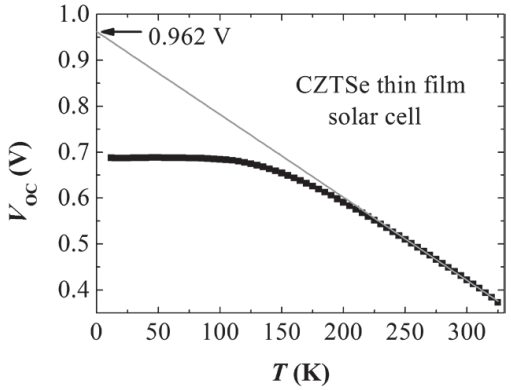

Figure 1. Temperature dependence of V_{oc} of a CZTSe thin film solar cell.

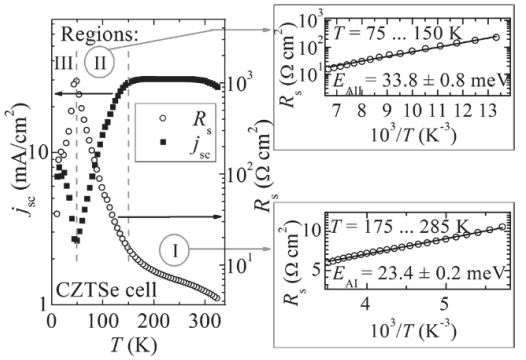

Figure 2. Temperature dependence of j_{sc}. Insets show found activation energies in region I and II.

In general, the activation energy $E_{A,V_{oc}}$ and also I_{00} depend mostly on the dominating recombination mechanism in the solar cell. In the case of bulk recombination $E_{A,V_{oc}} \approx E_g$, where E_g is the band gap energy of the absorber material.

Linear fitting of the temperature dependence of V_{oc} showed that $E_{A,V_{oc}} = 962$ meV (see figure 1), which is in good agreement with the band gap energy of CZTSe that is expected to be in the vicinity of 1 eV [4, 18], and hence the dominating recombination mechanism seems to be bulk recombination.

According to the temperature dependence of j_{sc} (see figure 2) three different temperature regions can be distinguished. Similar behaviour was also seen in CZTS [13]. At temperatures $T > 150$ K (region I) the series resistance R_s decreases with increasing temperature, indicating the thermal activation of carriers. In this region, R_s can be calculated by

$$R_S = R_{S0} \exp(E_A/kT), \tag{3}$$

where R_{s0} covers all parameters that are temperature-independent and E_A is an activation energy. Using equation (3), the activation energy $E_{AI} = 23.4 \pm 0.2$ meV was found in the temperature range 175 K to 285 K (region I). Similar values in kesterites have been published before, for example 29–48 meV [19, 20]. In our sample, the activation energy of 23.4 meV is related to grain boundaries or some shallow acceptor-like defect.

At intermediate temperatures (region II, $T = 50$ K to 150 K) another thermally activated process appears. Using equation (3), the activation energy $E_{AII} = 33.8$ meV was found in the temperature range $T = 75$ K to 150 K. In our previous studies [3, 4, 21] this activation energy was related to potential fluctuations of the valence band edge; it is the energy needed by holes to cross barriers that were created by these potential fluctuations. According to the literature, the root mean square depth of the potential well γ in CZTSe is usually in the range $\gamma = 20$–30 meV [3, 4, 21]. At the same time it is shown that in region II, the dependence of the series resistance on temperature changes and a typical Mott's variable-range hopping conduction starts to emerge [22]. This behaviour is expected in all heavily doped materials, where spatial potential fluctuations create deep potential wells for holes. But at the same time, we also expect an increasing role of bulk recombination in region II, as previously seen in CZTS [13]. At low temperatures ($T \lesssim 150$ K), the carriers, here holes, can occupy shallow acceptor states in the band gap. These states can arise from intrinsic defects or impurities or their interaction. At a sufficiently high concentration of these states, but below the critical Mott concentration, overlapping of carriers wave functions could form a so-called impurity band [23]. In such a case charge carriers can move from one shallow impurity state to another one at its spatial neighbourhood and conduction in the impurity band is expected [22]. These different processes could all be present and therefore we do not focus so much on activation energy here.

At low temperatures (region III, $T = 10$ K–50 K) the maximum of series resistance is present. By analyzing j_{sc} and *I*–*V* graphs (see figure 3), it can be seen that *I*–*V* curves have similar shapes symmetrically to both sides of 50 K. Also, impedance curves have quite similar patterns symmetrically to the temperature of $T = 50$ K in the Nyquist plot (compare the complex impedances at 10 K and 100 K in figure 4). The sudden drop in resistance below 50 K seems to be related to blocking of the interface recombination. The rapid change in the series resistance can occur because of cooling of the recombination processes: generated holes are not able to tunnel through the potential barrier into the interface region between CZTSe and CdS and therefore the interface recombination rate must be very small at these very low temperatures ($T = 10$ K–50 K) [13].

IS is a powerful non-destructive tool for characterizing semiconductors. IS detects the ac current response of a system to a small ac voltage signal with varied frequency. The impedance can be calculated by $Z = V/I$. From complex impedance the capacitance can be calculated, but this requires a certain equivalent circuit to be known. The temperature dependence of Z' and $-Z''$ of the CZTSe thin film solar cell is shown in figure 4.

Our measured impedance curves in the Nyquist plot in the whole temperature range can be fitted by applying an equivalent circuit, where a series resistor is followed by a resistor and a capacitor connected in parallel and followed by additional elements (R_{p2} and CPE) connected in parallel (circuit

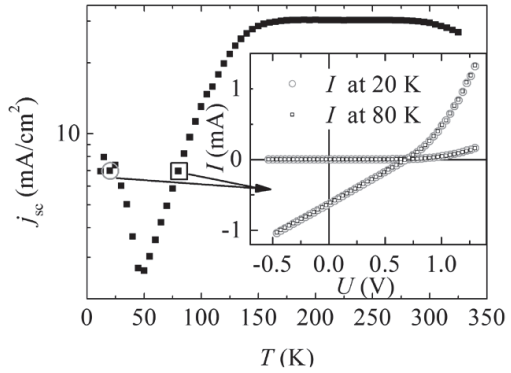

Figure 3. Temperature dependence of j_{sc}. Inset shows *I–V* curve shape similarity between both sides of 50 K at different temperatures.

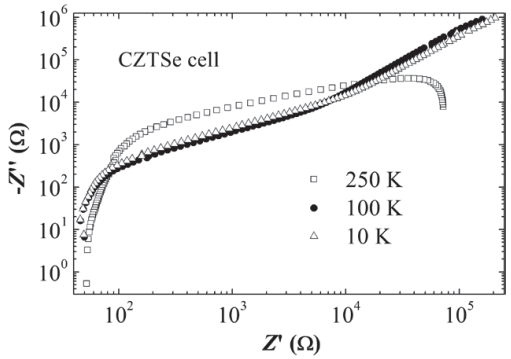

Figure 4. Nyquist plots. Selection of impedance curves of the CZTSe thin film solar cell in the logarithmic scale at temperatures 250 K, 100 K and 10 K.

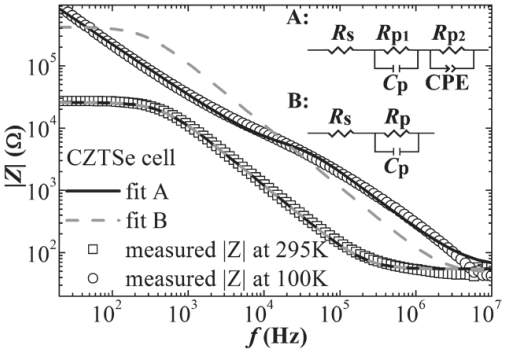

Figure 5. Measured impedance of the CZTSe solar cell and fitting results with corresponding equivalent circuits. A better fit was obtained by A. Commonly used equivalent circuit B is not suitable at lower temperatures $T \lesssim 150$ K. At room temperature no enormous difference was seen.

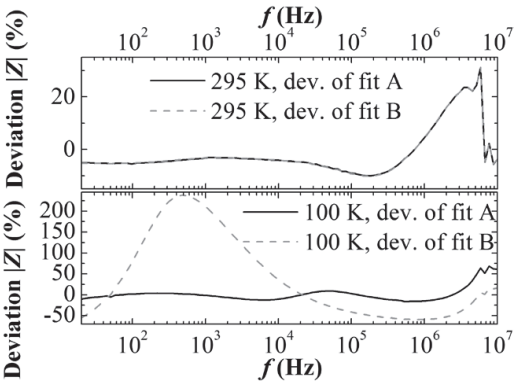

Figure 6. Fitting deviations of |Z| versus frequency at temperatures 295 K and 100 K of the CZTSe solar cell.

A in figure 5). The used complex impedance of a CPE, Z_{CPE} is given by

$$Z_{CPE} = \frac{1}{C_{CPE} \cdot (i * \omega)^P}, \tag{4}$$

where C_{CPE} is equal to capacitance C, if parameter $P = 1$. ω stands for angular frequency. But fitting of high temperature IS curves is also satisfactory with an equivalent circuit, where a series resistor is followed by a resistor and a capacitor connected in parallel (circuit B in figure 5). In figure 5 both theoretical fittings and experimental data curves are shown. In figure 6 the deviation between theoretical and experimental impedance data is shown. It is clearly seen that at room temperature there is no difference between fittings with circuits A and B, but the deviation between fitted and measured |Z| increases at higher frequencies. At low temperatures, i.e. $T \lesssim 150$ K, the equivalent circuit B was not suitable at all, and the equivalent circuit A fitting deviation of measured |Z| is enormously high (more than 50%) at quite high frequencies. Obviously, condition $R_s \ll (\omega C)^{-1}$ [10] is not satisfied at higher frequencies. It was checked by calculations and found that this condition is satisfied at frequencies $f < 3.7$ MHz at 100 K and at $f < 250$ kHz at room temperature. Moreover, measurement instrumentation capabilities have limits and affect measurements data. At low frequency, the fitting deviations of |Z| were not significant. Hence, IS results at higher frequencies are not trustworthy, and wide fitting deviations of |Z| coincide with neglecting the condition $R_s \ll (\omega C)^{-1}$.

At every measured temperature values of the equivalent circuit elements can be found by exploiting the *Z* view program for fitting. In turn, the R_s values can be used to calculate the capacitance. When assuming series inductance to be insignificant or absent, equivalent circuit B can be described by the following equation [24]:

$$Z = R_S + \frac{R_P}{1 + (\omega R_P C)^2} - i\frac{R_P^2 C\omega}{1 + (\omega R_P C)^2}, \tag{5}$$

where ω, C and R_P are angular frequency, capacitance and parallel resistance, respectively. After rewriting (5), the capacitance can be found by

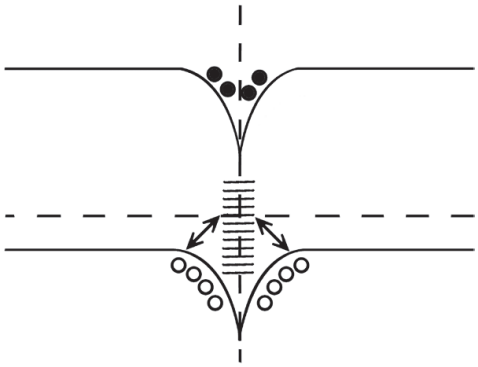

Figure 7. Grain boundary located between grains in the thin film solar cell. Some interface states are affected at quite low temperatures and these impact fittings of measured data.

$$C = \frac{-Z''}{[(Z' - R_S)^2 + (-Z'')^2] \cdot \omega}, \quad (6)$$

where Z' and $-Z''$ are the real and imaginary part of the complex impedance, respectively. Equation (6) can be used for capacitance calculation, if equivalent circuit B is applied for the fittings. In equivalent circuit A, CPE is used and in this case equations (5) and (6) would take a much more complicated form and the calculation of capacitance would not be straightforward. Thus, in the case of our studied CZTSe thin film solar cell capacitance should be derived by using equivalent circuit B and valid results are obtained only at higher temperatures ($T = 150$ K to 325 K). However, IS results are also beneficial in this low temperature range, because they add complementary or confirmative details about processes.

Temperature dependence of electrical parameters seen by IS in the CZTSe thin film solar cell at $T \lesssim 150$ K can be explained by grain boundaries, see figure 7. It seems that some interface states at grain boundaries are affected and change electrical properties of the studied cell at low temperatures. These states may not show a real capacitance, but can be explained by CPE in the equivalent circuit due to grain boundaries with different properties. This extra capacity is caused by holes being captured by interface states in grain boundaries, which are below the Fermi level, and released by states, which are above the Fermi level. If the cell is contacted and being electrically disturbed, then the band bending and hence crossing between Fermi level and interface states change. As a result, charging or discharging of these states occurs and capacitance can be detected.

As a result of this kind of capacitance change at low temperatures $T \lesssim 150$ K, where grain boundary states are affected, we need to add extra elements to our equivalent circuit. At high temperatures ($T = 150$ K–325 K), where grain boundary states do not contribute to capacitance, both equivalent circuits give excellent results. This low temperature ($T = 10$ K–150 K) behaviour, which requires the use of CPE and is present in the studied CZTSe thin film solar cells, was not seen in our previous research on monograin solar cells, where the role of grain boundaries was not so notable [7, 8].

4. Conclusions

IS and current–voltage characteristics were used for characterizing the CZTSe thin film solar cell. Different temperature ranges where electrical properties change were seen. Fittings of impedance data showed that some interface states at grain boundaries are affected at low temperatures. These states can be described by CPE in equivalent circuits due to grain boundaries with different properties. Linear fitting of temperature dependence of V_{oc} showed activation energy $E_A = 962$ meV, which is in good agreement with the band gap of CZTSe. Hence the dominating recombination mechanism seemed to be bulk recombination in the studied thin film solar cell. From temperature dependence of j_{sc} the activation energies were found. In the temperature range from 175 K to 285 K the activation energy of 23.4 meV is related to the energy needed to cross the grain boundaries or some shallow acceptor-like defect. At intermediate temperatures, from 75 K to 150 K different processes like carrier localization in potential wells, radiative recombination and Mott's variable-range hopping conduction start to come into effect, showing an activation energy of $E_{AII} = 33.8$ meV. In conclusion we have shown that temperature dependent impedance and *I–V* studies can give a valuable insight into electronic processes related to grain boundaries and interfaces in solar cells.

Acknowledgment

This work was supported by the Estonian Science Foundation grant ETF 9369, by the institutional research funding IUT 19–28 of the Estonian Ministry of Education and Research, and by FP7 project CHEETAH, EC grant agreement no. 609788, by project KESTCELLS (FP7-PEOPLE-2012-ITN-316488) and by European Regional Development Funds (ERDF, FEDER Programa Competitivitat de Catalunya 2007–2013). The authors from IREC and the University of Barcelona belong to the M-2E (Electronic Materials for Energy) Consolidated Research Group and the XaRMAE Network of Excellence on Materials for Energy of the 'Generalitat de Catalunya'. S G thanks the Government of Spain for the FPI fellowship (BES-2014–068533) and E S for the 'Ramon y Cajal' fellowship (RYC-2011–09212).

References

[1] Ito K and Nakazawa T 1988 Electrical and optical properties of stannite-type quaternary semiconductor thin films *Japan. J. Appl. Phys.* **27** 2094

[2] Lee Y S, Gershon T, Gunawan O, Todorov T K, Gokmen T, Virgus Y and Guha S 2015 $Cu_2ZnSnSe_4$ thin-film solar cells by thermal co-evaporation with 11.6% efficiency and improved minority carrier diffusion length *Adv. Energy Mater.* **5** 1401372–5

[3] Grossberg M, Krustok J, Raudoja J, Timmo K, Altosaar M and Raadik T 2011 Photoluminescence and Raman study of $Cu_2ZnSn(Se_xS_{1-x})_4$ monograins for photovoltaic applications *Thin Solid Films* **519** 7403–6

[4] Grossberg M, Krustok J, Timmo K and Altosaar M 2009 Radiative recombination in $Cu_2ZnSnSe_4$ monograins

studied by photoluminescence spectroscopy *Thin Solid Films* **517** 2489–92

[5] Oueslati S, Brammertz G, Buffiére M, Köble C, Oualid T, Meuris M and Poortmans J 2015 Photoluminescence study and observation of unusual optical transitions in $Cu_2ZnSnSe_4$/CdS/ZnO solar cells *Sol. Energy Mater. Sol. Cells* **134** 340–5

[6] Yakushev M V, Forbes I, Mudryi A V, Grossberg M, Krustok J, Beattie N S, Moynihan M, Rockett A and Martin R W 2015 Optical spectroscopy studies of $Cu_2ZnSnSe_4$ thin films *Thin Solid Films* **582** 154–7

[7] Kask E, Raadik T, Grossberg M, Josepson R and Krustok J 2011 Deep defects in Cu_2ZnSnS_4 monograin solar cells *Energy Proc.* **10** 261–5

[8] Kask E, Grossberg M, Jospeson R, Salu P, Timmo K and Krustok J 2013 Defect studies in $Cu_2ZnSnSe_4$ and $Cu_2ZnSn(Se_{0.75}S_{0.25})_4$ by admittance and photoluminescence spectroscopy *Mater. Sci. Semicond. Process.* **16** 992–6

[9] Weiss T P, Redinger A, Luckas J, Mousel M and Siebentritt S 2013 Admittance spectroscopy in kesterite solar cells: defect signal or circuit response *Appl. Phys. Lett.* **104** 202105

[10] Goodman A M 1963 Metal–semiconductor barrier height measurement by the differential capacitance method—one carrier system *J. Appl. Phys.* **34** 329–38

[11] Fernandes P A, Sartori A F, Salomé P M P, Malaquias J, da Cunha A F, Graça M P F and González J C 2012 Admittance spectroscopy of Cu_2ZnSnS_4 based thin film solar cells *Appl. Phys. Lett.* **100** 233504

[12] Friesen G, Özsar M E and Dunlop E D 2000 Impedance model for CdTe solar cells exhibiting constant phase element behaviour *Thin Solid Films* **361–362** 303–8

[13] Danilson M, Kask E, Pokharel N, Kauk-Kuusik M, Varema T and Krustok J 2015 Temperature dependent current transport properties in Cu_2ZnSnS_4 solar cells *Thin Solid Films* **582** 162–5

[14] López-Marino S *et al* 2013 ZnSe etching of Zn-Rich $Cu_2ZnSnSe_4$: an oxidation route for improved solar-cell efficiency *Chem. Eur. J.* **19** 14814–22

[15] Krustok J, Raadik T, Grossberg M, Giraldo S, Neuschitzer M, López-Marino S and Saucedo E 2015 Temperature dependent electroreflectance study of $Cu_2ZnSnSe_4$ solar cells *Mater. Sci. Semicond. Process.* **39** 251–4

[16] Krustok J, Josepson R, Danilson M and Meissner D 2010 Temperature dependence of $Cu_2ZnSn(Se_xS_{1-x})_4$ monograin solar cells *Solar Energy* **84** 379–83

[17] Rau U and Schock H W 1999 Electronic properties of Cu(In,Ga)Se_2 heterojunction solar cells—recent achievements, current understanding, and future challenges *Appl. Phys.* A **69** 131–47

[18] Raulot J M, Domain C and Guillemoles J F 2005 *Ab initio* investigation of potential indium and gallium free chalcopyrite compounds for photovoltaic application *J. Phys. Chem. Solids* **66** 2019–23

[19] Leitão J P, Santos N M, Fernandes P A, Salomé P M P, da Cunha A F, González J C, Ribeiro G M and Matinaga F M 2011 Photoluminescence and electrical study of fluctuating potentials in Cu_2ZnSnS_4-based thin films *Phys. Rev.* B **84** 024120

[20] Kosyak V, Karmarkar M A and Scarpulla M A 2012 Temperature dependent conductivity of polycrystalline Cu_2ZnSnS_4 thin films *Appl. Phys. Lett.* **100** 263903

[21] Krustok J, Josepson R, Raadik T and Danilson M 2010 Potential fluctuations in $Cu_2ZnSnSe_4$ solar cells studied by temperature dependence of quantum efficiency curves *Physica* B **405** 3186–9

[22] Mott N F 1976 Impurity band conduction. Experiment and theory the metal–insulator transition in an impurity band *J. Phys. Colloq.* **37** C4-301–6

[23] Song X, Böttger P H M, Karlsen O B, Finstad T G and Taftø J 2012 Impurity band conduction in the thermoelectric material ZnSb *Phys. Scr.* **T148** 014001

[24] Bayhan H and Kavasoğlu A S 2003 Admittance and impedance spectroscopy on Cu(In,Ga)Se_2 solar cells *Turk. J. Phys.* **27** 529–35

APPENDIX B

Curriculum Vitae

Ees- ja perekonnanimi	Erkki Kask
Sünniaeg ja -koht	22. juuni 1984, Noarootsi, Eesti
Kodakondsus	Eesti
E-post	erkki.kask@ttu.ee

Hariduskäik

Õppeasutus	*Lõpetamise aeg*	*Haridus/kraad*
Tallinna Tehnikaülikool	...	doktorantuur
Tallinna Tehnikaülikool	2010	loodusteaduse magistri (rakendusfüüsika) kraad, tehnilise füüsika õppekava
Tallinna Tehnikaülikool	2008	loodusteaduse bakalaureuse kraad, tehnilise füüsika õppekava
Noarootsi Gümnaasium	2005	keskharidus

Keelteoskus

Keel	*Tase*
eesti	emakeel, kõrgtase
inglise	kesktase
rootsi	kesktase
soome	algtase

Täiendusõpe

17.11.2015 – 21.11.2015 6th European Kesterite Workshop, Newcastle, UK

15.06.2015 – 20.06.2015 INP-Grenoble (IMEP-LAHC), Grenoble, Prantsusmaa

08.09.2013 – 15.09.2013 International Summer School on Photovoltaics and New Concepts of Quantum Solar Energy Conversion, Quantsol 2013, Hirschegg, Kleinwalsertal, Austria.

14.05.2012 – 18.05.2012 EMRS konverents, Strasbourg, Prantsusmaa

19.03.2012 – 17.04.2012 Politechnika Warszawska, Poola, Varssavi.

09.05.2011 – 13.05.2011 EMRS konverents, Nice, Prantsusmaa

Märts 2011	TÜ ja TTÜ Doktorikooli „Funktsionaalsed materjalid ja tehnoloogiad“ teaduskonverents.

Teenistuskäik

01.02.2016 – …	Tallinna Tehnikaülikool, Füüsikainstituut, nooremteadur (osalise ajaga)
01.02.2013 – 31.01.2016	Tallinna Tehnikaülikool, Füüsikainstituut, assistent (osalise ajaga)
01.09.2012 – 31.01.2013	Tallinna Tehnikaülikool, Füüsikainstituut, tunnitasuline
21.05.2012 – …	Aditro Estonia OÜ, Payroll Analyst (osalise ajaga)
01.09.2010 – 31.01.2011	Tallinna Tehnikaülikool, Füüsikainstituut, tunnitasuline
01.03.2009 – 01.05.2009	Balti Kriminaalpreventatsiooni ja Sotsiaalse Rehabilitatsiooni Instituut, IT spetsialist
07.04.2008 – 06.08.2009	Astangu Kutserehabilitatsiooni Keskus, hooldaja abiline, asendusteenistus
15.09.2006 – 31.03.2008	Haapsalu Tööotsijate Ühing, IT spetsialist
19.05.2004 – 31.08.2004	Haapsalu Tööotsijate Ühing, haljastustööline
19.05.2003 – 31.08.2003	Haapsalu Tööotsijate Ühing, tööline
27.05.2002 – 05.07.2002	Uusimaa OY, suvetööline trükikojas

Kaitstud lõputööd

„μ-Raman spektroskoopia rakendused nelikühendite optilisteks mõõtmisteks“,

magistritöö, juhendaja prof. Jüri Krustok, 2010.

„EPR metoodika ja kasutusalade edasiarendus“, bakalaureusetöö, juhendaja prof. Kalju Lott, 2008.

Teadustegevuse kirjeldus

Osalemine projektides

2014 – 2019	Uued materjalid ja tehnoloogiad päikeseenergeetikale, täitja
2014 – 2017	Päikesepaneelide maksumuse vähendamine läbi materjalide optimeerimise ning väljundenergia suurendamise - Euroopa teadus-ja arendusasutuste koostöös – CHEETAH, põhitäitja
2012 – 2016	Kesteriitsete absorbermaterjalide optilised uuringud, põhitäitja
2012 – 2015	Mittetoksilistest ja maapõues laialt levinud materjalidest valmistatud monoterakiht päikesepatareide arendamine, põhitäitja
2010 – 2013	Rekombinatsioonilised kaod CZTS(Se) päikesepatareides, põhitäitja

Tunnustused

2013	LETS stipendium
2012	World Federation of Scientists

Juhendatud lõputööd

2015 Xingxing Kong, „Schottky kontaktide analüüs Cu_2ZnSnS_4 monoterakihtide baasil“, magistritöö, kaasjuhendajana

2013 Mihkel Tiganik, „Metastabiilsed olekud Cu_2ZnSnS_4 monoteralistes päikesepatareides“, bakalaureusetöö, kaasjuhendajana

Curriculum Vitae

First name and surname	Erkki Kask
Date and place of birth	22nd of June, 1984, Noarootsi, Estonia
Citizenship	Estonian
E-mail	erkki.kask@ttu.ee

Education

Educational institution	*Graduation year*	*field of study/degree*
Tallinn University of Technology	...	doctoral studies
Tallinn University of Technology	2010	Master of Science in Natural Sciences (Applied Physics), Engineering Physics curriculum
Tallinn University of Technology	2008	Bachelor of Science in Natural Sciences, Engineering Physics curriculum
Noarootsi Gümnaasium	2005	secondary education

Language competence

Language	*Level*
Estonian	native language, fluent
English	average
Swedish	average
Finnish	basic skills

Special courses

17.11.2015 – 21.11.2015 6th European Kesterite Workshop, Newcastle, UK

15.06.2015 – 20.06.2015 INP-Grenoble (IMEP-LAHC), Grenoble, France

08.09.2013 – 15.09.2013 International Summer School on Photovoltaics and New Concepts of Quantum Solar Energy Conversion, Quantsol 2013, Hirschegg, Kleinwalsertal, Austria

14.05.2012 – 18.05.2012 EMRS Spring Meeting, Strasbourg, France

19.03.2012 – 17.04.2012 Politechnika Warszawska, Poland, Warsaw

09.05.2011 – 13.05.2011 EMRS Spring Meeting, Nice, France

March 2011	TU and TUT Graduate school „Functional materials and technologies“ conference.

Professional employment

01.02.2016 – …	Tallinn University of Technology, Department of Physics, Early Stage Researcher (part time)
01.02.2013 – 31.01.2016	Tallinn University of Technology, Department of Physics, Teaching Assistant (part time)
01.09.2012 – 31.01.2013	Tallinn University of Technology, Department of Physics, hourly pay teaching staff
21.05.2012 – …	Aditro Estonia OÜ, Payroll Analyst (part time)
01.09.2010 – 31.01.2011	Tallinna University of Technology, Department of Physics, hourly pay teaching staff
01.03.2009 – 01.05.2009	Balti Kriminaalpreventatsiooni ja Sotsiaalse Rehabilitatsiooni Instituut, Computer Support Servicer
07.04.2008 – 06.08.2009	Astangu Kutserehabilitatsiooni Keskus, Social Care Worker
15.09.2006 – 31.03.2008	Haapsalu Tööotsijate Ühing, Computer Support Servicer
19.05.2004 – 31.08.2004	Haapsalu Tööotsijate Ühing, landscaping worker
19.05.2003 – 31.08.2003	Haapsalu Tööotsijate Ühing, worker
27.05.2002 – 05.07.2002	Uusimaa OY, Summer Intern in Printing House

Defended dissertations

“μ-Raman spectroscopy applications for optical measurements of quaternary compounds”, master’s thesis, supervisor prof. Jüri Krustok, 2010.

"Development of methods and applications of EPR", bachelor's thesis, supervisor prof. Kalju Lott, 2008.

Research activity

Projects

2014 – 2015	New materials and technologies for solar energetics, executor
2014 – 2017	Cost-reduction through material optimisation and higher energy output of solar photovoltaic modules - joining Europes's research and development efforts in support of its PV industry CHEETAH, research staff
2012 – 2016	Optical studies of kesterite type absorber materials, research staff
2012 – 2015	Development of CZTS monograin powders towards abundant and non-toxic materials for solar cells, research staff
2010 – 2013	Recombination losses in CZTS(Se) solar cells, research staff

Recognition

2013	LETS scholarship
2012	World Federation of Scientists scholarship

Supervised dissertations

2015 Xingxing Kong, „Schottky contact analysis for Cu_2ZnSnS_4 monograin membranes", Master's thesis, co-supervisor

2013 Mihkel Tiganik, „Metastabilities in Cu_2ZnSnS_4 monograin solar cells", Bachelor's thesis, co-supervisor

List of publications

1. **E. Kask**, J. Krustok, S. Giraldo, M. Neuschitzer, S. López-Marino, E. Saucedo. Temperature dependent electrical characterization of thin film $Cu_2ZnSnSe_4$ solar cells. Journal of Physics D: Applied Physics 49(8) (2016) 085101.
2. M. Danilson, **E. Kask**, N. Pokharel, M. Grossberg, M. Kauk-Kuusik, T. Varema, J. Krustok. Temperature dependent current transport properties in Cu_2ZnSnS_4 solar cells. Thin Solid Films 582 (2015) 162-165.
3. **E. Kask**, M. Grossberg, R. Josepson, P. Salu, K. Timmo, J. Krustok. Defect studies in $Cu_2ZnSnSe_4$ and $Cu_2ZnSn(Se_{0.75}S_{0.25})_4$ by admittance and photoluminescence spectroscopy. Materials Science in Semiconductor Processing 16(3) (2013) 992 - 996.
4. **E. Kask**, T. Raadik, M. Grossberg, R. Josepson, J. Krustok. Deep defects in Cu_2ZnSnS_4 monograin solar cells. Energy Procedia 10 (2011) 261-265.

DISSERTATIONS DEFENDED AT
TALLINN UNIVERSITY OF TECHNOLOGY ON
NATURAL AND EXACT SCIENCES

1. **Olav Kongas**. Nonlinear Dynamics in Modeling Cardiac Arrhytmias. 1998.
2. **Kalju Vanatalu**. Optimization of Processes of Microbial Biosynthesis of Isotopically Labeled Biomolecules and Their Complexes. 1999.
3. **Ahto Buldas**. An Algebraic Approach to the Structure of Graphs. 1999.
4. **Monika Drews**. A Metabolic Study of Insect Cells in Batch and Continuous Culture: Application of Chemostat and Turbidostat to the Production of Recombinant Proteins. 1999.
5. **Eola Valdre**. Endothelial-Specific Regulation of Vessel Formation: Role of Receptor Tyrosine Kinases. 2000.
6. **Kalju Lott**. Doping and Defect Thermodynamic Equilibrium in ZnS. 2000.
7. **Reet Koljak**. Novel Fatty Acid Dioxygenases from the Corals *Plexaura homomalla* and *Gersemia fruticosa.* 2001.
8. **Anne Paju**. Asymmetric oxidation of Prochiral and Racemic Ketones by Using Sharpless Catalyst. 2001.
9. **Marko Vendelin**. Cardiac Mechanoenergetics *in silico*. 2001.
10. **Pearu Peterson**. Multi-Soliton Interactions and the Inverse Problem of Wave Crest. 2001.
11. **Anne Menert**. Microcalorimetry of Anaerobic Digestion. 2001.
12. **Toomas Tiivel**. The Role of the Mitochondrial Outer Membrane in *in vivo* Regulation of Respiration in Normal Heart and Skeletal Muscle Cell. 2002.
13. **Olle Hints**. Ordovician Scolecodonts of Estonia and Neighbouring Areas: Taxonomy, Distribution, Palaeoecology, and Application. 2002.
14. **Jaak Nõlvak**. Chitinozoan Biostratigrapy in the Ordovician of Baltoscandia. 2002.
15. **Liivi Kluge**. On Algebraic Structure of Pre-Operad. 2002.
16. **Jaanus Lass**. Biosignal Interpretation: Study of Cardiac Arrhytmias and Electromagnetic Field Effects on Human Nervous System. 2002.
17. **Janek Peterson**. Synthesis, Structural Characterization and Modification of PAMAM Dendrimers. 2002.
18. **Merike Vaher**. Room Temperature Ionic Liquids as Background Electrolyte Additives in Capillary Electrophoresis. 2002.
19. **Valdek Mikli**. Electron Microscopy and Image Analysis Study of Powdered Hardmetal Materials and Optoelectronic Thin Films. 2003.
20. **Mart Viljus**. The Microstructure and Properties of Fine-Grained Cermets. 2003.
21. **Signe Kask**. Identification and Characterization of Dairy-Related *Lactobacillus.* 2003.
22. **Tiiu-Mai Laht**. Influence of Microstructure of the Curd on Enzymatic and Microbiological Processes in Swiss-Type Cheese. 2003.
23. **Anne Kuusksalu**. 2–5A Synthetase in the Marine Sponge *Geodia cydonium*. 2003.

24. **Sergei Bereznev**. Solar Cells Based on Polycristalline Copper-Indium Chalcogenides and Conductive Polymers. 2003.
25. **Kadri Kriis**. Asymmetric Synthesis of C_2-Symmetric Bimorpholines and Their Application as Chiral Ligands in the Transfer Hydrogenation of Aromatic Ketones. 2004.
26. **Jekaterina Reut**. Polypyrrole Coatings on Conducting and Insulating Substracts. 2004.
27. **Sven Nõmm**. Realization and Identification of Discrete-Time Nonlinear Systems. 2004.
28. **Olga Kijatkina**. Deposition of Copper Indium Disulphide Films by Chemical Spray Pyrolysis. 2004.
29. **Gert Tamberg**. On Sampling Operators Defined by Rogosinski, Hann and Blackman Windows. 2004.
30. **Monika Übner**. Interaction of Humic Substances with Metal Cations. 2004.
31. **Kaarel Adamberg**. Growth Characteristics of Non-Starter Lactic Acid Bacteria from Cheese. 2004.
32. **Imre Vallikivi**. Lipase-Catalysed Reactions of Prostaglandins. 2004.
33. **Merike Peld**. Substituted Apatites as Sorbents for Heavy Metals. 2005.
34. **Vitali Syritski**. Study of Synthesis and Redox Switching of Polypyrrole and Poly(3,4-ethylenedioxythiophene) by Using *in-situ* Techniques. 2004.
35. **Lee Põllumaa**. Evaluation of Ecotoxicological Effects Related to Oil Shale Industry. 2004.
36. **Riina Aav**. Synthesis of 9,11-Secosterols Intermediates. 2005.
37. **Andres Braunbrück**. Wave Interaction in Weakly Inhomogeneous Materials. 2005.
38. **Robert Kitt**. Generalised Scale-Invariance in Financial Time Series. 2005.
39. **Juss Pavelson**. Mesoscale Physical Processes and the Related Impact on the Summer Nutrient Fields and Phytoplankton Blooms in the Western Gulf of Finland. 2005.
40. **Olari Ilison**. Solitons and Solitary Waves in Media with Higher Order Dispersive and Nonlinear Effects. 2005.
41. **Maksim Säkki**. Intermittency and Long-Range Structurization of Heart Rate. 2005.
42. **Enli Kiipli**. Modelling Seawater Chemistry of the East Baltic Basin in the Late Ordovician–Early Silurian. 2005.
43. **Igor Golovtsov**. Modification of Conductive Properties and Processability of Polyparaphenylene, Polypyrrole and polyaniline. 2005.
44. **Katrin Laos**. Interaction Between Furcellaran and the Globular Proteins (Bovine Serum Albumin β-Lactoglobulin). 2005.
45. **Arvo Mere**. Structural and Electrical Properties of Spray Deposited Copper Indium Disulphide Films for Solar Cells. 2006.
46. **Sille Ehala**. Development and Application of Various On- and Off-Line Analytical Methods for the Analysis of Bioactive Compounds. 2006.
47. **Maria Kulp**. Capillary Electrophoretic Monitoring of Biochemical Reaction Kinetics. 2006.

48. **Anu Aaspõllu.** Proteinases from *Vipera lebetina* Snake Venom Affecting Hemostasis. 2006.
49. **Lyudmila Chekulayeva**. Photosensitized Inactivation of Tumor Cells by Porphyrins and Chlorins. 2006.
50. **Merle Uudsemaa**. Quantum-Chemical Modeling of Solvated First Row Transition Metal Ions. 2006.
51. **Tagli Pitsi**. Nutrition Situation of Pre-School Children in Estonia from 1995 to 2004. 2006.
52. **Angela Ivask**. Luminescent Recombinant Sensor Bacteria for the Analysis of Bioavailable Heavy Metals. 2006.
53. **Tiina Lõugas**. Study on Physico-Chemical Properties and Some Bioactive Compounds of Sea Buckthorn (*Hippophae rhamnoides* L.). 2006.
54. **Kaja Kasemets**. Effect of Changing Environmental Conditions on the Fermentative Growth of *Saccharomyces cerevisae* S288C: Auxo-accelerostat Study. 2006.
55. **Ildar Nisamedtinov**. Application of ^{13}C and Fluorescence Labeling in Metabolic Studies of *Saccharomyces* spp. 2006.
56. **Alar Leibak**. On Additive Generalisation of Voronoï's Theory of Perfect Forms over Algebraic Number Fields. 2006.
57. **Andri Jagomägi**. Photoluminescence of Chalcopyrite Tellurides. 2006.
58. **Tõnu Martma**. Application of Carbon Isotopes to the Study of the Ordovician and Silurian of the Baltic. 2006.
59. **Marit Kauk**. Chemical Composition of $CuInSe_2$ Monograin Powders for Solar Cell Application. 2006.
60. **Julia Kois**. Electrochemical Deposition of $CuInSe_2$ Thin Films for Photovoltaic Applications. 2006.
61. **Ilona Oja Açik**. Sol-Gel Deposition of Titanium Dioxide Films. 2007.
62. **Tiia Anmann**. Integrated and Organized Cellular Bioenergetic Systems in Heart and Brain. 2007.
63. **Katrin Trummal**. Purification, Characterization and Specificity Studies of Metalloproteinases from *Vipera lebetina* Snake Venom. 2007.
64. **Gennadi Lessin**. Biochemical Definition of Coastal Zone Using Numerical Modeling and Measurement Data. 2007.
65. **Enno Pais**. Inverse problems to determine non-homogeneous degenerate memory kernels in heat flow. 2007.
66. **Maria Borissova**. Capillary Electrophoresis on Alkylimidazolium Salts. 2007.
67. **Karin Valmsen**. Prostaglandin Synthesis in the Coral *Plexaura homomalla*: Control of Prostaglandin Stereochemistry at Carbon 15 by Cyclooxygenases. 2007.
68. **Kristjan Piirimäe**. Long-Term Changes of Nutrient Fluxes in the Drainage Basin of the Gulf of Finland – Application of the PolFlow Model. 2007.
69. **Tatjana Dedova**. Chemical Spray Pyrolysis Deposition of Zinc Sulfide Thin Films and Zinc Oxide Nanostructured Layers. 2007.
70. **Katrin Tomson**. Production of Labelled Recombinant Proteins in Fed-Batch Systems in *Escherichia coli*. 2007.
71. **Cecilia Sarmiento**. Suppressors of RNA Silencing in Plants. 2008.

72. **Vilja Mardla**. Inhibition of Platelet Aggregation with Combination of Antiplatelet Agents. 2008.
73. **Maie Bachmann**. Effect of Modulated Microwave Radiation on Human Resting Electroencephalographic Signal. 2008.
74. **Dan Hüvonen**. Terahertz Spectroscopy of Low-Dimensional Spin Systems. 2008.
75. **Ly Villo**. Stereoselective Chemoenzymatic Synthesis of Deoxy Sugar Esters Involving *Candida antarctica* Lipase B. 2008.
76. **Johan Anton**. Technology of Integrated Photoelasticity for Residual Stress Measurement in Glass Articles of Axisymmetric Shape. 2008.
77. **Olga Volobujeva**. SEM Study of Selenization of Different Thin Metallic Films. 2008.
78. **Artur Jõgi**. Synthesis of 4'-Substituted 2,3'-dideoxynucleoside Analogues. 2008.
79. **Mario Kadastik**. Doubly Charged Higgs Boson Decays and Implications on Neutrino Physics. 2008.
80. **Fernando Pérez-Caballero**. Carbon Aerogels from 5-Methylresorcinol-Formaldehyde Gels. 2008.
81. **Sirje Vaask**. The Comparability, Reproducibility and Validity of Estonian Food Consumption Surveys. 2008.
82. **Anna Menaker**. Electrosynthesized Conducting Polymers, Polypyrrole and Poly(3,4-ethylenedioxythiophene), for Molecular Imprinting. 2009.
83. **Lauri Ilison**. Solitons and Solitary Waves in Hierarchical Korteweg-de Vries Type Systems. 2009.
84. **Kaia Ernits**. Study of In_2S_3 and ZnS Thin Films Deposited by Ultrasonic Spray Pyrolysis and Chemical Deposition. 2009.
85. **Veljo Sinivee**. Portable Spectrometer for Ionizing Radiation "Gammamapper". 2009.
86. **Jüri Virkepu**. On Lagrange Formalism for Lie Theory and Operadic Harmonic Oscillator in Low Dimensions. 2009.
87. **Marko Piirsoo**. Deciphering Molecular Basis of Schwann Cell Development. 2009.
88. **Kati Helmja**. Determination of Phenolic Compounds and Their Antioxidative Capability in Plant Extracts. 2010.
89. **Merike Sõmera**. Sobemoviruses: Genomic Organization, Potential for Recombination and Necessity of P1 in Systemic Infection. 2010.
90. **Kristjan Laes**. Preparation and Impedance Spectroscopy of Hybrid Structures Based on $CuIn_3Se_5$ Photoabsorber. 2010.
91. **Kristin Lippur**. Asymmetric Synthesis of 2,2'-Bimorpholine and its 5,5'-Substituted Derivatives. 2010.
92. **Merike Luman**. Dialysis Dose and Nutrition Assessment by an Optical Method. 2010.
93. **Mihhail Berezovski**. Numerical Simulation of Wave Propagation in Heterogeneous and Microstructured Materials. 2010.
94. **Tamara Aid-Pavlidis**. Structure and Regulation of BDNF Gene. 2010.

95. **Olga Bragina**. The Role of Sonic Hedgehog Pathway in Neuro- and Tumorigenesis. 2010.
96. **Merle Randrüüt**. Wave Propagation in Microstructured Solids: Solitary and Periodic Waves. 2010.
97. **Marju Laars**. Asymmetric Organocatalytic Michael and Aldol Reactions Mediated by Cyclic Amines. 2010.
98. **Maarja Grossberg**. Optical Properties of Multinary Semiconductor Compounds for Photovoltaic Applications. 2010.
99. **Alla Maloverjan**. Vertebrate Homologues of Drosophila Fused Kinase and Their Role in Sonic Hedgehog Signalling Pathway. 2010.
100. **Priit Pruunsild**. Neuronal Activity-Dependent Transcription Factors and Regulation of Human *BDNF* Gene. 2010.
101. **Tatjana Knjazeva**. New Approaches in Capillary Electrophoresis for Separation and Study of Proteins. 2011.
102. **Atanas Katerski**. Chemical Composition of Sprayed Copper Indium Disulfide Films for Nanostructured Solar Cells. 2011.
103. **Kristi Timmo.** Formation of Properties of $CuInSe_2$ and $Cu_2ZnSn(S,Se)_4$ Monograin Powders Synthesized in Molten KI. 2011.
104. **Kert Tamm**. Wave Propagation and Interaction in Mindlin-Type Microstructured Solids: Numerical Simulation. 2011.
105. **Adrian Popp**. Ordovician Proetid Trilobites in Baltoscandia and Germany. 2011.
106. **Ove Pärn**. Sea Ice Deformation Events in the Gulf of Finland and This Impact on Shipping. 2011.
107. **Germo Väli**. Numerical Experiments on Matter Transport in the Baltic Sea. 2011.
108. **Andrus Seiman**. Point-of-Care Analyser Based on Capillary Electrophoresis. 2011.
109. **Olga Katargina**. Tick-Borne Pathogens Circulating in Estonia (Tick-Borne Encephalitis Virus, *Anaplasma phagocytophilum*, *Babesia* Species): Their Prevalence and Genetic Characterization. 2011.
110. **Ingrid Sumeri**. The Study of Probiotic Bacteria in Human Gastrointestinal Tract Simulator. 2011.
111. **Kairit Zovo**. Functional Characterization of Cellular Copper Proteome. 2011.
112. **Natalja Makarytsheva**. Analysis of Organic Species in Sediments and Soil by High Performance Separation Methods. 2011.
113. **Monika Mortimer**. Evaluation of the Biological Effects of Engineered Nanoparticles on Unicellular Pro- and Eukaryotic Organisms. 2011.
114. **Kersti Tepp**. Molecular System Bioenergetics of Cardiac Cells: Quantitative Analysis of Structure-Function Relationship. 2011.
115. **Anna-Liisa Peikolainen**. Organic Aerogels Based on 5-Methylresorcinol. 2011.
116. **Leeli Amon**. Palaeoecological Reconstruction of Late-Glacial Vegetation Dynamics in Eastern Baltic Area: A View Based on Plant Macrofossil Analysis. 2011.

117. **Tanel Peets**. Dispersion Analysis of Wave Motion in Microstructured Solids. 2011.
118. **Liina Kaupmees**. Selenization of Molybdenum as Contact Material in Solar Cells. 2011.
119. **Allan Olspert**. Properties of VPg and Coat Protein of Sobemoviruses. 2011.
120. **Kadri Koppel**. Food Category Appraisal Using Sensory Methods. 2011.
121. **Jelena Gorbatšova**. Development of Methods for CE Analysis of Plant Phenolics and Vitamins. 2011.
122. **Karin Viipsi**. Impact of EDTA and Humic Substances on the Removal of Cd and Zn from Aqueous Solutions by Apatite. 2012.
123. **David Schryer**. Metabolic Flux Analysis of Compartmentalized Systems Using Dynamic Isotopologue Modeling. 2012.
124. **Ardo Illaste**. Analysis of Molecular Movements in Cardiac Myocytes. 2012.
125. **Indrek Reile**. 3-Alkylcyclopentane-1,2-Diones in Asymmetric Oxidation and Alkylation Reactions. 2012.
126. **Tatjana Tamberg**. Some Classes of Finite 2-Groups and Their Endomorphism Semigroups. 2012.
127. **Taavi Liblik**. Variability of Thermohaline Structure in the Gulf of Finland in Summer. 2012.
128. **Priidik Lagemaa**. Operational Forecasting in Estonian Marine Waters. 2012.
129. **Andrei Errapart**. Photoelastic Tomography in Linear and Non-linear Approximation. 2012.
130. **Külliki Krabbi**. Biochemical Diagnosis of Classical Galactosemia and Mucopolysaccharidoses in Estonia. 2012.
131. **Kristel Kaseleht**. Identification of Aroma Compounds in Food using SPME-GC/MS and GC-Olfactometry. 2012.
132. **Kristel Kodar**. Immunoglobulin G Glycosylation Profiling in Patients with Gastric Cancer. 2012.
133. **Kai Rosin**. Solar Radiation and Wind as Agents of the Formation of the Radiation Regime in Water Bodies. 2012.
134. **Ann Tiiman**. Interactions of Alzheimer's Amyloid-Beta Peptides with Zn(II) and Cu(II) Ions. 2012.
135. **Olga Gavrilova**. Application and Elaboration of Accounting Approaches for Sustainable Development. 2012.
136. **Olesja Bondarenko**. Development of Bacterial Biosensors and Human Stem Cell-Based *In Vitro* Assays for the Toxicological Profiling of Synthetic Nanoparticles. 2012.
137. **Katri Muska**. Study of Composition and Thermal Treatments of Quaternary Compounds for Monograin Layer Solar Cells. 2012.
138. **Ranno Nahku**. Validation of Critical Factors for the Quantitative Characterization of Bacterial Physiology in Accelerostat Cultures. 2012.
139. **Petri-Jaan Lahtvee**. Quantitative Omics-level Analysis of Growth Rate Dependent Energy Metabolism in *Lactococcus lactis*. 2012.
140. **Kerti Orumets**. Molecular Mechanisms Controlling Intracellular Glutathione Levels in Baker's Yeast *Saccharomyces cerevisiae* and its Random Mutagenized Glutathione Over-Accumulating Isolate. 2012.

141. **Loreida Timberg**. Spice-Cured Sprats Ripening, Sensory Parameters Development, and Quality Indicators. 2012.
142. **Anna Mihhalevski**. Rye Sourdough Fermentation and Bread Stability. 2012.
143. **Liisa Arike**. Quantitative Proteomics of *Escherichia coli*: From Relative to Absolute Scale. 2012.
144. **Kairi Otto**. Deposition of In_2S_3 Thin Films by Chemical Spray Pyrolysis. 2012.
145. **Mari Sepp**. Functions of the Basic Helix-Loop-Helix Transcription Factor TCF4 in Health and Disease. 2012.
146. **Anna Suhhova**. Detection of the Effect of Weak Stressors on Human Resting Electroencephalographic Signal. 2012.
147. **Aram Kazarjan**. Development and Production of Extruded Food and Feed Products Containing Probiotic Microorganisms. 2012.
148. **Rivo Uiboupin**. Application of Remote Sensing Methods for the Investigation of Spatio-Temporal Variability of Sea Surface Temperature and Chlorophyll Fields in the Gulf of Finland. 2013.
149. **Tiina Kriščiunaite**. A Study of Milk Coagulability. 2013.
150. **Tuuli Levandi**. Comparative Study of Cereal Varieties by Analytical Separation Methods and Chemometrics. 2013.
151. **Natalja Kabanova**. Development of a Microcalorimetric Method for the Study of Fermentation Processes. 2013.
152. **Himani Khanduri**. Magnetic Properties of Functional Oxides. 2013.
153. **Julia Smirnova**. Investigation of Properties and Reaction Mechanisms of Redox-Active Proteins by ESI MS. 2013.
154. **Mervi Sepp**. Estimation of Diffusion Restrictions in Cardiomyocytes Using Kinetic Measurements. 2013.
155. **Kersti Jääger**. Differentiation and Heterogeneity of Mesenchymal Stem Cells. 2013.
156. **Victor Alari**. Multi-Scale Wind Wave Modeling in the Baltic Sea. 2013.
157. **Taavi Päll**. Studies of CD44 Hyaluronan Binding Domain as Novel Angiogenesis Inhibitor. 2013.
158. **Allan Niidu**. Synthesis of Cyclopentane and Tetrahydrofuran Derivatives. 2013.
159. **Julia Geller**. Detection and Genetic Characterization of *Borrelia* Species Circulating in Tick Population in Estonia. 2013.
160. **Irina Stulova**. The Effects of Milk Composition and Treatment on the Growth of Lactic Acid Bacteria. 2013.
161. **Jana Holmar**. Optical Method for Uric Acid Removal Assessment During Dialysis. 2013.
162. **Kerti Ausmees**. Synthesis of Heterobicyclo[3.2.0]heptane Derivatives *via* Multicomponent Cascade Reaction. 2013.
163. **Minna Varikmaa**. Structural and Functional Studies of Mitochondrial Respiration Regulation in Muscle Cells. 2013.
164. **Indrek Koppel**. Transcriptional Mechanisms of BDNF Gene Regulation. 2014.
165. **Kristjan Pilt**. Optical Pulse Wave Signal Analysis for Determination of Early Arterial Ageing in Diabetic Patients. 2014.

166. **Andres Anier**. Estimation of the Complexity of the Electroencephalogram for Brain Monitoring in Intensive Care. 2014.
167. **Toivo Kallaste**. Pyroclastic Sanidine in the Lower Palaeozoic Bentonites – A Tool for Regional Geological Correlations. 2014.
168. **Erki Kärber**. Properties of ZnO-nanorod/In_2S_3/$CuInS_2$ Solar Cell and the Constituent Layers Deposited by Chemical Spray Method. 2014.
169. **Julia Lehner**. Formation of Cu_2ZnSnS_4 and $Cu_2ZnSnSe_4$ by Chalcogenisation of Electrochemically Deposited Precursor Layers. 2014.
170. **Peep Pitk**. Protein- and Lipid-rich Solid Slaughterhouse Waste Anaerobic Co-digestion: Resource Analysis and Process Optimization. 2014.
171. **Kaspar Valgepea**. Absolute Quantitative Multi-omics Characterization of Specific Growth Rate-dependent Metabolism of *Escherichia coli*. 2014.
172. **Artur Noole**. Asymmetric Organocatalytic Synthesis of 3,3'-Disubstituted Oxindoles. 2014.
173. **Robert Tsanev**. Identification and Structure-Functional Characterisation of the Gene Transcriptional Repressor Domain of Human Gli Proteins. 2014.
174. **Dmitri Kartofelev**. Nonlinear Sound Generation Mechanisms in Musical Acoustic. 2014.
175. **Sigrid Hade**. GIS Applications in the Studies of the Palaeozoic Graptolite Argillite and Landscape Change. 2014.
176. **Agne Velthut-Meikas**. Ovarian Follicle as the Environment of Oocyte Maturation: The Role of Granulosa Cells and Follicular Fluid at Pre-Ovulatory Development. 2014.
177. **Kristel Hälvin**. Determination of B-group Vitamins in Food Using an LC-MS Stable Isotope Dilution Assay. 2014.
178. **Mailis Päri**. Characterization of the Oligoadenylate Synthetase Subgroup from Phylum Porifera. 2014.
179. **Jekaterina Kazantseva**. Alternative Splicing of *TAF4*: A Dynamic Switch between Distinct Cell Functions. 2014.
180. **Jaanus Suurväli**. Regulator of G Protein Signalling 16 (RGS16): Functions in Immunity and Genomic Location in an Ancient MHC-Related Evolutionarily Conserved Synteny Group. 2014.
181. **Ene Viiard**. Diversity and Stability of Lactic Acid Bacteria During Rye Sourdough Propagation. 2014.
182. **Kristella Hansen**. Prostaglandin Synthesis in Marine Arthropods and Red Algae. 2014.
183. **Helike Lõhelaid**. Allene Oxide Synthase-lipoxygenase Pathway in Coral Stress Response. 2015.
184. **Normunds Stivrinš**. Postglacial Environmental Conditions, Vegetation Succession and Human Impact in Latvia. 2015.
185. **Mary-Liis Kütt**. Identification and Characterization of Bioactive Peptides with Antimicrobial and Immunoregulating Properties Derived from Bovine Colostrum and Milk. 2015.
186. **Kazbulat Šogenov**. Petrophysical Models of the CO_2 Plume at Prospective Storage Sites in the Baltic Basin. 2015.

187. **Taavi Raadik**. Application of Modulation Spectroscopy Methods in Photovoltaic Materials Research. 2015.
188. **Reio Põder**. Study of Oxygen Vacancy Dynamics in Sc-doped Ceria with NMR Techniques. 2015.
189. **Sven Siir**. Internal Geochemical Stratification of Bentonites (Altered Volcanic Ash Beds) and its Interpretation. 2015.
190. **Kaur Jaanson**. Novel Transgenic Models Based on Bacterial Artificial Chromosomes for Studying BDNF Gene Regulation. 2015.
191. **Niina Karro**. Analysis of ADP Compartmentation in Cardiomyocytes and Its Role in Protection Against Mitochondrial Permeability Transition Pore Opening. 2015.
192. **Piret Laht**. B-plexins Regulate the Maturation of Neurons Through Microtubule Dynamics. 2015.
193. **Sergei Žari**. Organocatalytic Asymmetric Addition to Unsaturated 1,4-Dicarbonyl Compounds. 2015.
194. **Natalja Buhhalko**. Processes Influencing the Spatio-temporal Dynamics of Nutrients and Phytoplankton in Summer in the Gulf of Finland, Baltic Sea. 2015.
195. **Natalia Maticiuc**. Mechanism of Changes in the Properties of Chemically Deposited CdS Thin Films Induced by Thermal Annealing. 2015.
196. **Mario Öeren**. Computational Study of Cyclohexylhemicucurbiturils. 2015.
197. **Mari Kalda**. Mechanoenergetics of a Single Cardiomyocyte. 2015.
198. **Ieva Grudzinska**. Diatom Stratigraphy and Relative Sea Level Changes of the Eastern Baltic Sea over the Holocene. 2015.
199. **Anna Kazantseva**. Alternative Splicing in Health and Disease. 2015.
200. **Jana Kazarjan**. Investigation of Endogenous Antioxidants and Their Synthetic Analogues by Capillary Electrophoresis. 2016.
201. **Maria Safonova**. SnS Thin Films Deposition by Chemical Solution Method and Characterization. 2016.
202. **Jekaterina Mazina**. Detection of Psycho- and Bioactive Drugs in Different Sample Matrices by Fluorescence Spectroscopy and Capillary Electrophoresis. 2016.
203. **Karin Rosenstein**. Genes Regulated by Estrogen and Progesterone in Human Endometrium. 2016.
204. **Aleksei Tretjakov**. A Macromolecular Imprinting Approach to Design Synthetic Receptors for Label-Free Biosensing Applications. 2016.
205. **Mati Danilson**. Temperature Dependent Electrical Properties of Kesterite Monograin Layer Solar Cells. 2016.
206. **Kaspar Kevvai**. Applications of ^{15}N-labeled Yeast Hydrolysates in Metabolic Studies of *Lactococcus lactis* and *Saccharomyces Cerevisiae*. 2016.
207. **Kadri Aller**. Development and Applications of Chemically Defined Media for Lactic Acid Bacteria. 2016.
208. **Gert Preegel**. Cyclopentane-1,2-dione and Cyclopent-2-en-1-one in Asymmetric Organocatalytic Reactions. 2016.